LWR SPENT FUEL DRY STORAGE BEHAVIOR AT 229°C

Hanford Engineering Development Laboratory

R.E. Einziger
J.A. Cook

NOTICE

Availability of Reference Materials Cited in NRC Publications

Most documents cited in NRC publications will be available from one of the following sources:

1. The NRC Public Document Room, 1717 H Street, N.W.
   Washington, DC 20555

2. The NRC/GPO Sales Program, U.S. Nuclear Regulatory Commission,
   Washington, DC 20555

3. The National Technical Information Service, Springfield, VA 22161

Although the listing that follows represents the majority of documents cited in NRC publications, it is not intended to be exhaustive.

Referenced documents available for inspection and copying for a fee from the NRC Public Document Room include NRC correspondence and internal NRC memoranda; NRC Office of Inspection and Enforcement bulletins, circulars, information notices, inspection and investigation notices; Licensee Event Reports; vendor reports and correspondence; Commission papers; and applicant and licensee documents and correspondence.

The following documents in the NUREG series are available for purchase from the NRC/GPO Sales Program: formal NRC staff and contractor reports, NRC-sponsored conference proceedings, and NRC booklets and brochures. Also available are Regulatory Guides, NRC regulations in the *Code of Federal Regulations,* and *Nuclear Regulatory Commission Issuances.*

Documents available from the National Technical Information Service include NUREG series reports and technical reports prepared by other federal agencies and reports prepared by the Atomic Energy Commission, forerunner agency to the Nuclear Regulatory Commission.

Documents available from public and special technical libraries include all open literature items, such as books, journal and periodical articles, and transactions. *Federal Register* notices, federal and state legislation, and congressional reports can usually be obtained from these libraries.

Documents such as theses, dissertations, foreign reports and translations, and non-NRC conference proceedings are available for purchase from the organization sponsoring the publication cited.

Single copies of NRC draft reports are available free, to the extent of supply, upon written request to the Division of Technical Information and Document Control, U.S. Nuclear Regulatory Commission, Washington, DC 20555. *

Copies of industry codes and standards used in a substantive manner in the NRC regulatory process are maintained at the NRC Library, 7920 Norfolk Avenue, Bethesda, Maryland, and are available there for reference use by the public. Codes and standards are usually copyrighted and may be purchased from the originating organization or, if they are American National Standards, from the American National Standards Institute, 1430 Broadway, New York, NY 10018.

GPO Printed copy price: _____

LWR SPENT FUEL DRY STORAGE BEHAVIOR AT 229°C

Hanford Engineering Development Laboratory

R.E. Einziger (WHC)
J.A. Cook (EG&G Idaho, Inc.)

OTHER REPORTS IN THIS SERIES

R. E. Einziger and J. A. Cook, Pretest Visual Examination and Crud Characterization of LWR Rods Used in the Long-Term, Low-Temperature Whole Rod Test, NUREG/CR-3285, HEDL-TME 83-9, Hanford Engineering Development Laboratory, Richland, WA, March 1984.

R. E. Einziger, R. L. Fish and R. L. Knecht, A Technical Description of the NRC Long-Term Whole Rod and Crud Performance Test, NUREG/CR-2889, HEDL-TME 82-32, Hanford Engineering Development Laboratory, Richland, WA, September 1982.

R. E. Einziger and R. L. Fish, Characterization of LWR Spent Fuel Rods Used in the NRC Low-Temperature Whole Rod and Crud Performance Test, NUREG/CR-2871, HEDL-TME 82-27, Hanford Engineering Development Laboratory, Richland, WA, September 1982.

LWR SPENT FUEL DRY STORAGE BEHAVIOR AT 229°C

R. E. Einziger
J. A. Cook

ABSTRACT

A whole rod test was conducted at 229°C to investigate the long-term stability of spent fuel rods under a variety of possible dry storage conditions. All combinations of BWR or PWR rods, inert or air atmospheres, and intact or defected rods were tested. After 2235 hours, visual observations, diametral measurements and radiographic smears were used to assess the degree of cladding deformation and particulate release. The same examinations plus metallography and x-ray analysis were conducted after 5962 hours.

None of the intact rods, the rods tested in inert atmosphere, or the defected PWR rod tested in unlimited air showed any measurable change from the pretest condition. The upper defect on the BWR rod tested in unlimited air had split open ∿0.5 in. after 2235 hours and had ∿10% cladding deformation. The crack grew to ∿2.5-in. after 5962 hours. X-ray analysis indicated that the UO_2 had oxidized to U_3O_8. The difference in behavior of the upper and lower defects is attributed to the air's accessibility to the fuel because of the defect's position with relation to the pellet-pellet interface.

The oxidized fuel appeared to form a powdery compact that remained for the most part in the split cladding. Only a fraction of the fuel that fell out of the cladding became airborne. Some crud spalled from the rods but appeared to have no airborne particulate in the 2- to 15-μm respirable range. This report discusses the details and meaning of the data from this test.

ACKNOWLEDGMENTS

CONTENTS

CONTENTS (Cont'd)

FIGURES

FIGURES (Cont'd)

FIGURES (Cont'd)

TABLES

ACRONYMS

BCL	Battelle Columbus Laboratories, Columbus, OH
BWR	Boiling Water Reactor
ct/s	Counts per second
DE	Destructive Examination(s)
DOE	Department of Energy, Washington, DC
EFPH	Effective Full-Power Hours
EG&G	EG&G Idaho, Inc., Idaho Falls, ID
GWd/t	Gigawatt days per ton
HBR	H. B. Robinson Reactor Unit 2
LANL	Los Alamos National Laboratory, Los Alamos, NM
LWR	Light Water Reactor
NDE	Nondestructive Examination(s)
NRC	Nuclear Regulatory Commission, Washington, DC
NUREG	Nuclear Regulatory Commission report prefix
PB	Peach Bottom Reactor Unit 2
PNL	Pacific Northwest Laboratories, Richland, WA
PWR	Pressurized Water Reactor
W	Westinghouse Electric Corporation
WHC	Westinghouse Hanford Company, Richland, WA

LWR SPENT FUEL DRY STORAGE BEHAVIOR AT 229°C

I. SUMMARY

Westinghouse Hanford Company and EG&G Idaho, Inc. conducted an experimental program for the Nuclear Regulatory Commission (NRC) to provide data on the long-term, low-temperature, dry storage performance of spent fuels. Spent fuel has an approximate in-reactor breach rate of 0.01% or less. Many breaches are small and difficult to detect; therefore, it is not possible or practical to separate breached and unbreached rods placed in dry storage. Thus the main concerns for this study of fuel performance were defective rod behavior and the dispersal potential of radionuclide carriers, such as fuel and crud. After an analysis of the existing UO_2 oxidation data and performance predictions, the whole rod experimental testing method was chosen.

The technical approach was based on literature indications that dry storage of spent fuel in unlimited air atmosphere was possible at temperatures below 250°C. No fuel oxidation was expected and no active cladding degradation mechanisms had been identified. A whole rod test was chosen since it represents an intermediate position between laboratory testing of small segments and demonstration testing of whole assemblies or groups of assemblies. The test was planned to run until significant degradation occurred or five years (when the temperature of a stored assembly would have dropped considerably), whichever was first.

The actual whole rod test was conducted with eight rods covering the eight combinations of rod type (BWR, PWR), atmosphere (inert, air), and rod condition (intact, defected). The rods used were from the H. B. Robinson Unit 2 pressurized water reactor (PWR) and the Peach Bottom-II boiling water reactor (BWR). The rods had been characterized in other programs and were visually inspected prior to the start of the test. Four of the rods were defected at the center and upper end of the fuel column with a 0.03-in. drill hole. Each rod was contained in an individual capsule that was placed in a 14-ft long whole rod furnace. The defected rods being tested in an unlimited air atmosphere had a set of filters at each end. A 15 psia Ar/1%He inert atmosphere or unlimited air was used. The test was conducted at 229°C for 5962 hours with an interim examination also conducted after 2235 hours. Examinations included capsule gas analysis, filter analysis, capsule swabbing, visual examination, physical measurements, metallography, ceramography and x-ray analysis.

Capsule gas analyses indicated no breaches of the intact rods. There were no visual or dimensional indications of rod degradation in any of the rods except the defected BWR rod tested in air. The upper defect had split open ~1/2 in. after 2235 hours and 2-1/2 in. after 5962 hours. Cladding diametral deformation as large as 16% occurred at the split defect. A destructive examination of the rod was conducted after 5962 hours. X-ray analysis showed that the fuel at the upper split defect had oxidized to U_3O_8, causing the

split. It required ~7% cladding strain before the crack propagated. This corresponded to ~100% local conversion of the UO_2 to U_3O_8. The center defect also had started to oxidize through U_4O_9 to U_3O_8 but had not progressed enough to split the cladding. The difference in behavior is probably due to the positioning of the defects. The center split was on the side of a pellet, which limited the availability of air, while the upper defect was at a pellet-pellet interface, which allowed freer access of the air to the fuel. This is probably the reason that the H. B. Robinson rod did not split open, since there is only a 7% chance that a defect will be at an interface. Because the most likely position of SCC cracks caused in-reactor is at the pellet-pellet interface, the behavior of this rod should not be considered abnormal.

Little crud spalled from the rod and little fuel fell out of the crack. Of the small amount of material that released to the capsule, less than 0.1% became airborne in the respirable range of 2 to 15 μm. Contamination from crud spallation during dry storage should be a manageable problem. Test results indicate that, to eliminate the potential of contamination from oxidation, breached spent fuel rods should be stored in an inert atmosphere or at a temperature as yet undetermined below the 229°C used in this experiment.

II. INTRODUCTION

The US Department of Energy and the utilities are attempting to license dry
storage of spent LWR fuel in the United States. The regulation under which
licensing must be granted is Title 10 CFR, Part 72 (Ref. 1). This regula-
tion indicates the following conditions related to fuel performance that
must be satisfied:

- The fuel cladding shall be protected against degradation and gross
  rupture.

- Surveillance shall be provided to ensure that limiting conditions
  are met.

- Adequate safety shall be provided under normal and accident
  conditions.

- Releases to the environment shall be within acceptable limits.

So that NRC could evaluate licensing applications for low-temperature
(<250°C) storage with respect to these criteria, WHC was asked to conduct
an experimental program to confirm the long-term, low-temperature (<250°C),
dry storage spent fuel performance predictions based on theoretical analysis
and on the results of high-temperature, short-term laboratory tests. In
particular, the dispersal potential of radionuclide carriers, such as fuel
and crud, was to be evaluated. The program was to include both PWR and BWR
rods, intact and defected rods, and inert or air atmospheres.

Dry storage of spent fuel in an unlimited air atmosphere below 250°C was
thought to be viable based on several considerations:

- In an unlimited air atmosphere, less than 10% of the cladding wall
  was expected to oxidize in 100 years of storage.

- Analyses and testing indicated that below 250°C there are no
  expected cladding breach mechanisms for normal rods.

- Pin hole cladding breaches, occurring in-reactor and not routinely
  identified and sorted out, were not expected to be a source of
  contamination. Based on information available, it was thought that
  below 250°C the UO_2 pellet, if in contact with air, oxidizes to
  U_3O_7 with little density change. As a result, the fuel pellet
  (or pieces) structure is maintained as is the cladding structural
  integrity, except for the original breach.

- For very conservative worst-case analyses, stress corrosion crack-
  ing (SCC) of the cladding is a possibility; but the consequence

3

should be limited to a release of fission gas. Fuel oxidation to U_3O_8 at the breach with subsequent cladding splitting and contamination was not viewed to be a problem.

Therefore, this study of the long-term, spent-fuel performance below 250°C concentrated on three points:

. Determining if any unforeseen cladding breach mechanisms appear.

. Determining the long-term behavior of breached fuel rods.

. Tracking crud dispersal behavior.

BWR rod segments had been tested in the laboratory but had never been part of a whole rod or demonstration test. This study provided the first testing of BWR rods, which represent ~40% of the spent fuel population. Although BWR rods operate with much lower internal pressure (2 to 10 atm) and have a thicker cladding (0.032 to 0.045 in.) than PWR rods (20 to 30 atm and 0.022 to 0.030 in. cladding), the BWR rods have approximately the same breach statistics as PWR rods (Ref. 2). The BWR rods also tend to release more fission gas (Ref. 3); hence, more corrosive fission products accumulate in the rod gap, at least in the unpressurized BWR vintage, than in the PWR rods. Thus, the BWR fuel rods have some attributes that may make them more susceptible to breach and others that make them less. This study compares BWR and PWR rod performance directly in both inert and oxidizing atmospheres.

The whole rod test initiated to study the low-temperature behavior of spent fuel rods under dry storage conditions represents an intermediate position between laboratory testing of small segments and demonstration testing of whole assemblies or groups of assemblies (Refs. 4&5). In some instances, such as studying rod/hardware interaction, demonstration testing is clearly preferred. In other instances, such as well controlled breach inducement, laboratory testing is preferred. Since storage programs look for the weak link in rod performance, whole rod testing offers some distinct advantages:

. It is more economical than demonstration testing, which requires extensive facilities.

. One whole rod is equivalent in material volume to ~24 laboratory samples.

. The complete rod, which has materials properties gradients along its length due to in-reactor temperature and fluence gradients, is tested.

. The internal atmosphere that controls many of the breach mechanisms in the rod is not disturbed.

4

- Test conditions can be controlled and varied more precisely than in a demonstration.

- Six whole rods are statistically equivalent to a whole assembly (Ref. 6).

This report presents the results of this investigation.

III. BACKGROUND

Prior to initiating the experimental program, the three points of interest (intact rod behavior, defected rod behavior and crud behavior) were reviewed and evaluated. Below 250°C there was no indication that intact rods could not be successfully stored in either an air or an inert atmosphere. While earlier data indicated that 250°C was a safe storage temperature for dry air storage of defected rods, later work now casts considerable doubt on that conclusion. Limited information is available on crud and its dispersal characteristics. The information about spent fuel performance that was used in designing this experiment is presented in the next section on fuel-cladding degradation mechanisms, fuel oxidation and crud.

A. DEGRADATION MECHANISMS

In an inert atmosphere, cladding degradation (not fuel oxidation) appears to be the limiting performance factor that sets an upper storage temperature limit. Four degradation mechanisms have been identified (Ref. 7) that might cause cladding breach during dry storage: stress-rupture, stress-corrosion cracking (SCC), hydriding and external oxidation. While each of these potential breach mechanisms could be active under certain conditions, control of the spent fuel environment during storage should ensure that cladding breach will not occur for long periods of time. Blackburn (Ref. 7) analyzed each mechanism discussed above and determined that stress-rupture was the most likely breach mode, although there was uncertainty about SCC. Based on his analysis, Blackburn recommended a maximum allowable cladding temperature of 380°C for spent fuel storage in an inert atmosphere. (This limit is based entirely on stress-rupture considerations for spent PWR fuel assemblies; higher temperatures could be allowed using stress-rupture considerations only for BWR fuel assemblies.)

Spent fuel rods are potentially susceptible to failure by stress-rupture since the internal pressure in the rod produces a tensile hoop stress in the cladding wall. While this mechanism was originally thought to be the most probable cause of breach (Ref. 7), high-temperature testing (Ref. 8) has indicated that this may not be the case. Accelerated high temperature (480°C to 570°C) tests were conducted (Ref. 8) on intact PWR rods (fabrication pressurization of 350 psi) to attempt to determine the dominant mode of cladding breach and degree of cladding degradation. Well characterized rods were used (Refs. 9,10,11&12) so that, if breach did not occur, the extent of the degradation could be determined. The test details have been previously described (Ref. 8). Cladding breach did not occur because of the creep strain up to 15% and the resulting drop in stress. In addition, there was:

.   No detectable release of fission gas from the fuel pellets.

.   Cracking of the external oxide layer.

7

Formation of oxygen-stabilized alpha Zircaloy[*] layer between the cladding and the ZrO_2. Penetration but blunting of cracks in the oxygen-stabilized alpha Zircaloy.

When these observations are factored into Blackburn's models (Ref. 7), an estimated 100-year cladding lifetime based on the stress-rupture mechanism can be obtained by extrapolation using the Larson-Miller (Ref. 13) technique for storage temperatures as high as 440°C. This prediction is still based on unirradiated stress-rupture properties that are probably representative above 400°C. Below 400°C, cladding will spend all or part of its lifetime in an irradiation-hardened state and part in an annealed state, so the use of unirradiated stress-rupture properties and the use or extrapolation of the higher temperature whole rod test results may be inappropriate. Recently a whole rod test (Ref. 14) was run for 2100 hours at 323°C using PWR rods that were overpressurized to 9.5 MPa at 23°C. The rods remained in the irradiation-hardened state with no apparent cladding annealing. No breaches occurred. Analysis of these results indicate that breach due to stress-rupture should not occur in 100 years if the cladding temperature is kept below 300°C. Experiments to determine long-term cladding behavior in the temperature range of 300°C to 400°C, where there is partially annealed cladding, have not yet been performed.

SCC as an active degradation mechanism in Zircaloy-clad fuel rods is not well understood. The corrosive environment responsible for SCC in fuel rods comes from the fission products generated during irradiation. The specific agent causing SCC has not been positively identified, although iodine is thought to be the prime candidate (Ref. 15). Gamma radiolysis of solid CsI (Ref. 16) to produce localized iodine vapor (thought to be responsible for in-reactor SCC, Ref. 17) may not be active during storage, thus reducing SCC effects. Analysis by Tasooji, Einziger and Miller, using the SCCIG model (Ref. 18), indicated that, even for rods that released 20% of the fission gas entrained in the fuel, SCC should not be a life-limiting degradation mechanism for temperatures below 400°C. This analysis was later extended by Tasooji and Miller (Ref. 19) to include the effects of Cd and Cs as corrosive species; the same conclusions were reached.

Oxidation of Zircaloy results in a brittle film that is created at the expense of the relatively ductile base metal. Degradation of the cladding mechanical properties could dictate the temperature and oxygen levels allowed during spent fuel storage or disposal. Cladding oxidation may limit the maximum allowable temperature in an unlimited air atmosphere. There have been many oxidation studies in water and steam, mostly at temperatures in excess of 500°C, but relatively few studies in a dry atmosphere. These few studies were also at temperatures above 500°C and were conducted for a short time (700 days maximum) (Ref. 20). Studies in steam by Hillner (Ref. 21)

---

[*]Zircaloy is a registered trademark of Westinghouse Specialty Metals Division, Pittsburgh, PA.

indicate that Zircaloy oxidation is a two-step process. The first step (pre-transition) follows a "$t^{1/3}$" dependence, while the second step (post-transition) follows a "t" dependence. This same two-step behavior and time-dependence were observed by Watson (Ref. 20) for oxidation of Zircaloy-2 in air between 500°C and 700°C. At reactor operating conditions (~350°C cladding temperature) transition occurs in ~150 days. Thus, when the rods enter dry storage, the exterior surface should have an oxide layer already growing as a post-transition oxide. It is not known whether the oxide will continue to grow at post-transition rates or revert to the slower pre-transition oxide growth rates at the lower storage temperatures. Bouse and Vandergraaf (Ref. 22) compared post-transition oxidation rate data above 500°C and found close agreement between oxidation in steam, water and air.

Zircaloy hydriding has been a matter of concern for in-reactor fuel rod performance (Ref. 23) and thus deserves attention with regard to storage. The primary concern in storage relates to the orientation of the hydrides formed in reactor. Proper processing of the Zircaloy during fabrication of the tubing and quality control of the moisture limits in the fuel pellets results in the in-reactor formation of an acceptable concentration of hydrides that are circumferentially oriented. Reorientation of the hydrides during cooldown under stress in storage to a radial direction (perpendicular to the hoop stress) could result in severe degradation of the cladding mechanical properties (e.g., make the cladding susceptible to failure from internal gas pressure). Hydrogen levels in PWR rods, in general, range from 40 to 100 ppm. Marshall and Loutham (Ref. 24) have shown that, when the concentration of hydrides oriented perpendicular to the stress vectors exceeds 40 ppm, a severe degradation of Zircaloy mechanical properties occurs. The lifetime and temperature determinations are usually made based on circumferential precipitation of hydrides. If the hydrides reorient radially during storage cooldown, the cladding may be weakened, stress-rupture predictions may not be valid, and predicted lifetimes may be significantly shortened. The critical stress for hydride reorientation is not well defined. During specimen tests that might be typical of storage conditions (i.e., 50 to 300 ppm H_2 and soak temperatures of 300°C to 400°C), reorientation generally commenced between 35 and 138 MPa (Refs. 25-28). The high-temperature and high-pressure whole rod data indicate that the stress threshold should be between 28 and 138 MPa, which is consistent with the literature. Unfortunately PWR rods have hoop stresses of 48 to 97 MPa in the 200°C to 300°C temperature range (the region of uncertainty). The variables affecting hydriding are discussed in more detail in Refs. 14 and 29.

B. CRUD

Crud, which is reactor primary cooling system corrosion products, deposits on the fuel rod surface. Once deposited it becomes neutron activated and is capable of trapping fissile material and fission products that may be in the system. This crud creates two main problems for reactor operations: 1) a thick layer of crud can cause localized overheating of the rod, which leads

to cladding rupture (Ref. 30), and 2) the activated crud is eroded and redeposited in the primary coolant piping system and, in turn, gives a radiation dosage to service workers. If crud spalls from the fuel rod during dry storage, it might cause a decommissioning contamination problem for some storage configurations.

The crud composition, quantity and deposition tendency are all system-dependent (Ref. 31). Crud thickness can vary from operating cycle to operating cycle within the same reactor (Ref. 32), but competing deposition and erosion processes eventually lead to a steady-state crud thickness that is dependent on the particular reactor. The tendency to form crud is strongly dependent on the water chemistry, with more crud forming at lower pH (Ref. 33). No relationship apparently exists between heat flux magnitude and either deposit distribution or quantity (Refs. 34&35).

Two types of crud are usually formed. An easily removed porous agglomerate of very fine iron-rich hydrated oxide particle (Refs. 2,30&36) is responsible for steam stagnation boiling in the reactor (Ref. 37). There is also a tenacious crystalline oxide layer that is dense and reflective. These two types of crud usually form in layers and may develop a sandwich-like structure. Crud has been generally characterized by its visual appearance, thickness, structure, chemical composition and radioactivity.

Both PWR and BWR fuel rods have patchy, flaky crud and show a wide spectrum of colors. These colors vary from black to dark brown, light brown to reddish orange and tan. This may be an indication of general crud composition since magnetite is black iron oxide and hematite is red iron oxide; on the other hand, hot cell and underwater lighting greatly affect the colors that appear on the fuel rods. Other than saying that crud is present and that it is either flaky or adherent, visual observations are a rather unsatisfactory means of crud evaluation.

The quantity of crud (i.e., thickness) is more important during reactor operations than in storage since a thick, localized crud layer may cause rod overheating and breach. Of major importance for storage is to determine how much crud is available to spall and how much will spall from the fuel rod. The maximum crud thickness on rods from 10 PWR reactors was ~3 mil, with many measurements being significantly less than 1 mil. While the BWR reactor Tsuruga had crud as thick as 8 mil, most of the remaining BWR measurements fell between 1 and 3 mil. By comparison, the SGHWR had a much heavier crud layer, and the CANDU rods exhibited a much thinner layer (0.4-mil maximum). While these are averages, they should not be mistakenly interpreted to imply a uniform distribution of crud on the rod. Crud thickness does not systematicly vary with burnup; it varies widely along a rod. The crud on PWR rods may be slightly thicker towards the top half of the rod, but this is a tenuous observation. Not enough data exists to determine axial distribution on BWR rods.

On both PWR and BWR rods, the crud is mainly Fe and Ni with lesser amounts of Cr and Cu. The Ni/Fe ratio in the crud is ~1.0 or less on PWR rods, while

10

it is almost zero on BWR rods; PWR crud is predominantly nickel-substituted spinel $Ni_xFe_{3-x}O_4$ with $x \approx 1$, while BWR crud is mostly Fe_2O_3. Not enough data has been collected to determine if there is an axial variation of crud composition.

Since a basic concern about crud in storage is its effect on decontamination and decommissioning of the facility, an important characteristic of crud is its radioactivity. While this activity is predominantly ^{58}Co, ^{60}Co, ^{54}Mn, ^{51}Cr and ^{59}Fe, the only isotopes of any practical importance are ^{60}Co and ^{54}Mn, due to their long half-lives and abundance. Sufficient information is lacking to determine if crud activity has an axial dependence.

There does not appear to be a typical crud for BWR and PWR rods. Based on a full crud description given in Ref. 38, some general crud characteristics are given in Table 1. (This is not to say that crud is uniform or that it won't fall outside the range specified in Table 1.)

TABLE 1

GENERAL CRUD CHARACTERISTICS

Feature	PWR	BWR
Color	Gray, Reddish Orange, Brown, Tan, Black, Reddish Brown	Orange, Brown, Reddish Brown
Thickness		
Maximum	3 mil	8 mil
Average	<1 mil	1 to 3 mil
Axial Variation	Yes	Yes
Chemical Composition		
Major Elements	Ni, Fe, Cr	Ni, Fe, Cr, Cu
Ni/Fe Ratio	<1	<<<1
Structure	$Ni_xFe_{3-x}O_4$	Fe_2O_3, NiO
Axial Variation	?	?
Radioactivity		
Maximum Observed ($\mu Ci/cm^2$)	140	1250
Range ($\mu Ci/cm^2$)	0.1 to 140	97 to 1250
Major Component After 10 Years	^{60}Co	^{60}Co

C. FUEL OXIDATION

If a breached fuel rod is unknowingly placed in dry unlimited air storage or if a breach occurs in a fuel rod while in dry storage in air, fuel oxidation rather than cladding degradation may become the controlling mechanism for the release of contamination. This contamination can result from three sources:

- If oxidation of UO_2 results in formation of U_3O_8 or UO_3, fuel will swell due to the decreased density. This swelling can lead to disintegration of the pellet itself and also stress the cladding, resulting in defect expansion. Particulates can then fall out of the fuel rod.

- Gases may be released from the grain boundaries of the oxidized fuel.

- Crud flaking may be accelerated due to cladding deformation.

To determine the potential for contamination, oxidation rates and oxidation products must be known.

UO_2 oxidation has been observed as low as room temperature (Refs. 39-44) but the oxidation rate and final oxidation products are strongly temperature-dependent. Early studies indicated that, below 250°C, UO_2 oxidizes to U_3O_7 (Refs. 39,42,45-51,52,53), which has approximately the same density as UO_2 even though the phase diagram gives no indication that this should be a limiting composition. Above 250°C, the UO_2 oxidizes to U_3O_8 (Refs. 46,47,50, 54-60), which has a much lower density. Powder samples experiments with widely varying surface-to-volume ratios and pellet studies (Ref. 53) were conducted only at the higher temperatures with large reaction rates. While these early studies generally agreed that, above 250°C, oxides higher than U_3O_7 were formed, the effects of microstructure and moisture were not considered. Studies on irradiated fuel (Refs. 55,61&62) provided no conclusive evidence that radiation either enhanced or decreased oxidation rates.

Boase and Vandergraaf (Ref. 52) found that oxidation of unirradiated UO_2 pellets in the 320°C to 460°C temperature range followed a nonisokinetic nucleation and growth pattern. All the reaction product was U_3O_8. Irradiated unclad CANDU pellets showed the same oxidation behavior. When the pellets were ground to powder prior to the oxidation tests, the oxidation rate increased for both irradiated and unirradiated fuel. This indicated that much of the work on unirradiated powders would not be suitable for determining fuel rod behavior.

Simpson and Wood (Ref. 63) interpreted the sigmoidal oxidation curve of unirradiated UO_2 in terms of an incubation period (zero weight gain intercept of the steady-state slope) and an oxidation rate (at ~50% conversion)

cr material U_3O_8. An alternative definition for an incubation period that is more closely related to the containment capability of spent fuel cladding is the time of first fuel spallation. When fuel rods or fuel rod segments are considered, a more suitable definition of incubation is the time at which defects start to enlarge. Hastings and Novak (Ref. 64) define this for bare particulate as the time when 0.6% weight gain occurs. One must, therefore, be careful when comparing incubation periods to state the type of incubation period and use the one appropriate to the physical situation.

A summary of fuel characteristics and test conditions for base fuel fragments/pellet oxidation studies is given in Table 2. A majority of work is on unirradiated pellets or CANDU and AGR fuel, all of which have a higher density than PWR fuel. If microstructure turns out to be an important parameter, then work on fuels with higher density might not be applicable to LWR fuel. Fuel in storage will be in an irradiated state and in a field produced by surrounding fuel rods. Only one experiment (Ref. 65) qualifies in this classification; and it was done at 230°C. The majority of the tests are with no external fields. No experiments were conducted on the same fuel with and without a field, and only one experiment (Ref. 64) was conducted on the same fabrication of fuel in both the unirradiated and irradiated state.

The effect of irradiation on other variables is again dependent on the definition of incubation. We choose to use time of spallation as the incubation criteria when possible. For the Canadian data, a 0.6% weight gain criteria was used. The published data is plotted in Figure 1. Two studies using essentially the same materials came to opposite results. Boase and Vandergraaf (Ref. 22) found no effect of radiation on steady-state weight gain, yet Hastings and Novak (Ref. 64) found a large enhancement of weight gain rate with irradiation. No conclusion on radiation effects can be drawn from Gilbert's work (Ref. 65) due to material differences between the irradiated and unirradiated samples. Insufficient data are available to determine the effects of radiation on fuel oxidation.

Oxidation studies on bare fuel are useful only if they can help predict the behavior of defected fuel rods. The experiments on defected rods or rod segments are listed in Table 3. None of the tests controlled the moisture in the test air, and the only field was the self-field or the field provided by surrounding rods included in the same test train. A number of breached rods were tested in an argon atmosphere as a control and, as expected, these rods showed no sign of degradation. The usual form of defect is a drilled hole, although some saw slits were used.

It is extremely difficult to make good correlations of incubation period and oxidation rates between fuel rods and bare pellet fragments. Accurate weight change measurements are not practical on whole LWR fuel rods, and frequent visual and diametral measurements are both difficult and costly. Scatter in bare fuel oxidation data necessitates that the bare fuel come from a companion rod in order to make meaningful comparisons. CANDU fuel studies indicate

TABLE 2

BARE FUEL OXIDATION EXPERIMENTS

Form	Reactor Name	Type	Burnup (MWd/MTU)	Density (g/cc)	External Radiation Field (R/h)	Atmosphere	Temp Range (°C)	Linear Power (kW/m)	Ref.
Cubes	--		0	10.8	No	Air	175 - 275	0	63
Disks	--		0	10.8	No	Air	275 - 500	0	63
Fragments	Hinkley Point	AGR	12.4	10.7	No	Air	175 - 200	?	63
Fragments	Windscale	AGR	26.7	?	No	Air	175 - 200	?	63
Fragments	Bruce	CANDU	7.1	10.6	No	Air	175 - 250	20-45	64
Fragments	Pickering	CANDU	7.9	10.6	No	Air	175 - 250	35-45	64
Pellets	Bruce	CANDU	0	10.6	No	Air	175 - 250	0	64
Pellets	--		0	10.55	No	Air	150 - 345	0	65
Pellets	--		0	10.55	No	$Air/1\%NO_2$	150 - 345	0	65
Fragments	Point Beach	PWR	29.2	?	$10^3, 10^5$	Air	230	?	65
Pellets	--		0	10.42	No	Air	332 - 454	0	22
Fragments	Pickering	CANDU	8.2	?	No	Air	350 - 420	?	22
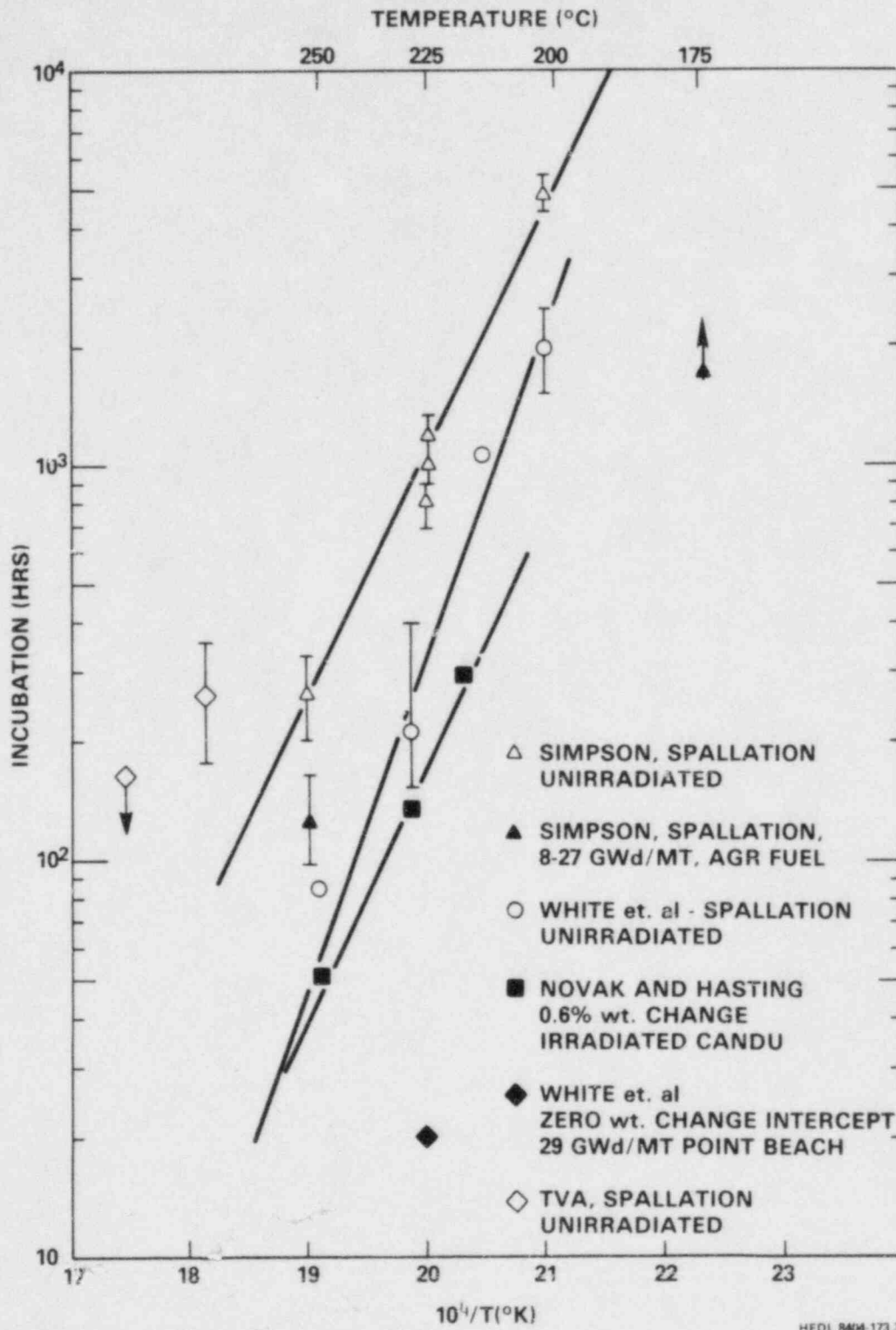
FIGURE 1. Bare Fuel Oxidation Incubation Time.

TABLE 3

DEFECTED RODS OXIDATION EXPERIMENTS

Reactor Name	Type	Burnup (GWd/MTU)	Linear Power (kW/m)	No. of Rods	Type of Defects	Atmosphere	Duration (h)	Temp Range (°C)	No. of Rods in Test Train	Ref.
N/A	CANDU	0	0	7	0.5-mm drill hole 25- x 0.5-mm slit 25- x 1.5-mm slit	Unlimited Air	?	267 - 370	1	22
Pickering	CANDU	8.2	?	3	0.5-mm drill hole 25- x 0.5-mm slit 25- x 1.5-mm slit	Unlimited Air	?	250 - 370	1	22
Pickering	CANDU	7.9	35 - 45	3	1 or 6 0.8-mm drill holes	Unlimited Air	Up to 685	220 - 250	1	66
Bruce	CANDU	7.9	20 - 45	2	1 or 6 0.8-mm drill holes	Unlimited Air	Up to 685	220 - 250	1	66
N/A	CANDU	0	0	4	1 to 6 0.8-mm drill holes	Unlimited Air	Up to 900	230 & 250	1	66
?	BWR	17.2	?	1	1- to 5-cm long natural splits	Replenished Air	2100	325	7	67
?	BWR	23.7	?	1	1- to 8-cm long natural splits	Argon	2100	325	7	67

N/A = Not applicable.
? = Information unavailable.

16

that relative weight changes are not proportional to the number of defects; this indicates that penetration of the air through fuel-cladding gaps and fuel cracks is taking place (Ref. 66). As a result, the fuel surface area and the fuel particulates available for oxidation are very sensitive to defect geometry and are quite uncertain.

While it is difficult to apply bare fuel fragment oxidation results to fuel rods, a number of significant conclusions can be drawn from the rod oxidation studies themselves. Both CANDU studies (Refs. 22&66), in which irradiated and unirradiated rod behavior was compared, indicated that cladding splitting and rod weight gains were taking place at least an order of magnitude faster in the irradiated rod. The only study on BWR fuel (Ref. 67) indicated, by oxygen depletion in the air, that fuel was oxidizing almost immediately at 325°C. All the rods tested at 250°C or above exhibited cladding splitting. Fuel particulate oxidation states ranged from U_3O_7 to U_3O_8. The oxidation to U_3O_8 appeared to be localized since cladding diametral change did not extend very much beyond the cladding crack tip. The CANDU work (Ref. 66) indicated that no cladding splitting took place with less than 2% cladding strain. The incubation period and the rate of cladding splitting both have an Arrhenius temperature behavior with approximately the same activation energies.

IV. TEST DESCRIPTION

A. TEST MATRIX AND ROD SELECTION

Eight rods representing the eight combinations of rod type (BWR or PWR), atmosphere (inert, unlimited air) and rod condition (intact, defected) were tested (see Table 4). Two additional rods were chosen for initial crud analysis.

The H. B. Robinson Unit 2 assembly B05 is well characterized in all aspects (see Figure 2). Generally, characteristics vary little over the cross section of the assembly. Extensive eddy current traces give no indication of any cladding incipient cracks. Based on the characterization in the literature, any of the rods would probably be suitable for the NRC testing purposes. The five rods picked for the test are shown by location in the assembly in Figure 2. Rods that are to remain intact were picked from positions away from control rods and were bounded by well characterized rods. The rod chosen to be cut for initial crud analysis was central to the assembly where it would not receive coolant edge effects. Peach Bottom assembly PH462 had limited characterization (see Figure 3). All the rods underwent eddy current inspection at pool-side. General Electric stated that eddy current inspection showed no incipient crack indications in any rods except those that breached. The lower (12 vs 25 GWd/t) burnup presently attained in the Peach Bottom-II fuel is not of major concern since:

1) Irradiation hardening, yield strength and ultimate strength of the cladding have saturated; hence, additional burnup should not change the mechanical properties of the cladding.

2) Gas release is already higher than would be the case for a modern vintage 8 x 8 rod. Modern pressurized BWR fuel has a gas release of <1% up to 25 GWd/t. The Peach Bottom-II fuel had a gas release of almost 3%. Since the fission product release is approximately proportional to the burnup, considering the volume of the fuel and surface area of the cladding, the Peach Bottom-II rods have an internal fission product concentration that is nearly the same as a pressurized rod from an 8 x 8 assembly.

3) The in-reactor breach of rods is usually associated with power transients, not burnup. The Peach Bottom-II assemblies underwent reactor operations that are unusually severe for BWR assemblies.

Care was taken not to choose tie, spacer, or gadolinium rods for testing. Tie rods and spacer rods, while identical to other rods in fuel configuration, are either too long or too wide for testing purposes. Gadolinium rods are different than normal fuel rods due to a mixture of Gd_2O_3 with the UO_2.

TABLE 4

RODS FOR THE LOW-TEMPERATURE, WHOLE ROD TEST

Reactor Type	Reactor*	Assembly & Rod No.	Rod Condition**	Capsule Atmosphere	Capsule Pressure @ 23°C (psi absolute)
PWR	HBR	B05-08	Intact	Ar + 1% He	15 ± 1
PWR	HBR	B05-G7	Defected	Ar + 1% He	15 ± 1
BWR	PB2	PH462-E5	Intact	Ar + 1% He	15 ± 1
BWR	PB2	PH462-D6	Defected	Ar + 1% He	15 ± 1
PWR	HBR	B05-B8	Intact	Air	15 ± 1
PWR	HBR	B05-E7	Defected	Air	Open capsule with filters
BWR	PB2	PH462-E4	Intact	Air	15 ± 1
BWR	PB2	PH462-E3	Defected	Air	Open capsule with filters
PWR	HBR	B05-J7	Crud	---	---
BWR	PB2	PH462-E6	Crud	---	---

*HBR = H.B. Robinson Unit 2.
 PB2 = Peach Bottom-II.
**Intact = No through-cladding cracks.
 Defected = Will have mechanically machined breach.
 Crud = Rod to be cut for crud examination.

Since Assembly PB-PH462 had in-reactor problems from control rod insertions, test rods were picked from the region of the assembly away from the control rod blade. Since the assembly has multi-zoned enrichment, the test rods were chosen to have the same enrichment as the characterized rods. Within these constraints, eight rods were available. There is no particular justification for the five picked from the group of eight. The positions of the five rods are shown in Figure 3.

The cladding on each of the four fuel rods was defected near the fuel mid-plane and near the top of the fuel column using a 1/32-in. diameter drill. The defect at the fuel centerline of each rod was made first; drilling was

20
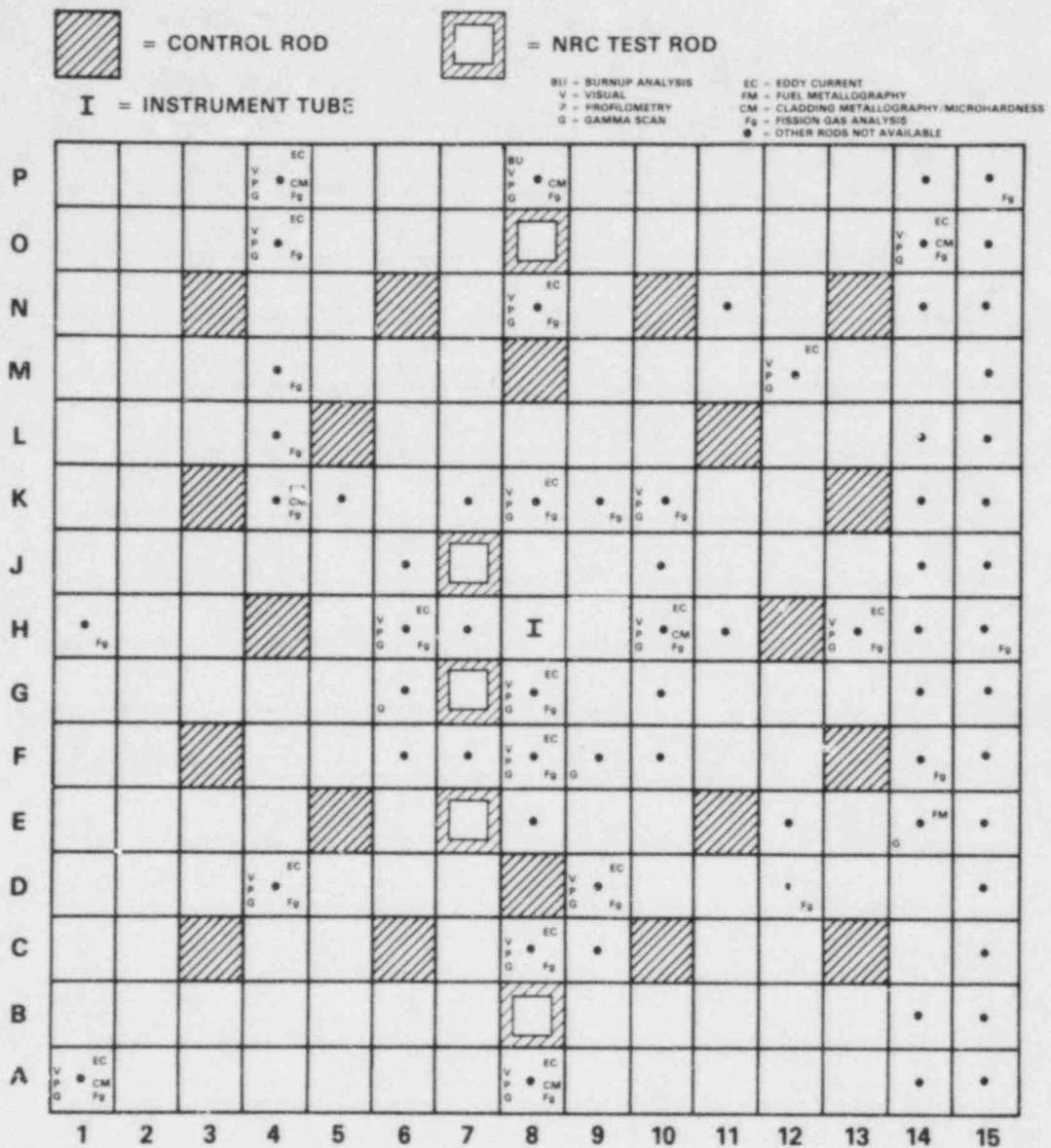
FIGURE 2. Rod Characterization of H. B. Robinson Unit 2 Assembly B05.

CONTROL ROD

	1	2	3	4	5	6	7
G	1.69	1.94	2.93 Gd$_2$O$_3$	2.93	2.93	1.94	1.94
F	1.94	2.93		2.93 FG	2.93 FG	Gd$_2$O$_3$	1.94
E	1.94	2.93	2.93	2.93	2.93	2.93	
D	FAILED MET 1.69	2.93		Gd$_2$O$_3$	2.93	2.93 Gd$_2$O$_3$	2.93
C	1.69	ENLARGED 2.93 Gd$_2$O$_3$	2.93	2.93	2.93 FAILED MET		2.93
B	1.69		2.93	2.93	2.93	2.93	1.94
A	1.33	1.69	1.69	1.94	1.94	1.94	1.69

CONTROL ROD

Gd$_2$O$_3$ - Contains Gd$_2$O$_3$ in the rod
FG   - Fission Gas Analysis.
MET   - Metallography
Bottom number is initial enrichment.
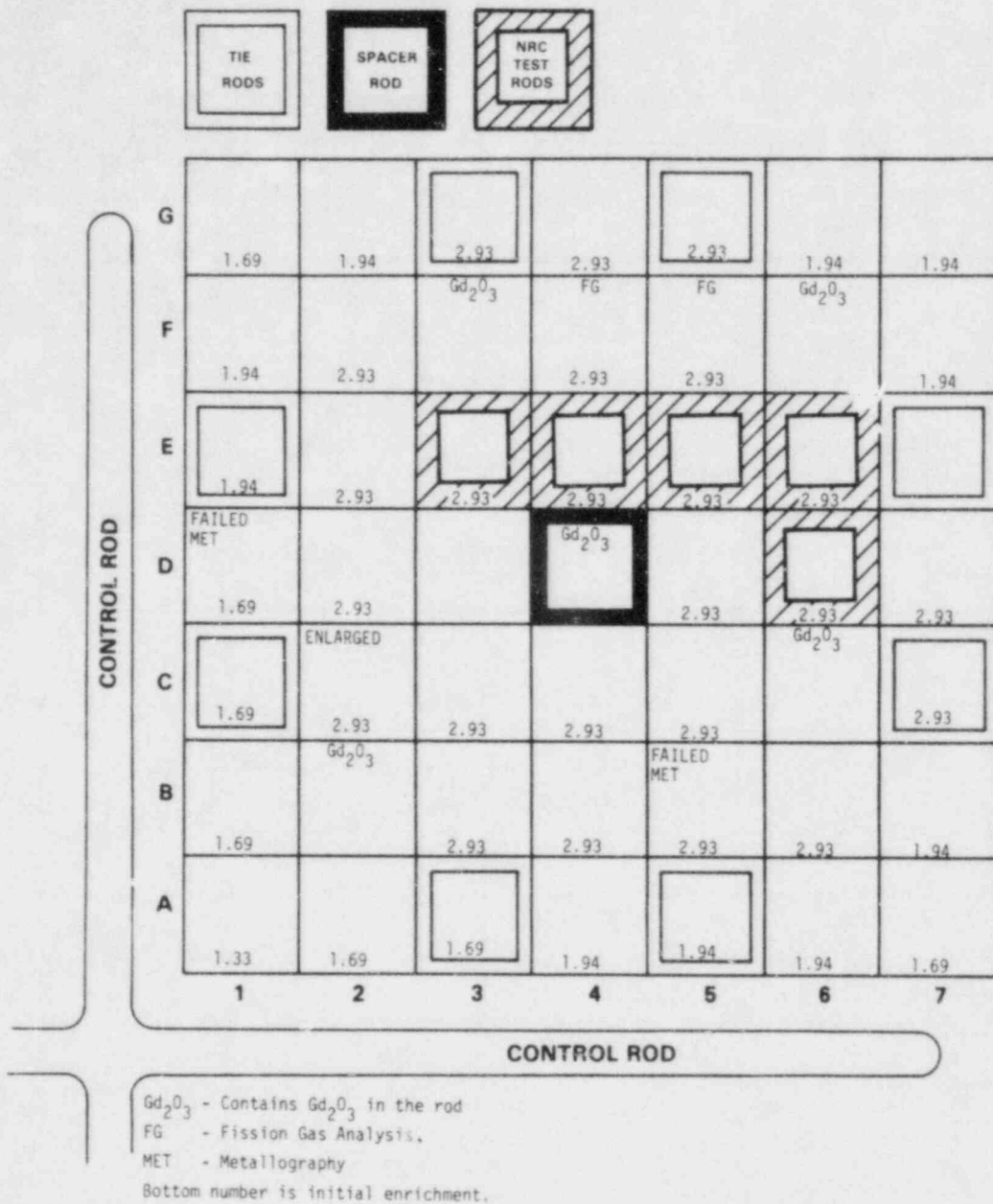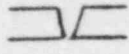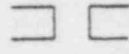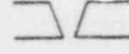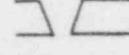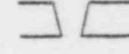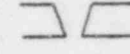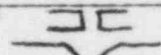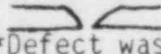
HEDL 8208 154 21

FIGURE 3.   Rod Characterization of Peach Bottom-II Assembly PH462.

22

halted when a positive Kr^{85} signal from the rod plenum gas was detected. Drilling of the second defect in each rod was halted when a change in the resistance to the drill was felt as the fuel pellet was reached. Care was taken not to significantly penetrate the fuel pellet since drill breakage would occur. A summary of the defect locations is shown in Table 5.

TABLE 5

PRETEST ROD DEFECT CHARACTERISTICS

Rod No.	Order of Defect	Distance from Top of Rod (in.)	Defect* Appearance	Confirmation of Opening**	Confirmation Technique
HBR-B05-E7	1	70.5	⊐⊏	Yes	Stack Monitor
HBR-B05-E7***	2	11			
PB-PH462-E3	3	88	⊐ ⊏	Yes	Stack Monitor Photo
PB-PH462-E3	4	22	⊐⊏		
PB-PH462-D6	5	88.5	⊐⊏	Yes	Stack Monitor
PB-PH462-D6	6	20.5	⊐⊏		
HBR-B05-G7	7	81	⊐⊏	Yes	Stack Monitor
HBR-B05-G7	8	11	⊐⊏		

* ⊐⊏ = Complete 31-mil penetration of cladding.
⊐⊏ = <31-mil diameter opening at inside cladding wall.
**Defect was confirmed to be through the wall.
***No pretest photo was taken of this defect.

Due to the taper on the drill bit and the depth of drill penetration, two types of defects were made in the cladding. In the first type, only the tip of the drill taper penetrated the inside cladding wall before drilling ceased due to either a Kr^{85} signal or a change in resistance to the drill. This resulted in a "V" shaped defect with only a small cladding penetration. In the second type of defect, the shank of the drill penetrated the cladding completely, resulting in an effective opening of 31 mil.

23

B. TEST EQUIPMENT

The tests were conducted in a shielded 14-zone, 14-ft long clamshell furnace capable of holding eight encapsulated unmodified LWR fuel rods (see Figure 4). Each rod was placed in a stainless steel capsule, with a 0.690 in. inside diameter, which was used as a test vehicle. The capsules were either sealed with a valve and leak checked (see Table 6) or had two in-line filters connected in series at both ends so the test capsule would be open to the cell atmosphere (see Figure 5). The sealed capsules were welded shut at one end and capped with a Swagelok® valve at the other. They were leak tested by spraying the capsule parts with a stream of gas that could be detected by a leak detector connected to the shutoff valve. Selection of particulate filters was based on observed fuel particle sizes of 8 to 11 μm from ruptured fuel rods. A 15-μm filter was used to catch large particulates and to allow fuel particles similar to those observed by Lorenz to pass through. A 2-μm filter was placed at the exit to collect all the particles that passed through the 15-μm filter. The capsules were placed around an instrument tree containing ten axially located Chromel-Alumel® thermocouples. Comparison of the measurement thermocouples on the instrument tree and the control thermocouples in the furnace zone indicated a 3°C radial temperature gradient with

TABLE 6

CAPSULE LEAK RATES

Capsule No.	Rod No.	Atmosphere	Pretest Rate (cc/s)	1st Interim Rate (cc/s)
1	PB-PH462-E5	Argon	3.4×10^{-7}	N.O.*
2	HBR-B05-G7	Argon	9.1×10^{-7}	1.4×10^{-7}
3	HBR-B05-08	Argon	5×10^{-7}	N.O.
4	PB-PH462-D6	Argon	4.3×10^{-7}	7.4×10^{-7}
5	HBR-B05-B8	Air	2.3×10^{-7}	N.O.
6	PB-PH462-E4	Air	7.9×10^{-3}	N.O.

---

*N.O. = not opened.

®Swagelok is a registered trademark of Crawford Fitting Co., Solon, OH.
®Chromel-Alumel is a registered trademark of Richmond Machine Products Corp., Staten Island, NY.
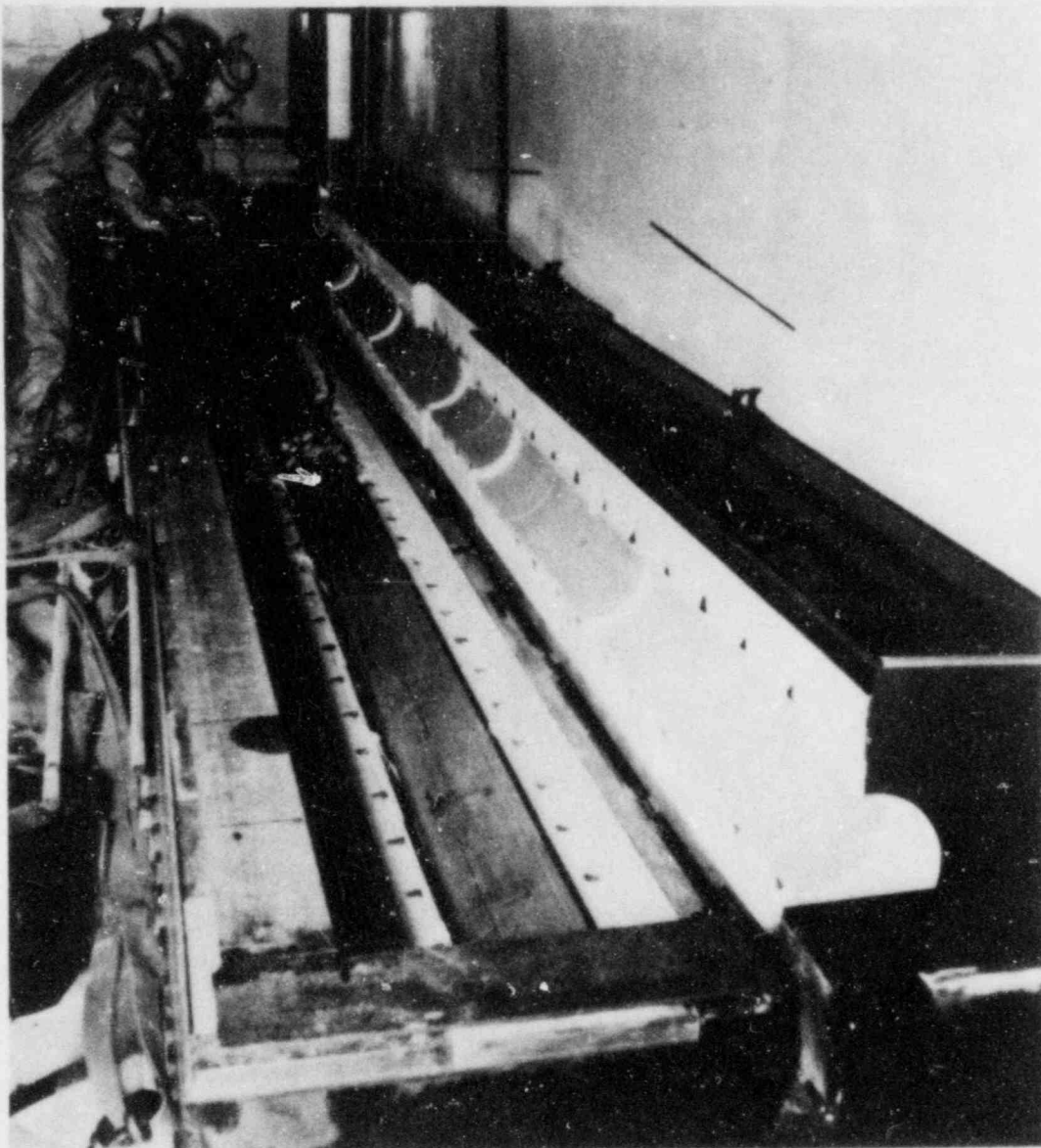
HEDL 8404-173.27

FIGURE 4. Whole Rod Furnace.
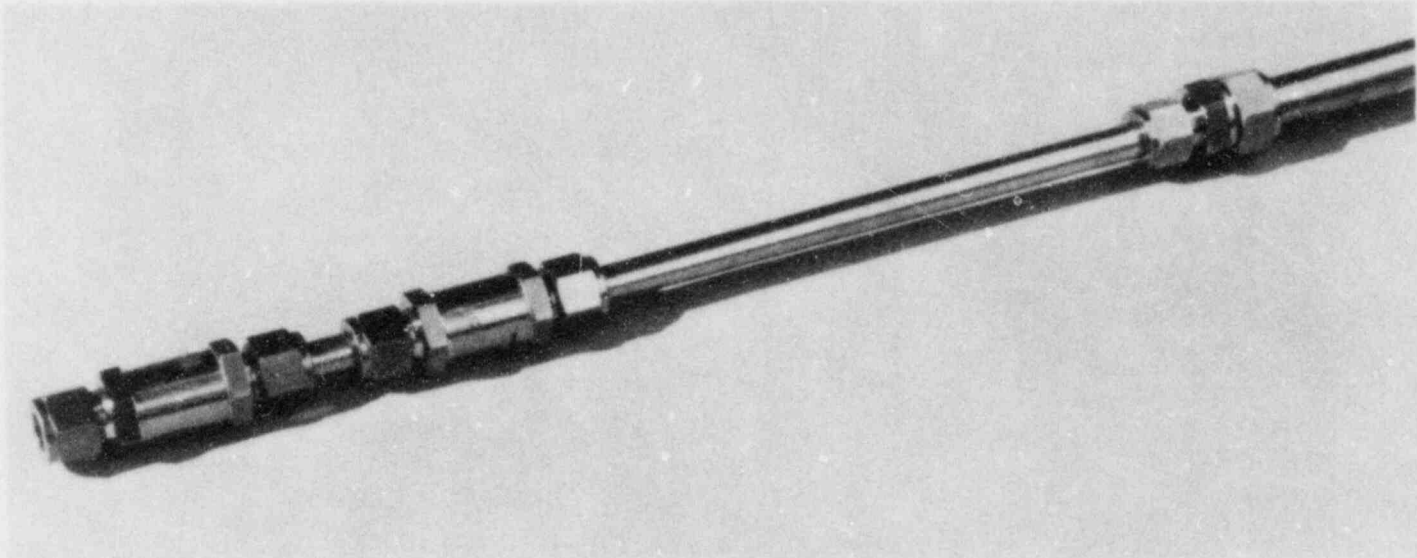
FIGURE 5. Capsule Filter Arrangement.

HEDL 8404-173.28

the center of the furnace being hottest. The axial variation of the hot zone temperature was $\pm 2°C$ with a time variation of $\pm 2°C$. The thermocouples were calibrated against a standard thermocouple and found to be less than 1°C too high. No correction was made for this.

C. TEST CONDITIONS

Four rods were tested in a dry inert atmosphere and four rods in an unlimited cell air atmosphere. The inert atmosphere of ~15 psia of a Ar/1% He mixture was chosen based on leak detection capabilities. The unlimited air tests were divided into two groups: 1) intact rods enclosed in capsules with sufficient air so that the oxygen wouldn't be depleted by cladding oxidation and 2) defected rods in open capsules with filters on both ends. The two intact rods needed to be placed in closed capsules; otherwise there was no way of detecting a breach. As calculated (Ref. 69), even at an upper test temperature of 250°C, only ~1 atm of air is needed to accommodate cladding oxidation in the closed air capsule without significantly depleting the oxygen.

It was desirable to operate the test at the highest possible temperature yet have some assurance that the UO_2 will not convert to U_3O_8 during the test. As indicated in Section III, UO_2 was thought to convert to U_3O_8 above $250 \pm 10°C$. Below this temperature, UO_2 was thought to convert to U_3O_7. Errors on the temperature-controlling system were: controllers ($\pm 5°C$), thermocouples ($\pm 2.5°C$) and zero point condensators ($\pm 0.5°C$). Combining these possible temperature errors with a lower bound on the U_3O_8 formation temperature led to a test temperature of 230°C.

The test was brought to temperature over a 12-hour period, and other than power outages, ran continuously until terminated for interim examinations. The furnace cooled down at an initial rate of 5°C per hour. The test was operated at $229 \pm 1°C$ for 2235 hours, at which time the first interim examination took place. After the examination, the test ran an additional 3727 hours for a total of 5962 hours before a second interim examination. During this interim examination, the tests indicated in Table 7 were conducted. Heatup and cooldown times were not included when determining the time at temperature.

D. FUEL ROD CHARACTERIZATION

Normal pretest procedure is to nondestructively characterize those rods actually being tested and to destructively characterize companion rods from the same assembly. For the present test, as many existing data as possible were used to establish the test rod condition without actual test rod characterization. An overall view of the available characterization of fuel rods and the relationship between characterized rods and actual test rods with the

27

TABLE 7

INTERIM FUEL ROD EXAMINATIONS

Rod No.	Orig Atmos-phere	Analysis			Visual Exam	Cladding Strain	Defect Size	Gamma Scan	Metal-lography	Micro-Hardness	Cera-mography	Fuel X-Ray Dif-fraction
		Capsule Gas	Filter	Swab								
HBR-B05-E7	Air		1,2	1,2	1,2	1,2	1,2	2				
PB-PH462-E3	Air		1,2	1,2	1,2	1,2	1,2	2	2	2	2	2
PB-PH462-D6	Argon	1,2		2	1,2	2	2	2				
HBR-B05-G7	Argon	1,2			1							
PB-PH462-E5	Argon	2		2	2	2		2				
HBR-B05-08	Argon	2										
HBR-B05-B8	.ir	2										
PB-PH462-E4	Air	2										

1 = 2235-hour examination.
2 = 5962-hour examination.

28

assemblies is given in Figures 2 and 3 and Table 8. The only pretest characterization conducted on the test rods was a visual examination. It is obvious that the H. B. Robinson Unit 2 fuel is characterized much more extensively than the Peach Bottom-II fuel. In fact, the H. B. Robinson Unit 2 fuel is characterized as well as any assembly that has been examined. This section only summarizes the pretest characterization; complete details are found in Refs. 38 and 70.

Nondestructive examinations (NDE) are conducted much more often (see Table 8) than destructive examinations (DE) for several reasons: 1) they are significantly less expensive, 2) many times they can be conducted at poolside, and 3) it can be used to detect reactor breaches and other rod changes (such as bowing, growth and creepdown) that affect reactor operations. In the reactor industry, NDE usually refers to eddy current (EC) and/or ultrasonic examination; sometimes visual, gamma scan and profilometry are also included. In a hot cell, complete NDE includes all the above tests. DE is most useful when looking for small changes in properties, verifying or determining reactor operating conditions (such as burnup) or obtaining input for mechanistic modeling codes. To measure changes, companion rods are usually destructively examined prior to testing. Test rods are examined after testing is complete. By its very nature, DE can only be done once; therefore, if more than an average rate for a phenomenological occurrance is desired, multiple duplicate experiments must be run. However, an advantage of DE techniques is their sensitivity to material conditions as compared to NDE.

1. Peach Bottom-II BWR Rods

The Philadelphia Electric Company's Peach Bottom Unit-II is a 1065-MW electric BWR located at Peach Bottom, Pennsylvania. It began commercial operation in July 1974. The core contains 764 General Electric (GE) assemblies. During the first cycle of operation, the core contained assemblies with average enrichments of either 1.10 wt% or 2.50 wt%. The burnup of each assembly was not precisely defined. The reported average assembly burnup was 11,900 MWd/t (Ref. 72). The reported average core burnup was 10,100 MWd/t (Ref. 72). The official GE average assembly burnup was 12,890 MWd/t. The power peaked at ~240 W/cm and was within 5% of that power level except for a month at the start of the run and three months near the end of the run when it dropped as low as 120 W/cm. Assembly PB-PH462 selected for this study is an improved-design 7 x 7 grid, which has a moisture getter in the plenum region (Ref. 72). The assembly was discharged from the reactor during the refueling outage between March 27 and June 24, 1976 due to rod failures associated with control rod manipulations (Ref. 73). In April 1977 the fuel assembly was shipped without incident from Peach Bottom-II to EG&G in a National Lead Industries dry shipment cask (Ref. 72). An extensive reactor description is given in Ref. 71.

The 49 rods, including 5 Gd_2O_3 rods for control improvement, 8 tie rods and 1 spacer rod, were held in the assembly with the assistance of 7 grid spacers.

29

TABLE 8

SUMMARY OF EXAMINATIONS CONDUCTED ON FUEL FROM
ASSEMBLIES HBR-B05 AND PB-PH462

Reactor Assembly	Fuel Rod Examinations	No. of Tests
HBR-B05	Nondestructive Examination	
	Visual	24
	Eddy Current	18
	Profilometry	18
	Gamma-Scan	22
	Destructive Examination	
	Fission Gas Analysis	26
	Burnup Analysis	2
	Fuel Ceramography	3
	Cladding Metallography	7
PB-PH462	Nondestructive Examination	
	Visual	8
	Eddy Current	49
	Destructive Examination	
	Fission Gas Analysis	2
	Cladding Metallography	2

The variation of initial enrichment within the assembly and the location of the different types of rods are shown in Figure 4. Note the orientation of the assembly with respect to the control rod blade, since the configuration is not symmetrical. The typical rod consists of sintered UO_2 pellets within a Zircaloy-2 sheath. The pellets are held in place by a spring in the plenum region that contains the moisture getter. The pellet length is proprietary but appears from PIE to be approximately equal to the diameter (Ref. 72). The rods were initially filled with between 1 and 10 psig of helium.

a. Nondestructive Examination

There were few visual differences between any of the Peach Bottom rods.
There were water marks and scratches at sporadic locations along the rods.
The top third had a very uniform, apparently thick crud layer. The center
third had some pitting in the thinner crud. The bottom third had thick,
pitted and nonuniform crud. In addition, between 150 in. and 160 in. from
the top, the deposits were reddish brown or bright red in color compared to
the variety of grays on the remainder of the rod. Representative photos at
the 20-in. and 148-in. levels from Rod PB-PH462-E9 show the variation in the
rod coating (Figure 6). All the rods from the assembly were examined by
eddy current (EC) at the Peach Bottom-II pool (Ref. 72). All rods had no
EC-indicated defects except for two breached rods and one "possible" breached
rod (see Figure 3). A letter detailing the methods, the standards, and the
results of this unpublished work is provided in Ref. 70. No pretest gamma
scans or profilometry was conducted on rods from this assembly.

b. Destructive Examination

Gas analyses were made in other projects on Rods PH-462-F4 and -F5. There
was an average void volume of ~73 cc, an average gas volume at STP of 127 cc
and a gas pressure of 25.2 psia. The high fission gas release of 2.94% at
this fairly low burnup is not unexpected. Unpressurized fuel tends to have
greater gas release than pressurized fuel (Ref. 74) due to the lower thermal
conductivity across the fuel-cladding gap. Pressurized BWR fuel would have
gas releases lower than 1% up to approximately the current burnup limits of
25 GWd/MTM. The molecular composition is ~40% fission gas, which is not
surprising since the rods were not pressurized.

Rods PH462-B5 and -D1 were metallographically studied in other projects.
The inner 40% of the cladding wall has radial hydrides, and the outer 60%
has circumferential hydrides. This is in contrast to the H. B. Robinson
Unit 2 rods, which had only circumferential hydrides. The radial hydrides
that weaken the cladding (Ref. 24) could be caused either by the particular
texture introduced during the manufacturing process or by excessive cladding
stress (Ref. 27) during operation. This hydride distribution may not be
typical of BWR rod cladding. In contrast to the H. B. Robinson Unit 2 rods
that showed a smooth uniform oxide layer, the outer oxide on the Peach
Bottom-II rods was nodular. The inner surface oxide was uniform. Oxide
thicknesses are ~0.4 mil on the ID and range up to a maximum of 1.3 mil on
the OD surface (Ref. 72). Since these samples were near the bottom of the
rod, the oxide thicknesses are significantly greater than those found on the
H. B. Robinson Unit 2 rods. Ceramographic studies of the fuel from the area
near the breaches in Rods PH462-D1 and -B5 have been conducted (Ref. 72).
Even though the examination is exhaustive with information on grain size,
void volume and pellet cracking, the information may not be representative
of the fuel structure in an unfailed rod since both PH462-D1 and -B5 failed
in-reactor.

31
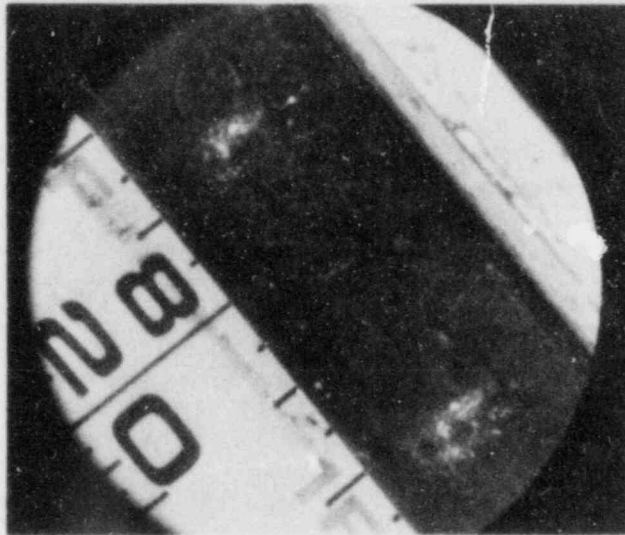
(a) **20**-in. ELEVATION FROM TOP OF ROD SHOWING UNIFORM ROD SURFACE COATING.
(SCRATCHES ~1 in. APART WERE FOUND AT GRID SPACER LOCATIONS.)
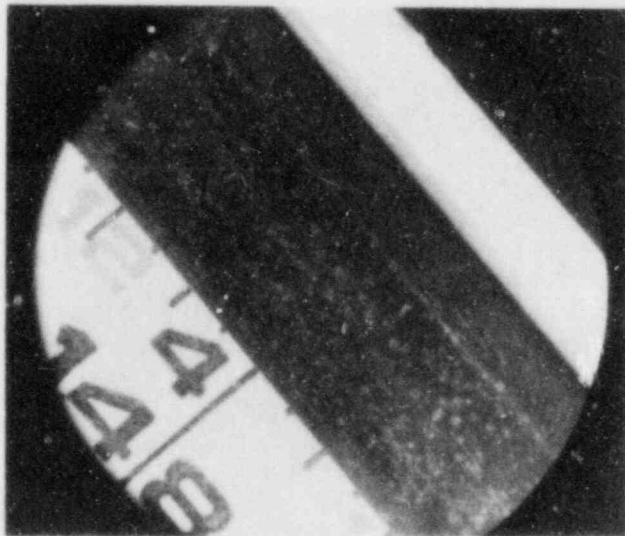
(b) **148**-in. ELEVATION FROM TOP OF ROD SHOWING POX-MARKED APPEARANCE OF ROD
SURFACE COATING.

HEDL 8304-056.13

FIGURE 6. Pretest Visual Examination of Peach Bottom Rod PH462-E9.

2. H. B. Robinson Unit 2 PWR Rods

The Carolina Power and Light Company's H. B. Robinson Unit 2 reactor is a 665-MW electric (2192-MWt) three-loop LWR located in Hartsville, SC. It began operation in March 1971 (Refs. 75&76). The core consists of 157 Westinghouse 15 x 15 assemblies with three enrichment zones (Ref. 76). Each assembly contains 204 fuel rods, 20 control rods and 1 possible in-core instrumentation tube. The rods are held in place with seven grids per assembly.

Assembly HBR-B05 was irradiated in the H. B. Robinson Unit 2 core during Cycles 1 and 2 for a total of 799 effective full power days (EFPD), then removed from the reactor on May 6, 1974. The peak power (327 W/cm) occurred in December 1971 shortly after irradiation began. By the end of irradiation in May 1974, the power had dropped to 212 W/cm.

During transportation of the H. B. Robinson Unit 2 assembly from the reactor to the hot cell and subsequent unloading of the cask, a series of events may have caused the assembly to overheat. As standard procedure, 25 gallons of water were drained from the transportation cask to allow for thermal expansion. As a result, the assembly was transported partially uncovered in a horizontal position. When the cask arrived at the hot cell, it was placed in a vertical position where it was also partially uncovered. After removal from the cask, the assembly was held in air before it was placed in the pool. When placed in the pool, large amounts of steam formed and an alarm sounded -- possibly due to the release of crud from the rod surfaces (Ref. 77). Later the assembly was held in a horizontal position for 7 hours during rod removal, but no steam was released when the assembly was put back into the pool (Ref. 77).

Although Assembly HBR-B05 may have experienced a temperature excursion during transportation, tests and calculations indicate that it was not long enough nor high enough to significantly change the condition of the fuel rods. A complete analysis of the temperature excursion is given in Ref. 70.

a. Nondestructive Examination

In general, the five H. B. Robinson test rods that were previously examined differed little in appearance. Water marks and small scratches were seen at sporadic locations on the rods. The top 20 in. of the rods showed a heavy crud layer that appeared to be flaky (see Figure 7). The rods looked very clean from the 20-in. to 120-in. level. As one traversed further down a rod, a thin adherent patchy layer (see Figure 8) became more apparent on the rod. The test rods did not differ from the other rods in the assembly that were examined in other programs (Refs. 78&79). A complete visual description is given in Ref. 38.
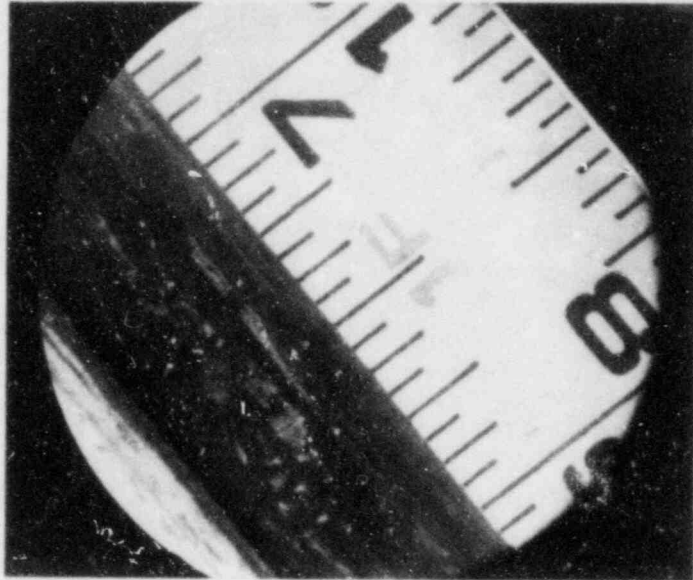
FIGURE 7.   Flaky Crud at 18.5 in. from Top of Rod HBR-B05-E7.
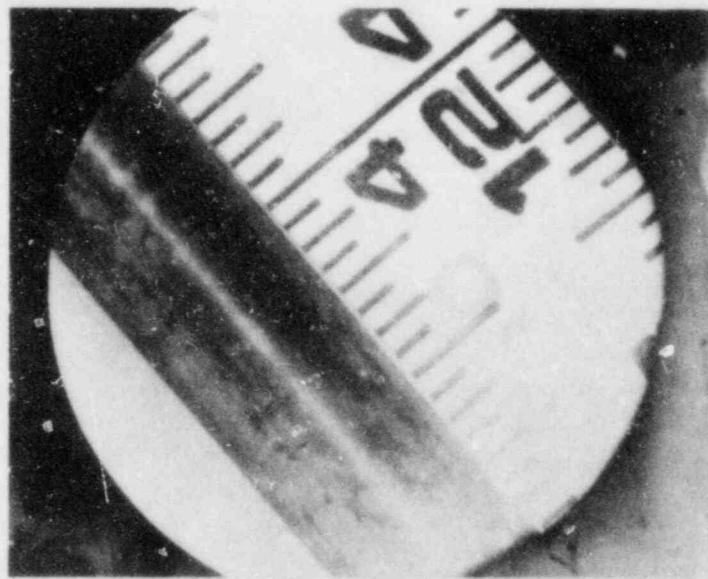
FIGURE 8.   Thin Adherent Crud Layer at 124 in. from Top of Rod HBR-B05-B8.

Eighteen rods were profilometered at BCL (Refs. 79-81). The main findings were the diameters, the ovality and the location of maximum ovality. No test rods were profilometered prior to testing. All the profiles can be bounded by a curve of $D \pm 1$ mil, where D is the average axially dependent diameter. There is no reason to believe that the test rods are not within this bound. No ridging indications were found.

Axial gamma scans were run on 22 rods or parts of rods (Refs. 79,80,82-84). No test rods were pretest gamma-scanned. Discounting the dips in the traces where the structural members changed the fluence, the profiles were very flat over the central 8 ft. The pellet stack height was very uniform at 143.5 ± 0.4 in. and contains, on the average, 6 ± 3 large pellet-to-pellet gaps.

Eighteen rods were EC-scanned at BCL (Refs. 78&79). Indications were found on four rods: B05-P4, -04, -N8 and -K10. Only Rod B05-04 had a completely uncorrelated indication, and only Rod B05-P4 was thought to exhibit any type of defect (Ref. 78). No test rods were EC-scanned.

2. Destructive Examination

Gas analysis was conducted on 28 rods at BCL (Refs. 79-81), EG&G (Ref. 76) and ORNL (Ref. 68&85). The average void volume of 24.7 ± 1.5 cc in the H. B. Robinson Unit 2 rods agrees well within a standard deviation with the void volume of 22.8 ± 1.2 cc measured for the Turkey Point fuel (Ref. 12). The internal pressure (220 ± 14 psia) for the H. B. Robinson Unit 2 rods is ∿70% lower than the internal pressure (373 ± 25 psia) in the Turkey Point rods. This is due to a lower preirradiation gas fill volume (528 ± 20 cc for Turkey Point vs 370 ± 10 cc for H. B. Robinson Unit 2). The fission gas release for both types of fuel were within one standard deviation (0.27 ± 0.08 for Turkey Point vs 0.21 ± 0.05 for H. B. Robinson Unit 2) (Ref. 8). Only Rod B05-H6, has gas volume and hence gas pressure significantly lower than a standard deviation for the average. The reference gives no indication as to whether there was an apparatus problem with this measurement. There is no systematic positional variation within the assembly, indicating that average values should be suitable as initial pretest conditions for the present test. Complete gas analyses data are given in Ref. 70.

Metallography was previously done along the length of Rods B05-K4 (Ref. 76) and B05-014 (Ref. 78). Rod B05-K4 showed hydrides that were primarily circumferentially oriented. Exterior and interior cladding oxide was measured on both rods. The oxide in both cases was very uniform. No globular oxidation was observed. The oxide thickness increased with increasing distance up the rod, which is to be expected due to the coolant axial temperature gradient. The exterior oxide layer showed no azimuthal dependence (Ref. 86). Rod B05-K4 had a slightly thinner oxide layer than Rod B05-014, but the data are not sufficient to determine if this difference is significant. The internal oxide layer is also slightly thinner than the external oxide layer.

Microhardness measurements (Ref. 80) were taken at a number of locations that adequately represent the assembly. There is no statistically significant variation in the measurement results among the rods or along the length of the rods (Ref. 78). The hardness was 250 ± 10 kHN. For comparison, Turkey Point fuel, also made by Westinghouse [operated to almost the same burnup (28.5 GWd/MTM) at nearly the same average power level (182 W/cm) and discharged from the reactor at nearly the same time (November 1975)] had a cladding hardness of 274 ± 30 kHN as-irradiated and 190 ± 15 when annealed at 482°C (Refs. 8&12).

Tensile specimens were tested over a range of temperatures (Refs. 80&81). The strength decreases linearly from 80° to 700°F while the ductility remains essentially constant.

Ceramographic examination of the H. B. Robinson Unit 2 fuel assembly (B05-K4 between the 2.26-m and 3.51-m elevations and B05-F7 between the 0.05-m and 0.89-m elevations) was conducted at both EG&G (Ref. 76) and ANL (Refs. 82&87). The pellet is cracked in the radial direction with usually between 4 and 13 fragments formed in a cross section. The one longitudinal sample, which was 2 diameters long, had twice as many fragments; therefore, ~16 to 170 fragments formed per pellet diameter (Ref. 75) of fuel volume. The length and width of the major cracks were also measured. The measured area from the cracks was compared to the measured area from the fuel pellet-to-cladding gap. Except at the 3.27-m elevation, the cracks provide a larger cross-section area for flow of gas through the rod than through the gap. The large cross section for gas flow would indicate that a grossly breached rod stored in air may have its full column exposed to the oxidizing atmosphere.

From the 2.26-m to 3.51-m elevations, little grain growth occurred. Average fuel grain size varied from 7 μm in the peak power range (2.26 m) to 4 μm near the top of the rod (Ref. 76). At the 0.89-m elevation, the grain size had a radial gradient with a mean diameter of ~6 μm in the central region and ~3 μm near the outer surface (Ref. 82). The porosity at the 3.52-m elevation is very similar to that at the 0.89-m elevation. The coarse porosity ranges from 30 to 250 m in diameter and occupies a volume fraction of 0.03 (Ref. 82).

Both PNL (Refs. 88&89) and LANL (Ref. 90) conducted radial microprobe measurements on unidentified fragments of H. B. Robinson Unit 2 fuel. Other than Pu and Ru, no elements showed radial gradients. The Pu concentration is ~70% higher on the surface, which can be probably attributed to its mode of formation; fissionable plutonium preferentially forms near the outer surface of the fuel pellet due to resonance absorption of thermal neutrons by ^{238}U. No reason has been postulated for the higher ruthenium concentration near the surface.

V. RESULTS

After 2235 hours and again after 5962 hours cumulative time at temperature, the test was stopped for interim examinations. These fall into three categories: capsule examinations, nondestructive rod examinations and destructive fuel examinations. The examinations conducted on each capsule or rod are listed in Table 7.

A. CAPSULE EXAMINATIONS

These examinations include capsule gas analysis, smearing the inside of the capsules and analyzing the particulates trapped on the filters. The results will help answer these questions:

- . Have any rods failed?
- . Has crud spalled from the rods?
- . Has fuel particulate spilled from the defect?
- . Have radionuclides migrated from the defect?

1. Gas Analysis

The valved end of each sealed capsule was connected to a gas collection bottle. Prior to the valve being opened, the connection line was evacuated to 10^{-4} torr. After opening the valve, the capsule gas was pumped into the evacuated collection bottle. The contents of the bottle were then analyzed with a mass spectrometer. No measurements were made of the volume of gas or the internal pressure of the capsule.

Due to faulty equipment, no meaningful gas analyses were obtained during the 2235-hour examination. The results of the 5962-hour examination are given in Table 10. No Kr or Xe was found in the capsules containing intact rods, indicating that none of the intact rods breached during the test. Capsules 1 and 3 were supposed to be filled with argon but had an air analysis. Capsule 1 was probably filled with the wrong gas. The misfill of Capsule 1 means that it is essentially a duplicate of the test in Capsule 6. A very small volume of gas was collected from Capsule 3, indicating that the valve leaked and that the capsule was being pumped out at the same time that the connection line was being evacuated. Whether the air was in the capsule during the test or in the connection line cannot be determined. If the air leaked into the capsule during the test, then Capsule 3 is a duplicate of Capsule 5.

37

TABLE 9

TEST ROD CHARACTERISTICS

	H. B. Robinson Unit 2	Peach Bottom-II
Assembly Type	15 x 15 PWR	7 x 7 BWR
Power Range (W/cm)	212 - 327	∿240
Peak Burnup (GWd/MTU)	30.9	11.9
Date Removed from Reactor	May 1974	March 1976
Fuel Enrichment (wt%)	2.55	2.93
Fuel Density (%TD)	92	95
Cladding Material	Zircaloy-4	Zircaloy-2
Cladding Thickness (mm)	0.62	0.94
Postirradiation Rod Diameter (mm)	10.64	14.30
Average Postirradiation Plenum Gas Pressure (psia)	220 ± 14	25 ± 2
Average Fission Gas Release (%)	0.21 ± 0.05	2.94

Capsule 2, which was filled with argon, contained 50% air at the end of the test. The elapsed time since the gas was purged at the first interim was 3727 hours. At a leak rate of 1.4×10^{-7} cc/s (see Table 10), only 2 cc of gas should have leaked into the capsule. Since the capsule contained ∿632 cc of gas (Ref. 69), a leaky capsule should not have caused the air contamination. The contamination probably occurred due to an insufficiently evacuated line connecting the capsule to the gas sampling bottle. This is consistent with the nitrogen-to-oxygen ratio of ∿4. Since Capsule 2 contained a breached rod, one would have expected a depletion of the O_2 (i.e., an increase in the N_2/O_2 ratio) if the ingress of air occurred during the test.

Such an oxygen depletion relative to nitrogen was found in Capsule 4, which also had the fission gases Kr and Xe in the gas inventory. The capsule had not been opened since the test started, i.e,. 3727 hours and had a leak rate of 7.4×10^{-7} cc/s. This corresponds to a leak of 9.9 cc or ∿3.1% air in the capsule based on a minimal capsule volume of 326 cc (Ref. 69). This agrees with the 3% N_2 found in the capsule sample after accounting for oxygen depletion. At one atmosphere, 326 cc of gas corresponds to 1.34×10^{-2} moles. If

TABLE 10

CAPSULE GAS ANALYSIS AFTER 5962 HOURS

Rod	Capsule No.	Rod Condition	Initial Atmosphere	Composition (vol%)								
				H_2	He	N_2	O_2	Ar	CO_2	Organic	Kr	Xe
PB-PH462-E5	1	Intact	Ar/1% He	<0.01	<0.01	78.3	20.7	0.93	0.09	--*	--	--
HBR-B05-G7	2	Defected	Ar/1% He	0.15	0.14	39.2	10.2	50.2	0.08	~0.09	--	--
HBR-B05-08	3	Intact	Ar/1% He	0.02	<0.01	79.2	19.5	0.97	0.29	--	--	--
PB-PH462-D6	4	Defected	Ar/1% He	0.08	0.90	2.4	0.01	96.5	0.02	~0.09	0.005	0.04
HBR-B05-B8	5	Intact	Air	<0.01	<0.01	78.6	19.8	0.92	0.65	--	--	--
PB-PH462-E4	6	Intact	Air	<0.01	<0.01	79.2	18.4	0.86	1.5	--	--	--

*-- Not detected.

3% of this gas was air, of which 20% was the oxygen that was consumed, then $\sim 8.0 \times 10^{-5}$ moles of oxygen was depleted. Because we are not sure whether UO_2 oxidizes to U_3O_7 or U_3O_8, one mole of O_2 can oxidize between 3 and 6 moles of UO_2. This corresponds to between 3 and 6 mil of the fuel column or 3 to 6 x 10^{-3} % of the fuel being oxidized. This small amount of oxidation, if it was present, could not be visually detected. During irradiation, ~ 1650 cc of fission gas were produced (Ref. 70). If we assume that the gas release is proportional to the amount of fuel being oxidized, then between 5×10^{-2} and 0.1 cc of gas should have been released. Of the 326 cc of gas collected, 0.045% was fission gas. This corresponds to 0.15 cc, which is close to the 0.1 cc one would expect due to oxidation of the fuel.

2. Filter Analysis

Each of the open capsules was terminated in a series of in-line sintered filters. A 15-μm pore filter was on the inside, and a 2-μm pore filter was on the outside. Fresh filters were put in place each time the capsule was opened. The filters used in the second 3727-hour duration test were weighed before and after testing to see if there was a noticable weight gain due to particulate accumulation. The results are given in Table 11. Even though the same balance was used for both weighings, no weight gains were measured. The negative weight changes in Table 11 are insignificant and are thought to result from balance drift.

TABLE 11

PRE- AND POSTWEIGHTS ON FILTERS USED
DURING SECOND (3727-HOUR) RUN

Filter No.	Size (μm)	Preweight* (g)	Postweights** (g)	Δ (g)
7E	15	120.0376	120.0339	-0.0037
7G	2	121.1048	121.1032	-0.0016
7F	15	119.9391	119.9340	-0.0051
7H	2	121.8607	121.8586	-0.0021
8E	15	120.6483	120.6393	-0.0090
8G	2	121.8205	121.8175	-0.0030
8F	15	120.8530	120.8509	-0.0021
8H	2	121.1264	121.1216	-0.0048

*One weighing.
**Average of 3 weighings.

40

Because Rod HBR-B05-E7 showed no signs of fuel oxidation in comparison to Rod PB-PH462-E3, the filters from Capsule 7 were flow tested to make sure that air was reaching the rod. Filters 7E and 7G and Filters 7F and 7H were tested in pairs. A flow of dry air was applied to the inlet of each filter containment capsule and the outlet flow of air bubbles in a beaker of water was visually observed. Neither filter set indicated blockage, and both sets had similar flows.

The filters were gamma spectrum analyzed, then activated for delayed neutron (DN) counting. The samples were analyzed as point sources with geometrical correction. The DN counter was calibrated against soil and pitchblende standards. Results are shown in Table 12 and Figure 9. After the first (2235-hour) test at 229°C, activity was found on only four of the filters, and no fissile material was detected. After the second (3727-hour) test, all the filters had some isotope and fissile particulate accumulation. As seen in Figure 9 no relationship between the filter pore size and the accumulation of material is apparent.

3.   Smear Analysis

The insides of the capsules were smeared to gather the crud that had spalled and any loose fuel particulate. The smears were either a tight bundle of cotton tipped swabs (2235 hours) or a trimmed gun barrel swab (5962 hours). The smears were fitted so that they contacted the complete inside wall of the capsule. After the rod was removed, the smear was pushed through the capsule and collected at the other end in a plastic bag. During the time when each smear was being executed, a control swab was left exposed to the cell atmosphere to gather any activity that might be airborne.

The capsules that were smeared and the smears that were analyzed are indicated in Table 13. DN analyses was not conducted on the controls due to a lack of activity indicated by the γ-scans. Since the weight gains and activity in the controls were much lower than on the capsule smears, the analyses of the control smears for each interim examination were averaged.

After 2235 hours, the activity of the loose material in the capsules was predominantly ^{60}Co, indicative of crud spallation (Table 14). The predominant fission product was ^{137}Cs, which migrated out of the artificial defects. Both rods indicated that some fissile material had come out of the defects; but the amount for the H. B. Robinson rod, which did not split the defect, was near the resolution limit and approximately an order of magnitude less than the fissile material from the open split in PB-PH462-E3.

High activity and contamination problems limited usefulness of the 5962-hour smear data. Problems with the bagging procedure when the first capsule (containing Rod PB-PH462-E3) was smeared led to contamination of the hot cell floor with a large portion of the loose material that was in the capsule. Even so, the resultant smear was too hot to be analyzed in its entirety.

41

TABLE 12

FILTER ANALYSIS FROM CAPSULES USED TO TEST DEFECTED RODS AT 229°C IN AIR ATMOSPHERE

Rod	Filter No.	Size (μm)	Isotope Analysis (μCi)*				Fissile** Analysis ^{234}U (μg)
			^{134}Cs	^{137}Cs	^{54}Mn	^{60}Co	
			2235 h at Temperature for Rods 2235 h at Temperature for Filters				
HBR-B05-E7	7G	2	$1.2 \pm 0.2 \times 10^{-5}$	$2.1 \pm 0.4 \times 10^{-4}$	---	$3.1 \pm 0.6 \times 10^{-4}$	---
HBR-B05-E7	7E	15	---	---	---	$5.1 \pm 1.0 \times 10^{-5}$	---
PB-PH462-E3	8G	2	---	$3.0 \pm 0.6 \times 10^{-5}$	$1.5 \pm 0.6 \times 10^{-5}$	$4.7 \pm 1.0 \times 10^{-4}$	---
PB-PH462-E3	8E	15	---	---	---	$2.0 \pm 0.4 \times 10^{-5}$	---
			5962 h at Temperature for Rods 3727 h at Temperature for Filters				
HBR-B05-E7	7E	15	---	$3.3 \pm 1.3 \times 10^{-5}$	---	$2.7 \pm 1.1 \times 10^{-5}$	$0.0078 \pm 30\%$
HBR-B05-E7	7G	2	---	$9.7 \pm 2.2 \times 10^{-5}$	---	$1.0 \pm 0.3 \times 10^{-4}$	$0.0947 \pm 5.4\%$
HBR-B05-E7	7F	15	---	---	---	$1.1 \pm 0.1 \times 10^{-3}$	$0.136 \pm 4.8\%$
HBR-B05-E7	7H	2	---	$4.9 \pm 1.6 \times 10^{-5}$	---	$1.3 \pm 0.4 \times 10^{-4}$	$0.0527 \pm 7\%$
PB-PH462-E3	8E	15	---	---	---	$4.3 \pm 0.7 \times 10^{-4}$	$0.138 \pm 5\%$
PB-PH462-E3	8G	2	---	$5.4 \pm 0.2 \times 10^{-5}$	---	$1.9 \pm 0.1 \times 10^{-3}$	$0.0615 \pm 7\%$
PB-PH462-E3	8F	15	---	$4.6 \pm 1.6 \times 10^{-5}$	---	$2.0 \pm 0.9 \times 10^{-5}$	$0.0226 \pm 12\%$
PB-PH462-E3	8H	2	$6.0 \pm 0.6 \times 10^{-4}$	$1.11 \pm 0.02 \times 10^{-2}$	---	$4.2 \pm 0.2 \times 10^{-3}$	$0.0069 \pm 34\%$

*Errors based on 2σ counting statistics and not including errors for a non-point-source configuration.
**Error based on 1σ counting statistics and uncertainty in calibration coefficient.

42

7G ^{2}	7E ^{15}	H.B. ROBINSON	7F ^{15}	7H ^{2}
$1.0 \pm 0.3 \times 10^{-4}$	$2.7 \pm 1.1 \times 10^{-5}$	^{60}Co	$1.1 \pm 0.1 \times 10^{-3}$	$1.3 \pm 0.4 \times 10^{-4}$
$9.7 \pm 2.2 \times 10^{-5}$	$3.3 \pm 1.3 \times 10^{-5}$	^{137}Cs	---	$4.9 \pm 1.6 \times 10^{-5}$
0.0947	0.0078	^{235}U (μg)	0.136	0.0527

8G ^{2}	8E ^{15}	PEACH BOTTOM	8F ^{15}	8H ^{2}
$1.9 \pm 0.1 \times 10^{-3}$	$4.3 \pm 0.7 \times 10^{-4}$	^{60}Co	$2.0 \pm 0.9 \times 10^{-5}$	$4.2 \pm 0.2 \times 10^{-3}$
$5.4 \pm 0.2 \times 10^{-5}$	---	^{137}Cs	$4.6 \pm 1.6 \times 10^{-5}$	$1.11 \pm 0.02 \times 10^{-2}$
---	---	^{134}Cs	---	$6.0 \pm 0.6 \times 10^{-4}$
0.0615	0.138	^{235}U (μg)	0.0226	0.0069
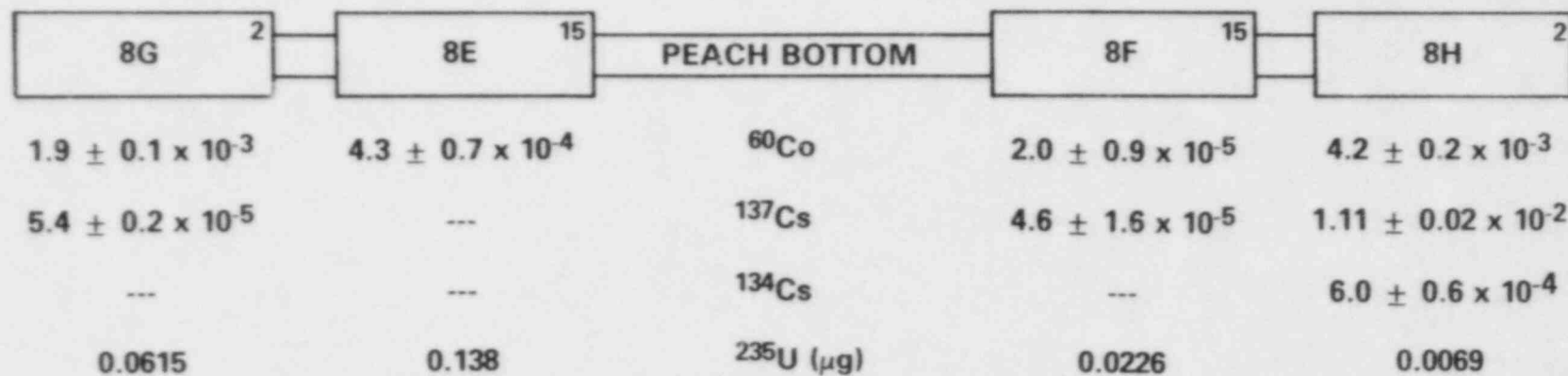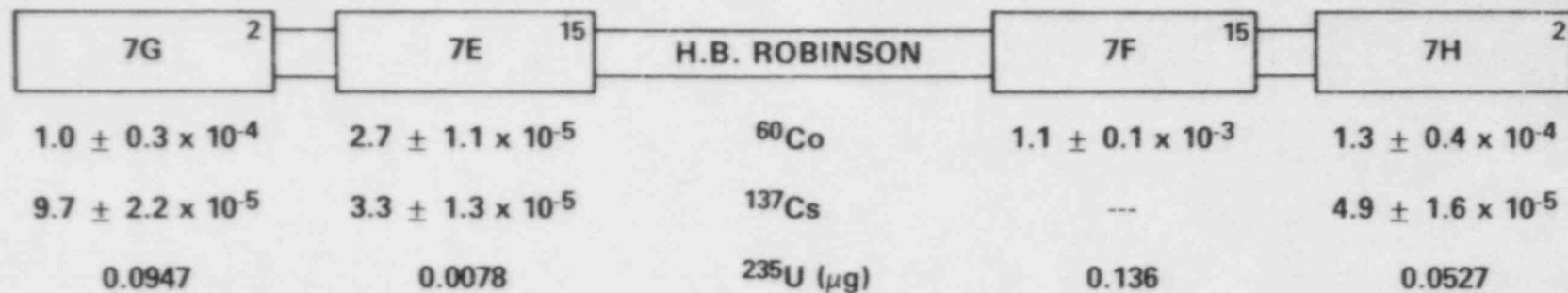
HEDL 8404-173.18

FIGURE 9. Positional Schematic of Filter Analysis (μCi) After Rods Were Tested for 5962 Hours at 229°C. (Number at the upper right of the filter boxes is the filter size in micrometers.)

TABLE 13

CAPSULE SMEAR TESTS

Rod	Capsule	Defected?	2235-h Interim		5962-h Interim		
			γ	DN	Wt	γ	DN
HBR-B05-E7	7	Defected	X	X		X	X
PB-PH462-D6	4	Defected			X	X	X
PB-PH462-E5	1	Intact			X	X	X
PB-PH462-E3	8	Defected	X	X		X*	X
Control			X	X	X	X	

*Relative only.

Analysis of a partial smear indicated fissile material was present in the loose powder in the capsule. Due to loss of material and use of a system not calibrated for the smear geometry, only the percentage of activity for the γ emitters was reported. ^{137}Cs predominates due to the fuel coming out of the rod breach, which is in contrast to the other rods in which ^{60}Co from the crud is dominant. The ^{137}Cs and fissile material found on the smears from the other rod seem unusually high since no material could be visibly seen on the smears. Also activity was present in the capsule containing intact rod PB-PH462-E5. Since the swabbing was conducted after the contamination incident and since the smears were counted in their original bags without unbagging, in all probability much of the ^{137}Cs and fissile material activity is probably due to residual contamination on the bag. Further interpretation of the ^{137}Cs and fissile counts from capsules containing PB-PH462-D6 and -E5 would not be justified.

An estimate of the amount of crud spalled was based on the weight gain of the smears and the radiation level of the ^{60}Co. The initial amount of crud in the rod is estimated from the linear average of the ^{60}Co determined from the grinding of crud from companion rods (Ref. 38) (see Table 15). This initial amount was compared to the crud picked up by the smears on the assumption that the amount of crud in the capsule was proportional to the ^{60}Co counts (see Table 16). Based on weight gain, the Peach Bottom rods spalled 7% to 15% of the crud during the last 3726 hours compared to 2% to 5% spallation determined by ^{60}Co counting. Spallation from the H. B. Robinson rod could only be calculated by ^{60}Co counting and was ∿6%. These numbers may be high due to the scraping of the rods during insertion and removal from the capsules, but the spallation calculated for the first 2235 hours indicates that this should be a small correction.

44

TABLE 14

POSTTEST SMEAR ANALYSES OF CAPSULES (μCi)

Isotope	2235-h Interim			5962-h Interim				
	HBR-B05-E7	PB-PH462-E3	Control	HBR-B05-E7	PB-PH462-D6	PB-PH462-E5	PB-PH462-E3 (% Total Activity)	Control
^{241}Am		$1.6 \pm 0.5 \times 10^{-3}$					0.91	
^{154}Eu		$2.4 \pm 1.0 \times 10^{-3}$					0.24	
^{155}Eu								
^{144}Ce		$1.0 \pm 0.1 \times 10^{-2}$					1.09	
^{125}Sb		$8 \pm 3 \times 10^{-3}$					0.60	
^{134}Cs		$3.1 \pm 0.3 \times 10^{-2}$	$2.3 \pm 0.9 \times 10^{-4}$				2.64	$1.1 \pm 0.1 \times 10^{-2}$
^{137}Cs	0.1 ± 0.01	$4.5 \pm 0.4 \times 10^{-1}$	$3.5 \pm 2.2 \times 10^{-3}$	1.7 ± 0.1	$11.4 \pm 0.5^*$	$2.7 \pm 0.1^*$	92.90	$4.7 \pm 7.7 \times 10^{-2}$
^{54}Mn		$2.2 \pm 0.6 \times 10^{-3}$						
^{60}Co	15 ± 2	1.1 ± 0.1	$1.7 \pm 0.7 \times 10^{-2}$	522 ± 20	530 ± 30	177 ± 1	1.32	$6.4 \pm 6.4 \times 10^{-2}$
Others							^{106}Ru-^{106}Rh 0.30	
Total Fissile (ng)	26 ± 5	250 ± 50	<10	774 ± 29	$2480 \pm 90^*$	$1120 \pm 40^*$	67,100**	NM***
Weight Change (mg)	NM	NM	NM	NM	83	39	NM**	0.67
Order of Smearing				1	3	4	2	

*Probably contaminated.
**Material lost while swabbing capsule.
***NM - Not measured.

TABLE 15

RADIATION ANALYSIS OF CRUD FROM TEST ROD COMPANIONS (Ref. 38)
(April 1983)

Distance from Top of Rod (in.)	Radioactivity (μCi/cm^2)						Areal Crud Density (mg/cm^2)
	^{54}Mn	^{60}Co	^{125}Sb	^{134}Cs	^{137}Cs	^{154}Eu	
Peach Bottom Rod PB-PH462-E6							
20	---	1.97	4.4×10^{-3}	2.2×10^{-4}	1.5×10^{-2}	1.0×10^{-4}	0*
60	1.75×10^{-2}	4.24	1.5×10^{-1}	4.4×10^{-4}	2.9×10^{-2}	1.2×10^{-3}	0.21
156	7.3×10^{-4}	1.17	1.0×10^{-2}	4.4×10^{-4}	1.3×10^{-2}	1.4×10^{-4}	0.16
H. B. Robinson Rod HBR-B05-H9							
15	8.2×10^{-4}	6.05	2.8×10^{-3}	5.5×10^{-3}	3.9×10^{-2}	8.3×10^{-4}	0.48
137	---	2.1	5.8×10^{-3}	2.3×10^{-3}	3.2×10^{-2}	2.3×10^{-3}	0.07
146	1.2×10^{-3}	3.3×10^{-1}	3.9×10^{-3}	1.8×10^{-3}	1.7×10^{-2}	1.8×10^{-3}	0.81

*No detectable weight gain.

TABLE 16

CRUD SPALLATION RANGE CALCULATIONS

	Symbol	HB Robinson Rod	Peach Bottom Rod
Average Areal Crud Density* (mg/cm^2)	ρ	0.45	0.12
Rod Surface Area (cm^2)	A	3.3×10^3	4.5×10^3
Total Crud Weight Per Rod (mg)	ρA	1.5×10^3	542
Measured Weight Increase of Smear (mg)	W		39 - 83
Crud Spalled (%)	W x 100/ρA		7 - 15
Average ^{60}Co Activity 4/83* (μCi/cm^2)	R	2.83	2.5
Total Rod ^{60}Co Activity (μCi)	RA	9.3×10^3	1.1×10^4
^{60}Co Count at 5962 Hours (μCi)	C_1	522	177 - 530
^{60}Co Count at 2235 Hours (μCi)	C_2	15	1.1
Crud Spalled - 5962 Hours (%)	100 x C_1/RA	5.6	1.6 - 4.8
Crud Spalled - 2235 Hours (%)	100 x C_2/RA	0.16	0.01

*Ref. 38.

B. NONDESTRUCTIVE ROD EXAMINATIONS

Four rods were nondestructively examined during each interim examination. The NDE consisted of videotape and periscope visual, diametral and defect size measurement and gross and/or isotopic gamma scans. The measurements made on the rods are listed in Table 3.

47

1. Visual Examination

Rods were identified by their location in the assembly. The Peach Bottom rods had a serial number stamped on the lower end fitting. A digit in the serial number was used to designate the zero degree orientation of the rod (Ref. 38). The H. B. Robinson rods had no serial numbers, consequently a mark was scratched in the upper end fitting with a vibrating tool to signify the zero degree orientation. The rod was placed in a "V" trough that contained an attached ruler with 1/16-in. divisions for video scans and still pictures. Zero was at the top of the rod. The fuel rod zero degree identification mark was placed upward in the "V" trough and a video scan taken. During the course of the video traverse, notations were made for locations of still photographs, crud condition, coloration changes and other notable characteristics. Two further video scans were made of each rod after a clockwise rotation of 120° and 240°.

Video tape and still photographs of typical cladding and defects were taken of all the rods prior to the test. The visual observations made during the interim examinations are listed in Table 17. Since nothing unusual was observed during the periscope examination and since the 2235-hour interim examination was primarily to check for fuel oxidation, photographs were taken of the defects only during the 2235-hour interim examination. After 5962 hours all rods were examined in the periscope. Nothing unusual was observed on the cladding at sites remote from the defects. No outstanding features or surface differences from the pretest appearance were apparent. Rod HBR-B05-E7, which had heavy crud above 20 in. from the top, still had heavy crud. (See Figure 10 for comparison with Figure 7.) Pictures of the typical surface condition were taken every two feet on all three Peach Bottom rods. A typical set of photos are given in Appendix A for comparison with a similar set of pretest photos in the appendix of Ref. 38. The test atmosphere could not be determined based on the surface appearances.

Each time a defect was examined, it was photographed. The exception was the defect located 14 in. from the top of HBR-B05-E7, which was not photographed before the start of the test. Other than the defect located 22 in. from the top of rod PB-PH462-E3, none of the defects appeared to have changed. An example is in Figure 11, with a complete photo record of the defects in Appendix A. As seen in Figure 12 after 2235 hours, the defect at 22 in. from the top of PB-PH462-E3 split open and continued to enlarge as the test continued.

2. Defect and Diameter Measurements

As described in Section IV.A, a 1/32-in. (0.031-in.) drill was used to put two defects in each of four fuel rods. Measurements of the defect size were not made prior to the start of the test. During the interim examinations, defects were measured with a filar eyepiece calibrated against a ruler placed

TABLE 17

FUEL ROD VISUAL EXAMINATIONS

Rod	Pretest			2235 Hours			5962 Hours		
	Video Tape	Typical Cladding	Defects	Video Tape	Typical Cladding	Defects	Video Tape	Typical Cladding	Defects
HBR-B05-E7	X	X	X			X		X	X
PB-PH462-E3	X	X	X			X	X	X	X
PB-PH462-D6	X	X	X			X		X	X
PB-PH462-E5	X	X					X	X	
HBR-B05-G7	X	X	X			X			
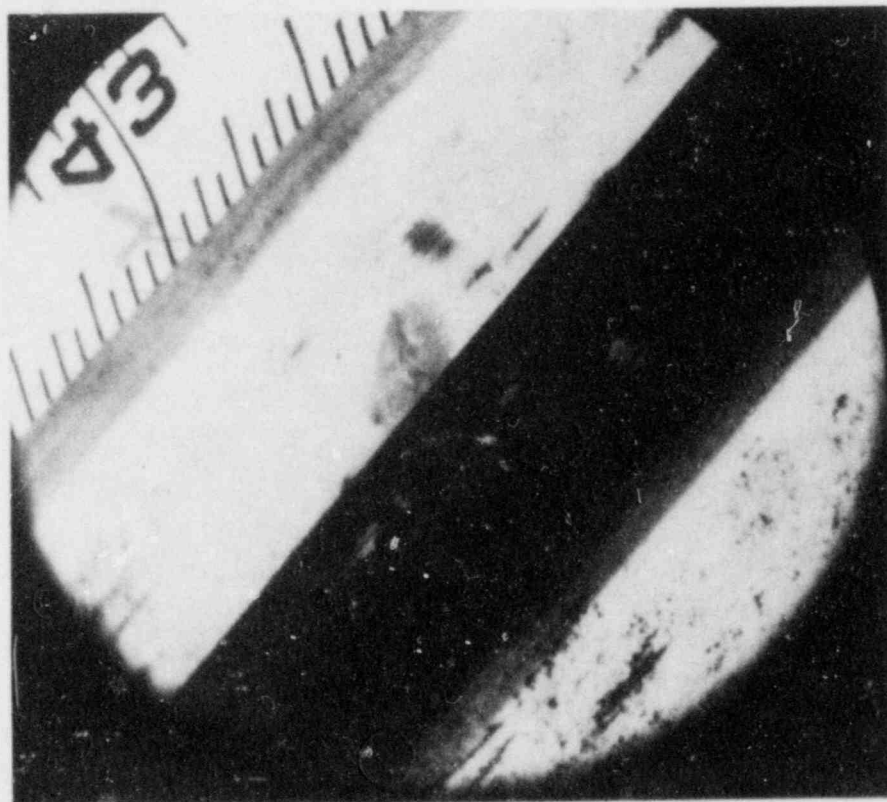
HEDL 8404-173.26

FIGURE 10. Heavy Crud Coating at 19 in. from Top of Rod HBR-B05-E7 After Testing for 5962 Hours at 229°C in Unlimited Air Atmosphere.

49
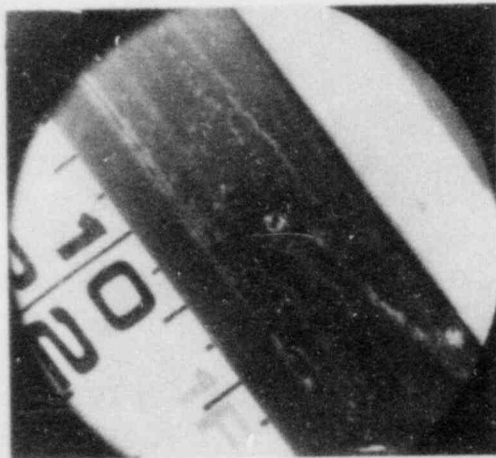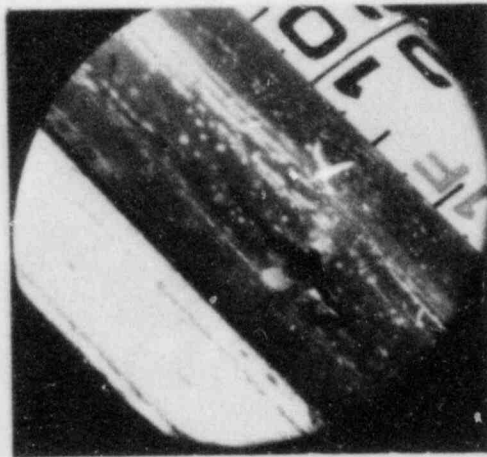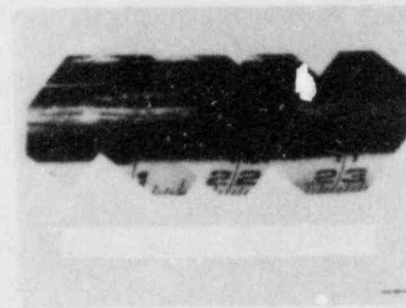
(a) **(b)** **(c)**

FIGURE 11. Artifical Defect at 88 in. from Top of Rod PB-PH462-E3: (a) Pretest, (b) After Testing for 2235 Hours, and (c) After Testing for 5962 Hours at 229°C in Unlimited Air Atmosphere.
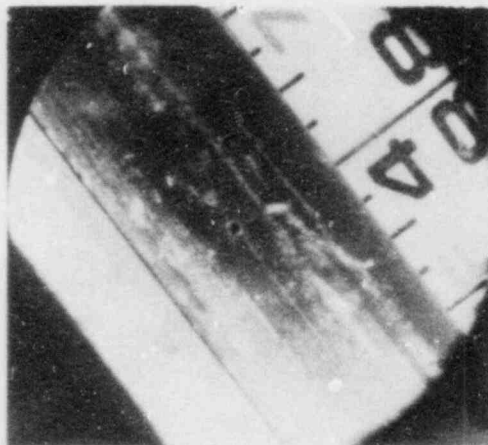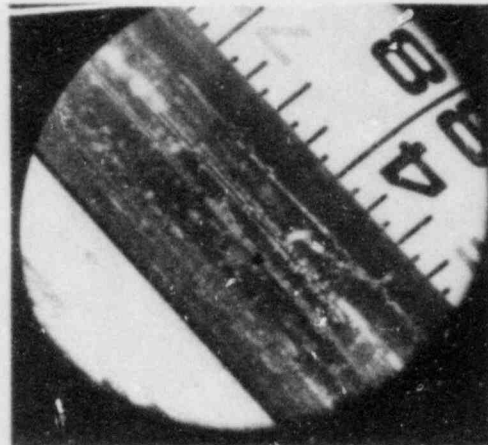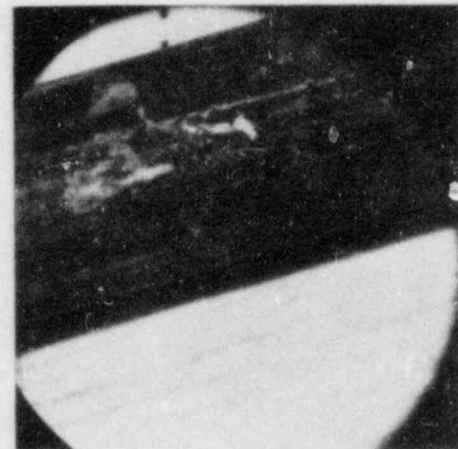
(a) **(b)** **(c)**

FIGURE 12. Artifical Defect at 22 in. from Top of Rod PB-PH462-E3: (a) Pretest, (b) After Testing for 2235 Hours, and (c) After Testing for 5962 Hours at 229°C in Unlimited Air Atmosphere.

on top of the defect. This filar eyepiece calibration was repeated a number
of times at each defect site to eliminate magnification problems in the
periscope.

The unsplit defects were measured only after 5962 hours at 229°C, and then
only the defects that appeared to penetrate the cladding with the full diam-
eter of the drill were measured. The results are given in Table 18. The
axial and transverse diameters are within 10%. The largest apparent growth
is 13% in the transverse direction for the upper defect on Rod HBR-B05-E7.
Without pretest diameter measurements, it is impossible to determine if the
holes have actually grown or if the drill just wandered during the defecting
process. Diameter measurements from the pretest photos without the use of
the filar eyepiece are not accurate enough for comparisons due to the large
error associated with the magnification factor.

TABLE 18

DEFECT SIZE AFTER TESTING FOR 5962 HOURS

Rod	Atmos-phere	Defect Location (in. from Rod Bottom)	Axial Diameter (mil)*	Transverse Diameter (mil)*
PB-PH462-E3	Air	72	31.2 ± 0.9	30.9 ± 0.4
PB-PH462-D6	Argon	73.5	31.2 ± 0.2	34.7 ± 0.9
HBR-B05-E7	Air	71	30.9 ± 0.8	33.3 ± 0.9
HBR-B05-E7	Air	138	34.6 ± 0.8	35 ± 1.0

*Errors are based on 1σ for measurements.

Figures 13 and 14 show the defect at 22 in. from the top of Rod PB-PH462-E3
after 2235 and 5962 hours at 229°C in unlimited air. In both cases, the crack
is widest adjacent to the original defect. As indicated in Table 19, the
crack is 0.45 in. long after 2235 hours and grows to 2.2 in. after 5962 hours.
By the time 5962 hours have elapsed, a secondary crack has started to form.
The crack, which is not straight through the cladding but rather at ~60°, is
fairly typical of the behavior of a tube under hoop stress. The original
0.031-in. diameter defect grew considerably. At 2235 hours it is oval with
~190% growth in the axial direction and 5.6 times the area. After 5962 hours
the defect has become more circular with only 145% axial growth but has not
significantly increased in area (5.8 times). The defect growth may be due to
contact between the cladding and swelling fuel. After contact is made, until
crack formation starts, the fuel could isotropically swell, thus enlarging
the hole.

UPPER CRACK TIP

ORIGINAL DEFECT

LOWER CRACK TIP

WIDEST CRACK WIDTH
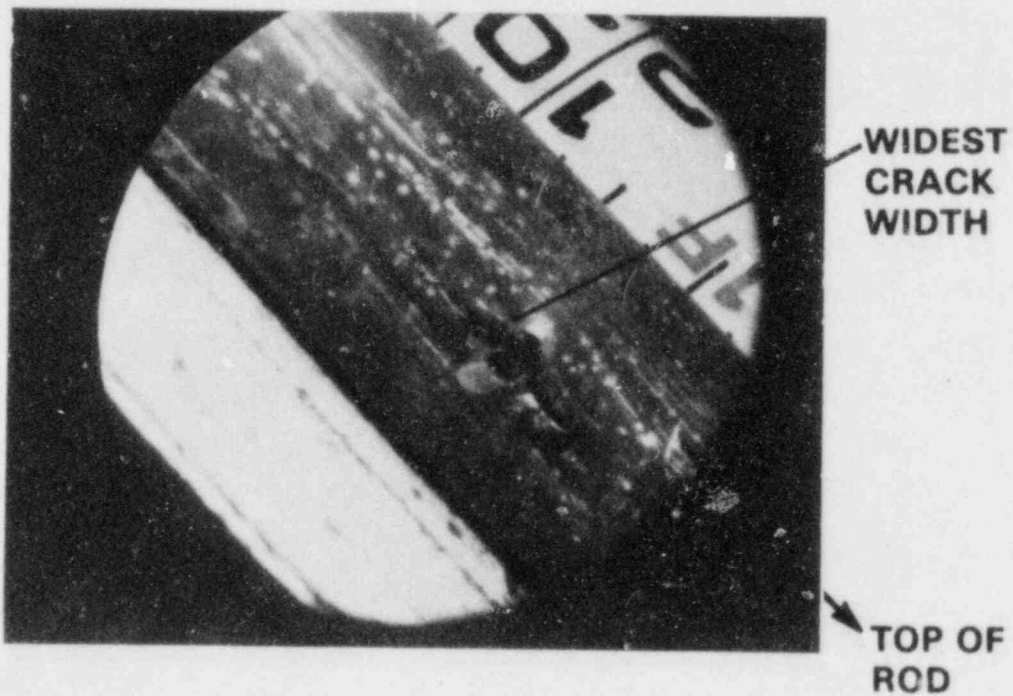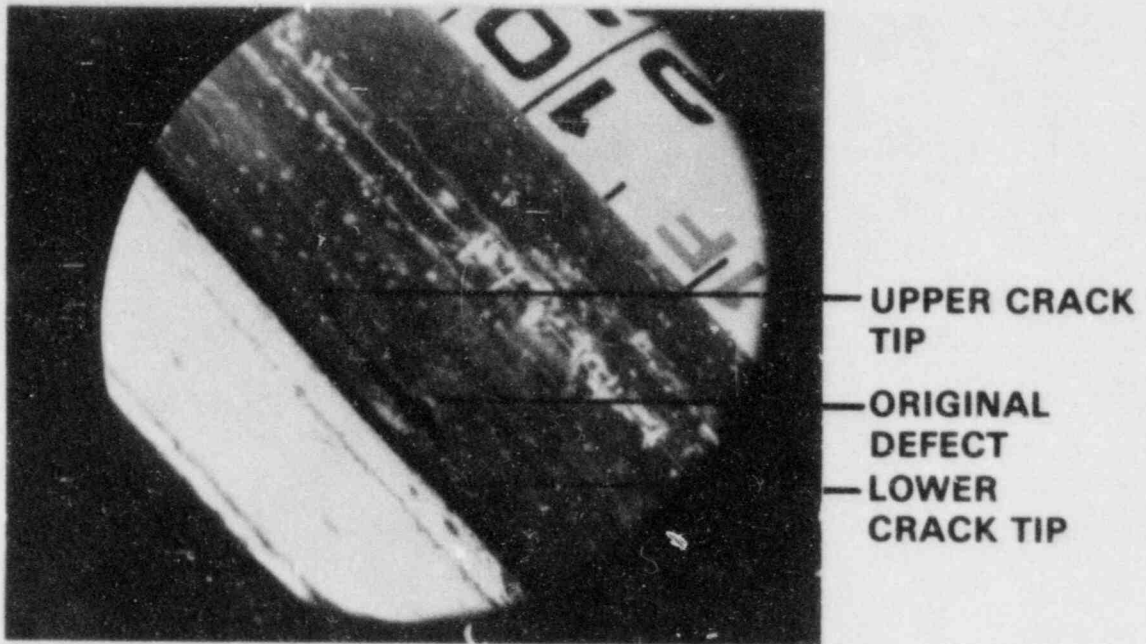
TOP OF ROD

HEDL 8404-173.38

FIGURE 13. Split Defect 22 in. from Top of Rod PB-PH462-E3 After Testing for 2235 Hours at 229°C in Unlimited Air Atmosphere.

52

UPPER CRACK TIP

60° CRACKED ZIRCALOY SURFACE

ORIGINAL DEFECT

LOWER CRACK TIP

SECONDARY CRACK

POINT OF LARGEST CRACK WIDTH

SECONDARY CRACK
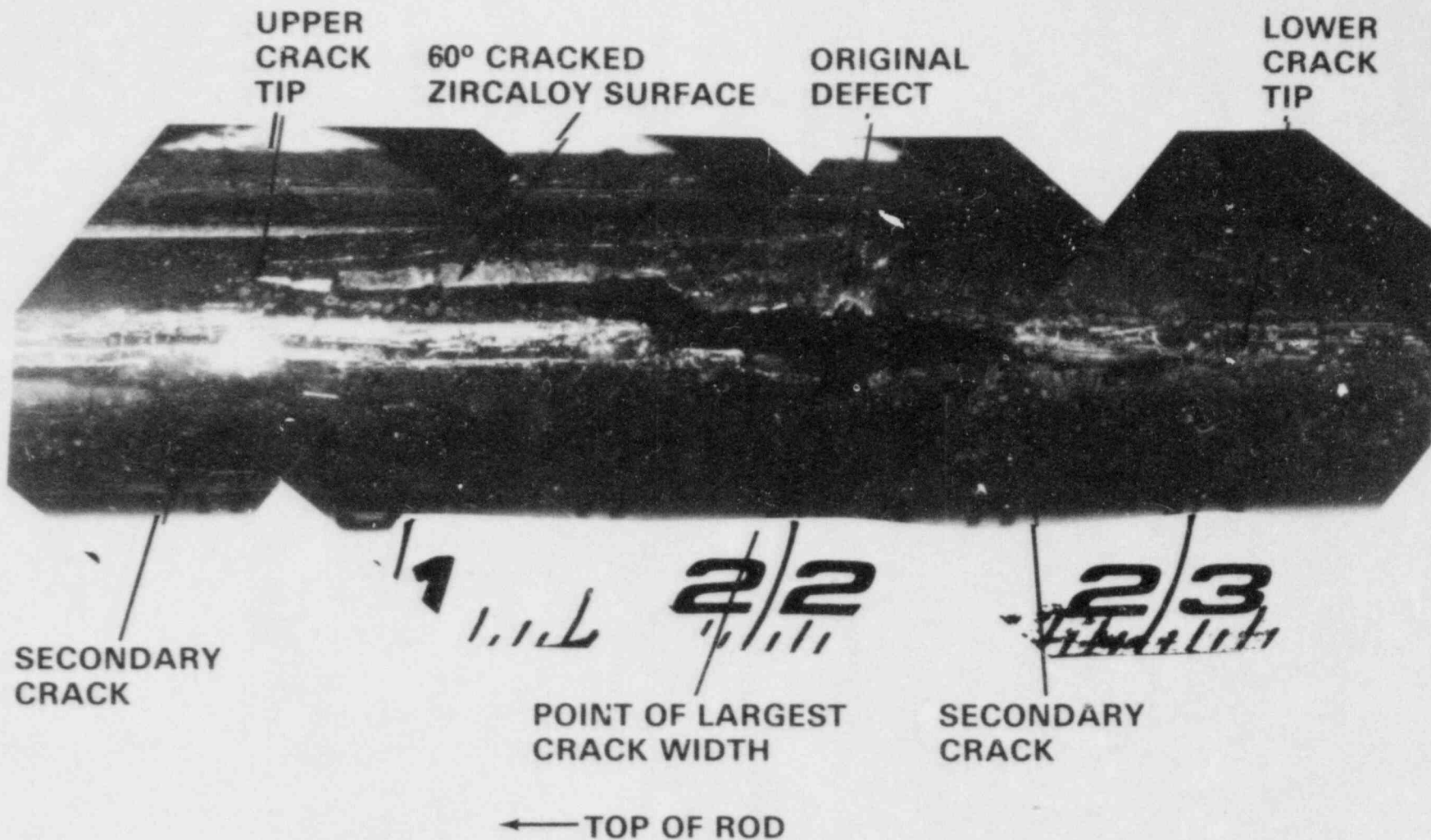
← TOP OF ROD

HEDL 8404-173.7

FIGURE 14. Split Defect 22 in. from Top of Rod PB-PH462-E3 After Testing for 5962 Hours at 229°C in Unlimited Air Atmosphere.

TABLE 19

CHARACTERISTICS OF DEFECT 22 in. FROM TOP OF
ROD PB-PH462-E3 TESTED AT 229°C IN UNLIMITED AIR ATMOSPHERE

	2235 Hours*	5962 Hours*
Axial Width of Original Defect (in.)	0.090 ± 0.006	0.076 ± 0.001
Transverse Width of Original Defect** (in.)	0.060 ± 0.006	0.074 ± 0.004
Nominal Transverse Growth of Original Defect (%)	93.5	139
Length of Split Up the Rod (in.)	0.167 ± 0.003	1.337 ± 0.006
Length of Split Down the Rod (in.)	0.277 ± 0.003	0.833 ± 0.005
Total Length of Split (in.)	0.444 ± 0.005	2.17 ± 0.01
Maximum Width of Split (in.)	0.054 ± 0.002	0.179 ± 0.002
Maximum Diametral Deformation (%)	9.8	15.8

---

*Errors are based on 1σ for measurements.
**Measured transverse width less the average split width adjacent to the original defect.

The rod diameters were measured at various axial positions with a vernier caliper, which was calibrated against a ruler on top of the rod. Although a number of measurements were taken at each location, the minimum measurement was used since nonperpendicularity of the vernier would result in a high reading. The pressure of the master-slave on the caliper resulted in +0.002-in. error on the readings. Since we are concerned with maximum rod growth, 0.004 in. was added to the diameters measurements.

The diameter measurements for Rod HBR-B05-E7 are shown in Figure 15. Since no pretest diameter measurements of the test rods were made, only the creep-down diameters could be compared on numerous companion rods. These companion rods form a tight band of diameter measurements with a +1-mil deviation. Within the capabilities of measurement, no diametral growth at any location on the rod is indicated.
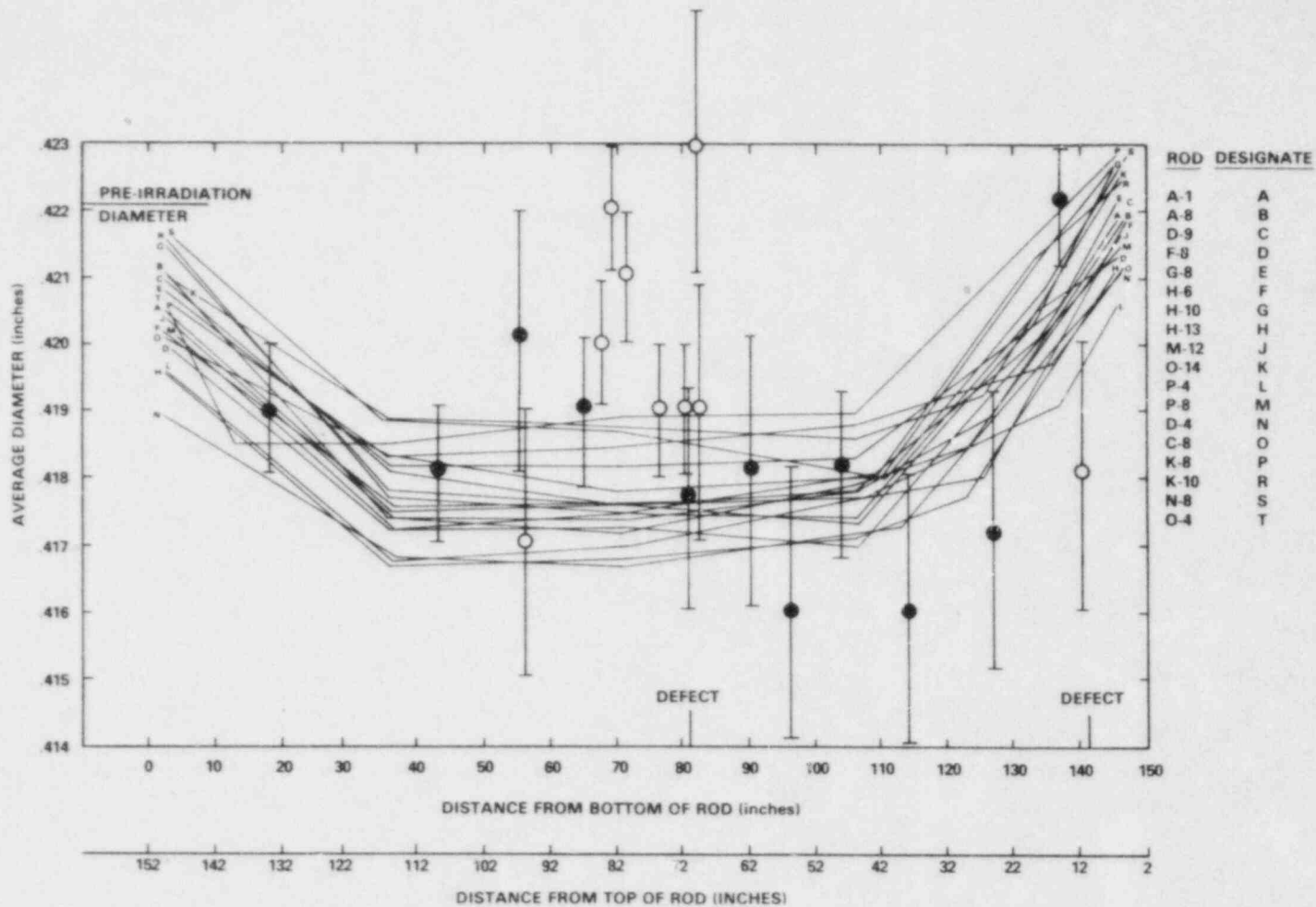
FIGURE 15. Caliper Measurements of Rod HBR-B05-E7 Diameter After Testing at 229°C in Unlimited Air Atmosphere Compared to Spiral Profilometry of HBR-B05 Rods (Ref. 70). O = 2235 Hours; ● = 5962 Hours.

The pretest diameters of the Peach Bottom BWR rods were also not measured, but BWR rods exhibit no creepdown. Pre- and post-irradiation diameters are approximately the same; therefore, the manufactured rod diameter (0.563 in.) can be used as a zero point. Diameter measurements on PB-PH462-D6, -E5 and -E3 at positions away from the split defect are listed in Table 20. Ignoring errors, one might conclude that there is an indication of deformation at the lower defect on Rod PB-PH462-E3 after 5962 hours, but the deformation is only 0.3%. Within measurement error, there is no indication of cladding deformation away from the crack site on Rod PB-PH462-E3.

TABLE 20

ROD DIAMETERS AT REPRESENTATIVE AXIAL LOCATIONS

Rod	Time (h)	Location from Top of Rod (in.)	Average Diameter (mil)*	Comment
PB-PH462-E3	2235	74	562	
		55	562	
		79	562	
PB-PH462-E3	5962	34	561	
		53	561	
		85	561	
		86	561	
		87	564	
		88	564	Defect
		88.75	564	
		89	562	
		90	561	
PB-PH462-D6	5962	20.5	561	Defect
		47	561	
		88.5	563	Defect
		108	562	
PB-PH462-E5	5962	36	560	
		43	560	
		72	560	
		108	561	
		132	560	
		156	561	

*Error of ±3 mil on measurements.

56

The cladding deformation at the split defect on Rod PB-PH462-E3 is shown in Figure 16. As illustrated, measurements were made across and perpendicular to the defect. At 2235 hours no difference in deformation between the orientations is apparent. At 5962 hours there is slightly more deformation in the perpendicular direction. After 2235 hours a peak deformation of 9.7% is measured at the site of the original defect; by 5962 hours the peak deformation has risen to 17%. More important than the amount of deformation is the axial progression of the deformation beyond the crack tip. At 2235 hours
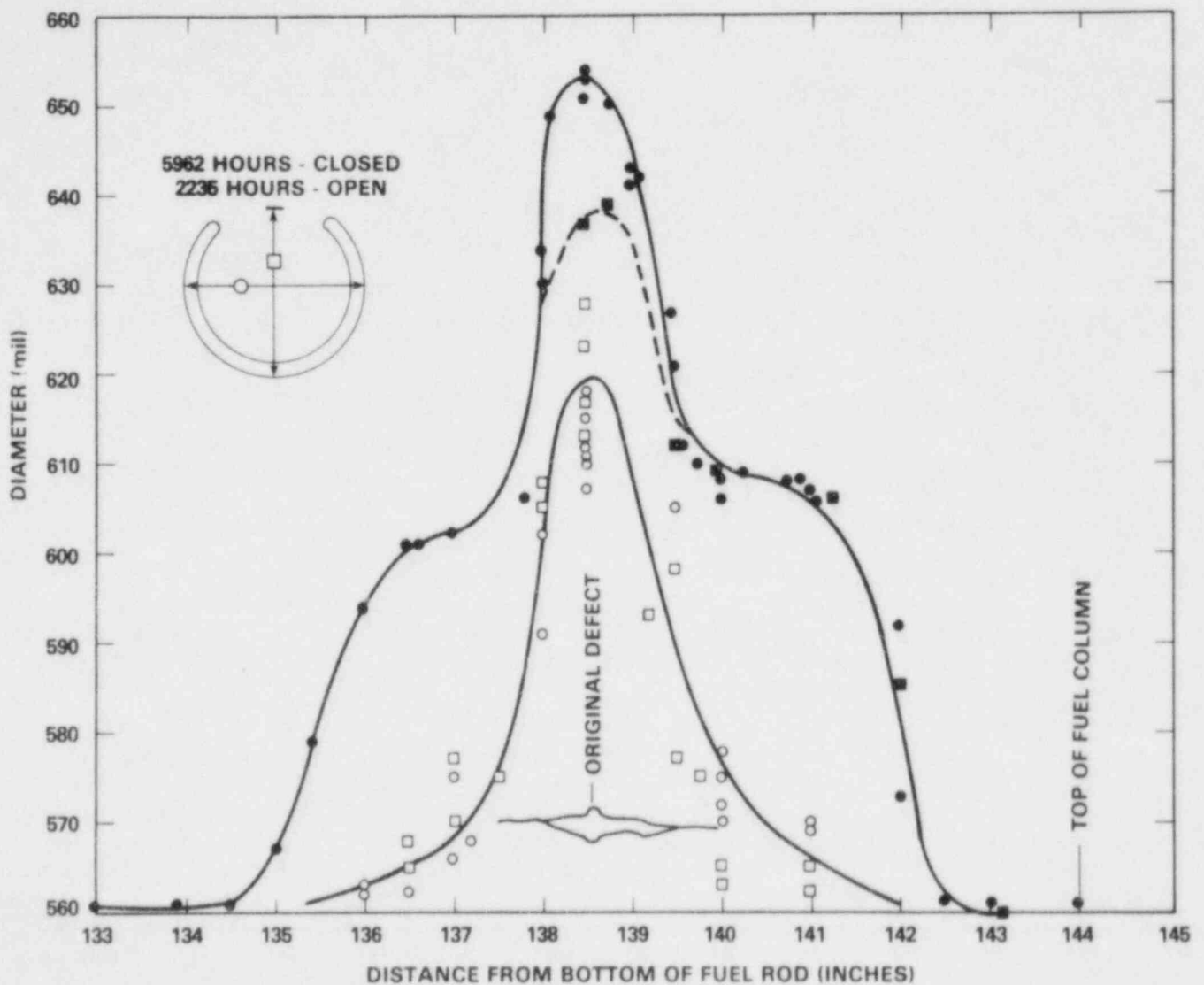
HEDL 8309-204.4

FIGURE 16. Diametral Profile at Position of Upper Defect in Rod PB-PH462-E3 After Testing at 229°C in Unlimited Air Atmosphere. (Original defect and crack geometry shown schematically at appropriate distance from bottom of fuel rod.)

the deformation does not drop to 5% until +1 in. from the defect site, although cladding splitting occurred for only ∿1/4 in. Preirradiation diameters were reached ∿2 in. beyond the crack tip. At 5962 hours, the deformation does not drop to 5% until 2 in. beyond the crack tip, and it is yet another inch before preirradiation diameters are reached.
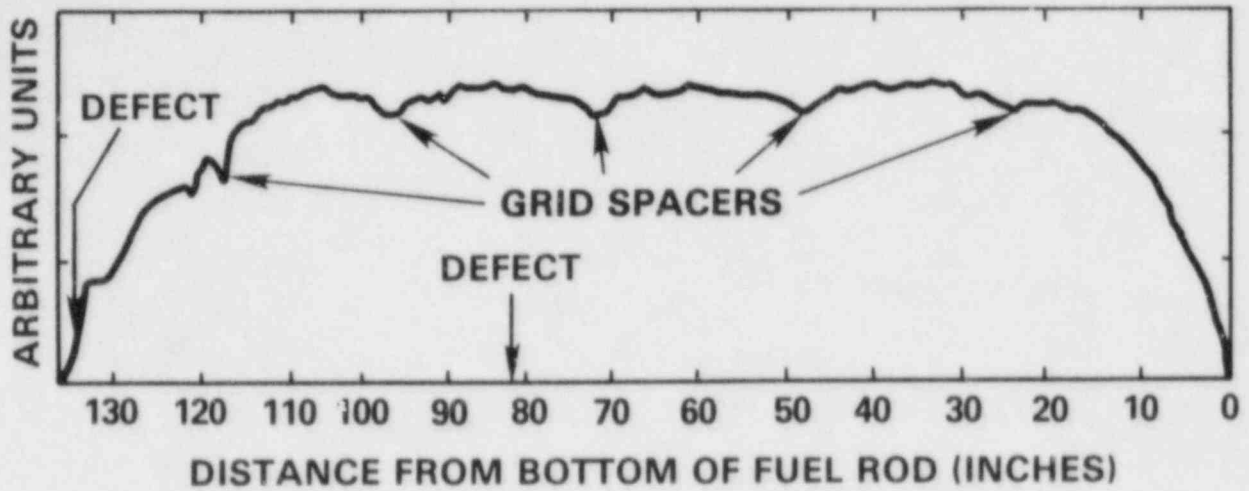
3. Gamma Scans

Gross and isotopic gamma scans were made on the four rods examined after 5962 hours. The main purposes of the gamma scans were to: (a) determine if the progression of the oxidation front could be determined by disruption of the pellet-pellet interfaces caused by the volume expansion that accompanies the $UO_2 \rightarrow U_3O_8$ transition and (b) determine the crud profile by looking at the most active constituents of crud, ^{60}Co and ^{54}Mn.

Rods PB-PH462-D6, PB-PH462-E5 and HBR-B05-E7 were scanned in the TAN underwater facility. The rods were placed in a sealed container that was, in turn, placed under the detector. The unit was calibrated against a ^{60}Co source on the traveling bed. The gross scan was taken continuously and counted all γ's above 0.5 MeV. Typical traces are shown in Figures 17 and 18. The flux depressions at the grid spacers are quite noticeable. The isotopic scans were taken stepwise in 6-in. intervals. A 10^3-s live time count was taken, and any isotope with less than 0.1 ct/s was considered as not detected. While a full energy spectrum was recorded, the isotopes analyzed were ^{152}Eu (344.2 keV), ^{134}Cs (604.6 keV), ^{137}Cs (661.6 keV), ^{54}Mn (834.8 keV), ^{154}Eu (1274.4 keV) and ^{60}Co (1332.4 keV). The results are tabulated in Appendix B.

Rod PB-PH462-E3 would not fit into the TAN γ-scanner and had to be scanned at TRA. The rod was cut into three sections, and each section was individually scanned. A 0.5-in. long by 0.080-in. wide collimator was used. A continuous gross scan and a 6-in. interval step-wise isotopic scan were made.

^{54}Mn was not detected in any of the isotopic scans even though an 8-h count was taken at one location. ^{60}Co, when detectable, was very low and only increased appreciably on the upper and lower end fittings (see Appendix B). This indicates that the Zircaloy itself and not the crud is the prime contribution to the ^{60}Co activity. Therefore, γ-scanning does not appear to be a suitable method of determining crud profiles. ^{137}Cs (∿92%) was the predominant activity with some contribution from ^{134}Cs (∿7.4%) and ^{125}Sb or ^{154}Eu (0.6%). The pellet-pellet interfaces (Figure 19) with peak-to-peak separation (0.51 in.) are quite clear in the center of the rod. At the ends of the rod though, the pellet-pellet interfaces are not discernable even in a rod where no oxidation has taken place (see Figure 20). This indicates that gamma scanning is not useful for nondestructively determining an oxidation front; profilometry is probably more useful. There appeared to be a dip in the profile of PB-PH462-E3 at the upper defect site (see Figure 21) that might be indicative of fuel fallout, but a similar dip was found in Rod

FIGURE 17.   Gross Gamma Scan of Defected Rod HBR-B05-E7 After 5962 Hours at 229°C in Unlimited Air Atmosphere.
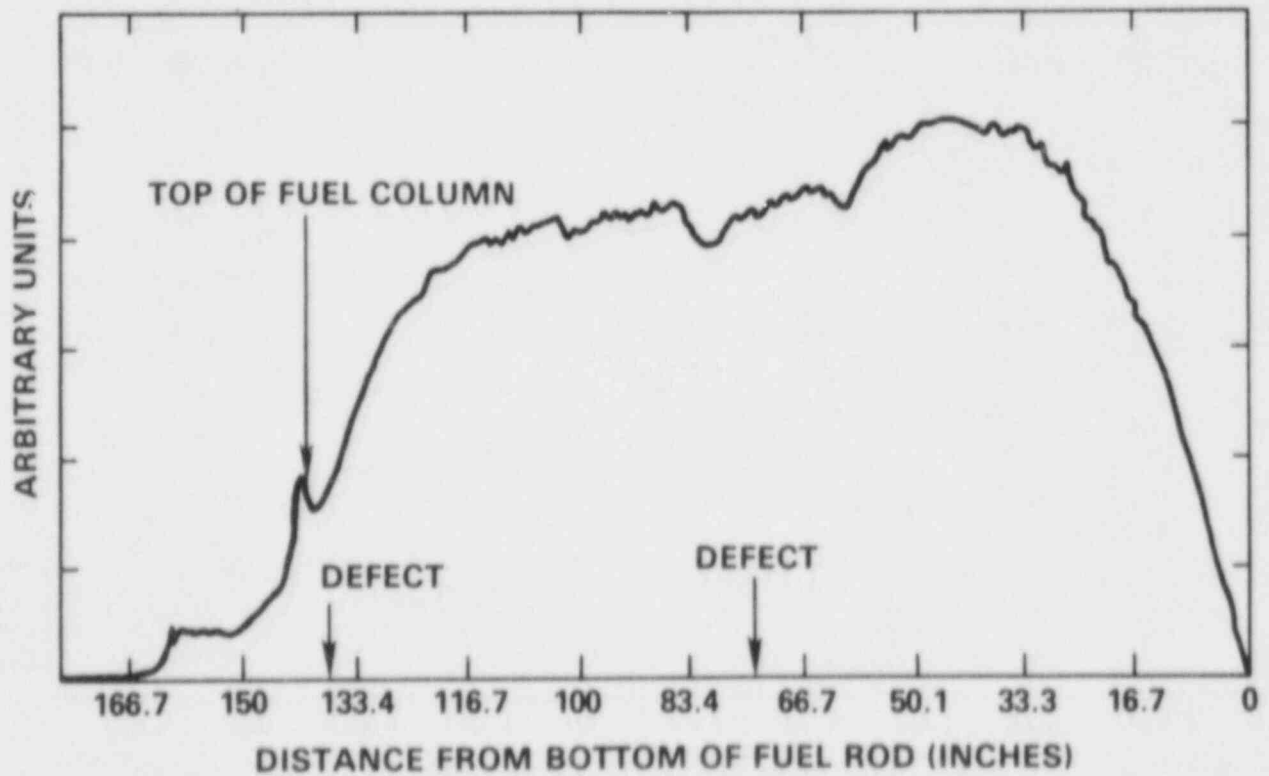
FIGURE 18.   Gross Gamma Scan of Defected Rod PB-PH462-D6 After 5962 Hours at 229°C in Argon Atmosphere.
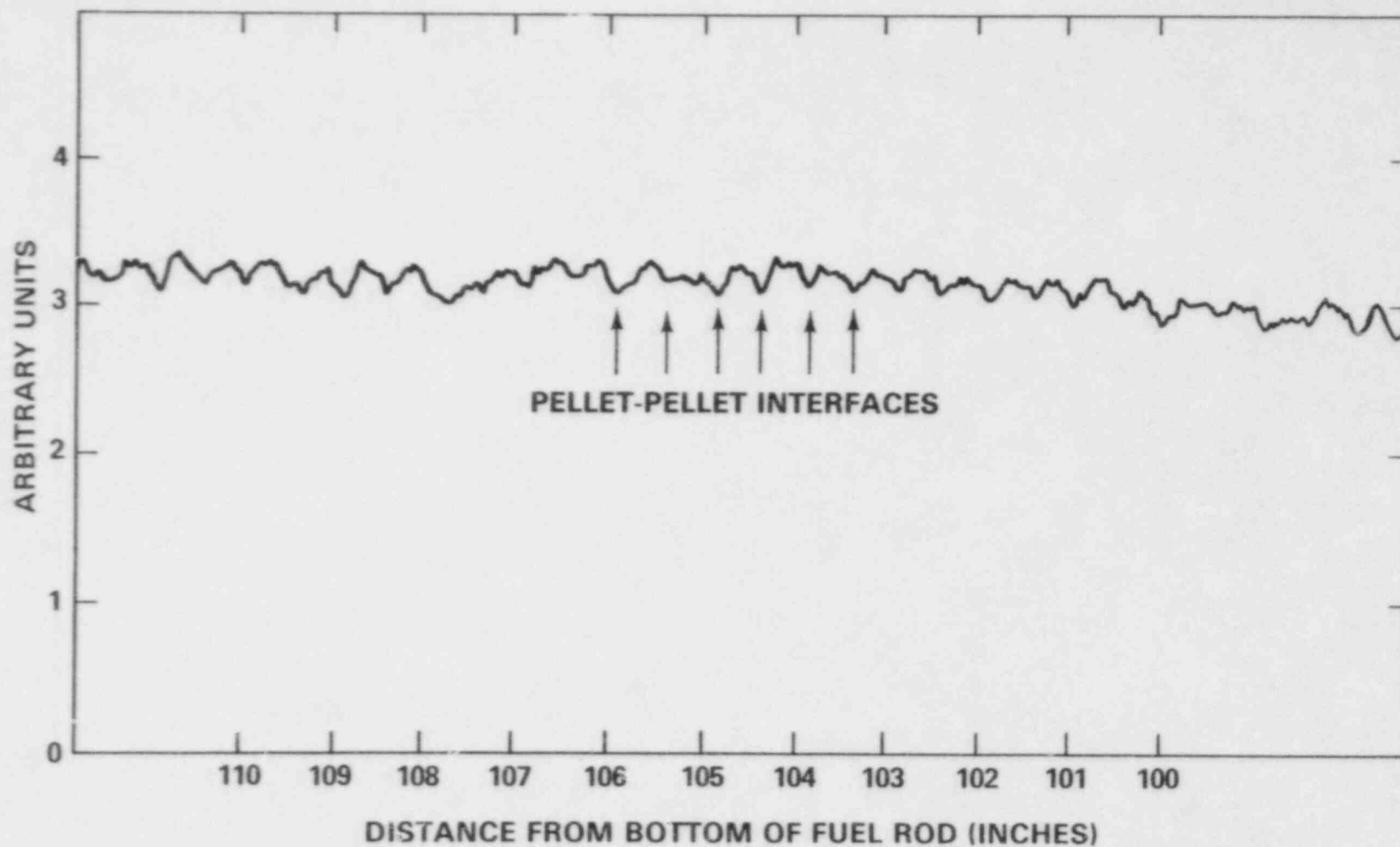
FIGURE 19. Detailed Gross Gamma Scan of Center of Defected Rod PB-PH462-D6 After Testing for 5962 Hours at 229°C in Argon Atmosphere.
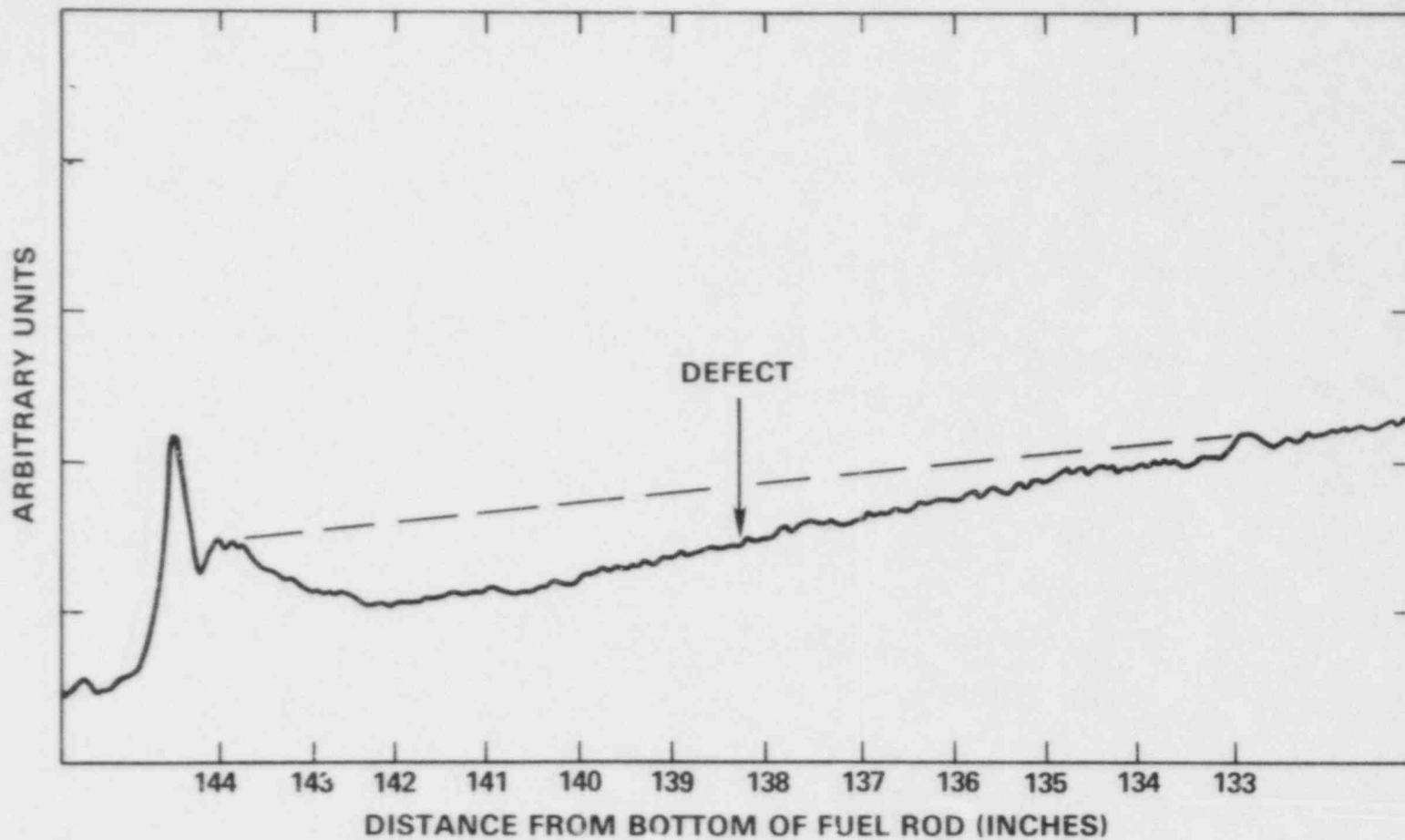
FIGURE 20. Detailed Gross Gamma Scan of Defected Rod PB-PH462-D6 After Testing for 5962 Hours at 229°C in Argon Atmosphere. (Dotted line shows extrapolation of more central gamma-scan data and is used for comparative purposes to show natural drop in gamma intensity due to lower burnup.)
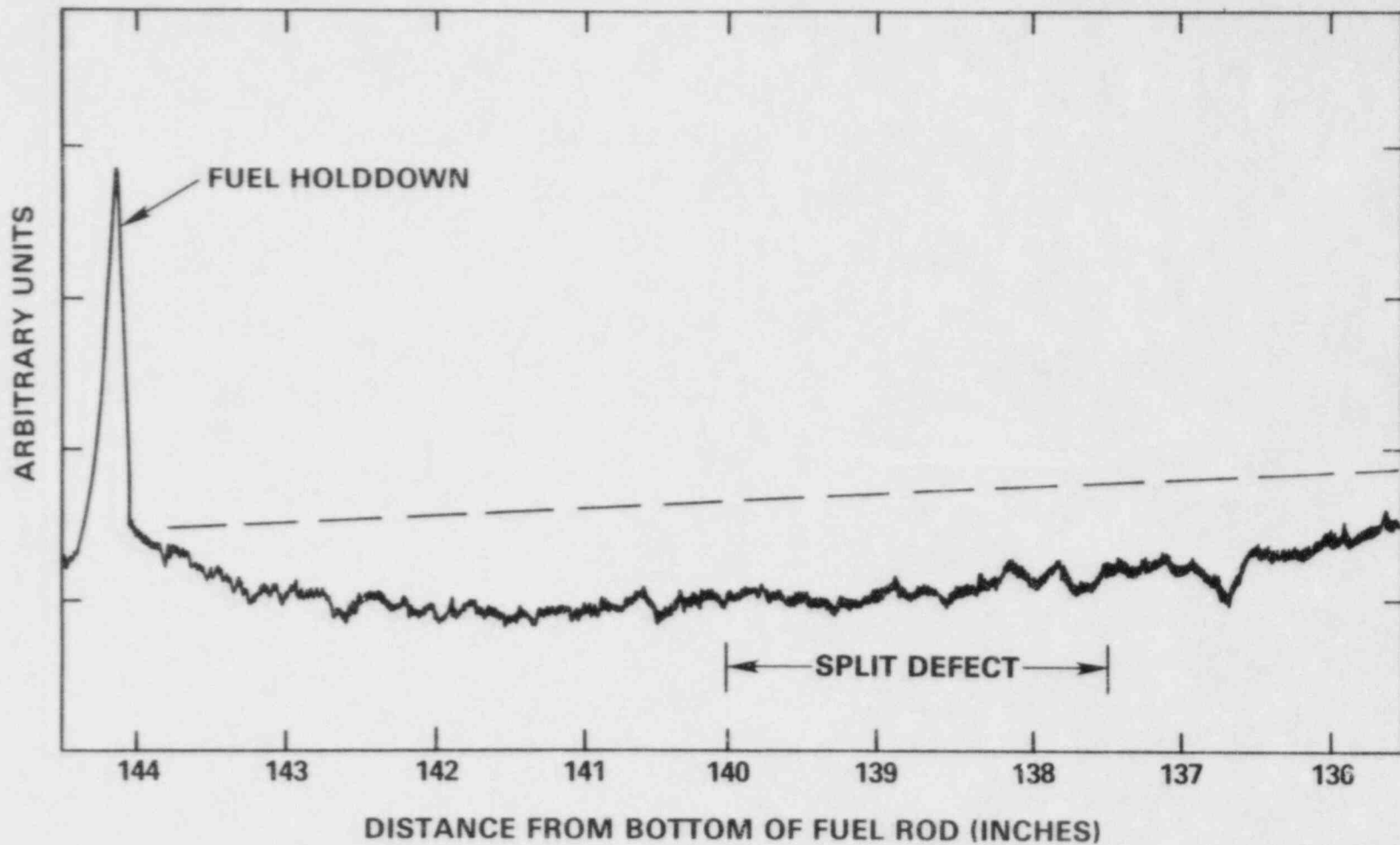
HEDL 8404-173.12

FIGURE 21. Detailed Gross Gamma Scan at Top End of Fuel Column of Defected Rod PB-PH462-E3 After Testing for 5962 Hours at 229°C in Unlimited Air Atmosphere. (Dotted line shows extrapolation of more central gamma scan data and is used for comparative purposes to show possible drop in gamma intensity due to loss of fuel.)

HEDL 8404-173.11

PB-PH462-D6 that had no fuel fallout (Figure 20). This dip is probably a feature of the lower burnup of the ends of the rod. The small amount of fuel fallout visually observed was not sufficient to be detected on top of the axially changing profile. In the center of the fuel rod, where there is a fairly flat profile, fuel fallout might be noticeable in a split defect.

C. DESTRUCTIVE EXAMINATIONS

After each visual examination of Rod PB-PH462-E3, the rod was turned over and any material that fell out of the split defect was collected for analysis. After 5962 hours, Rod PB-PH462-E3 was destructively examined to determine if:

1) A metallurgical reason existed why one defect in the cladding split opened and the other did not.

2) The oxidation front movement could be correlated with the cladding deformation.

3) The condition of the oxide and crud layers could be defined.

Metallographic and ceramographic examinations were conducted in the as-polished and etched state, and the fuel was analyzed by x-ray. In the process, fuel/cladding gap, cladding wall thickness, interior and exterior oxide thickness, crack patterns, pellet configurations and oxide grain structure were examined.

1. Fuel Particulate Fallout

After 2235 hours the fuel particulate in the crack appeared intact and not powdery. Any loose particulate in and around the split defect was collected and analyzed. A paint can lid was covered with double-sided tape and placed underneath but separated from the fuel rod. The rod was rotated until the defect was facing toward the tape and was then tapped twice with the manipulator arm. A fine but very limited fallout of black powder adhered to the tape, which was then removed from the paint can lid and rolled into a point source ball for gamma spectrum analysis (Table 21). The γ-scans of the secondary transfer bags used to determine exterior contamination indicate that the Eu and Sb are probably due to in-cell contamination.

The ^{60}Co indicates that crud and ZrO_2 were present. While the gamma spectroscopy did not detect any ^{235}U, delayed neutron counting indicated that 2.9 μg of fissile material was equivalent to ~3×10^{-6}% of the fuel rod inventory.

63

TABLE 21

ANALYSIS OF PARTICULATE OBTAINED BY TAPPING ROD
AT DEFECT SITE AFTER TESTING FOR 2235 HOURS
AT 229°C IN UNLIMITED AIR ATMOSPHERE

Isotope	Point Source on Counting Card (µCi)
^{241}Am	2.2 ± 0.2 E-2
^{144}Ce	8.4 ± 0.8 E-2
^{125}Sb	3.8 ± 0.4 E-2
^{134}Cs	10.4 ± 1.0 E-2
^{137}Cs	2.2 ± 0.2 E 0
^{154}Eu	2.4 ± 0.3 E-2
^{60}Co	2.2 ± 0.2 E-1
Total Fissile (µg)	2.9 ± 0.3

After 5962 hours, the fuel still appeared to be in chunks with only limited powder. Obviously from the capsule smears, some fuel powder did fall out of the crack during handling, and a fragment of fuel fell out when the rod was turned over. X-ray analysis was conducted on the fragment to determine the oxide phases. When the fragment was broken into smaller pieces (having a contact dose of less than 20 mR/h), it disintegrated into a very fine powder instead of fragmenting into three or four pieces as would have been expected of UO_2. A powder diffraction pattern was obtained using copper $K\alpha$ ($\lambda = 1.5418A$) radiation and a Debye-Sherrer powder camera with a diameter of 114.6 cm. The lattice "d" spacings and relative intensities are listed in Table 22. The Debye rings were broadened, possibly from radiation damage to the crystal structure incurred during irradiation. The pattern agrees well with those of $\alpha-U_3O_8$, having a very minor amount of UO_2.

2. Sample Preparation

After the visual examination, tape was placed over the split defect to prevent further particle fallout. Rod PB-PH462-E3 was cut into three pieces, each ∿54 in. long, using a tubing cutter and no lubricant. The segment ends were capped with rubber stoppers and stored in air until sample preparation began. After gamma scanning, two sections, each containing a defect, were cut from the rod. Axial orientation was maintained. The sections were placed in a secondary tube and vacuum impregnated with a low temperature epoxy. After the epoxy cured at room temperature, individual transverse and

64

TABLE 22

X-RAY DIFFRACTION PATTERN FOR FUEL PARTICLE THAT FELL OUT
OF CLADDING CRACK ON ROD PB-PH462-E3 AFTER TESTING FOR
5962 HOURS AT 229°C IN UNLIMITED AIR ATMOSPHERE

"d" (A)	I
4.150	65
3.407	100
2.632	80
2.075	15
1.722	40
3.15	Weak
1.96	Weak

longitudinal samples were cut, as shown in Figure 22, using an isomet saw
lubricated with water. The transverse sample in the center of the rod (Fig-
ure 22a) was cut slightly off-defect, then polished through the center of the
defect. Due to the powdery nature of the fuel, there was extensive fuel
pullout in a number of samples, which necessitated additional re-impregnation
and repolishing. As-polished photographs were taken of each sample through
the Kollmorgan periscope. A ruler with 1/32 in. as the smallest division was
included in each photograph. Magnification between 4.5 and 5 is indicated in
each photograph. Additional photographs at 103X and 515X were taken with the
sample in the as-polished and etched state. Calibration was made against a
micrometer stage with a smallest division of 0.01 mm. The cladding etch con-
sisted of 55% lactic acid, 19% nitric acid, 7% hydrofloric acid and 19%
water. It was applied from 45 to 120 seconds, depending on the sample. The
fuel etch (85% hydrogen peroxide and 15% sulfuric acid) was applied for 120
to 240 seconds, depending on the sample.

3.   Cladding Metallography

Some concern was expressed that the center defect in Rod PB-PH462-E3 had not
completely penetrated the cladding. As seen in Figure 23, the cladding has
been fully penetrated with a sharp clean hole.

The cladding thickness was measured at a limited number of locations, as
shown in Figure 24. In the neighborhood of the split defect, as much as 16%
wall thinning occurred. No thinning was observed 4 in. beyond the defect
nor at the center defect. The cladding dilation profile is superimposed on
the wall thinning data in Figure 24. As would be expected from a biaxial
stress, the radial strain is similar in magnitude to the thickness strain.
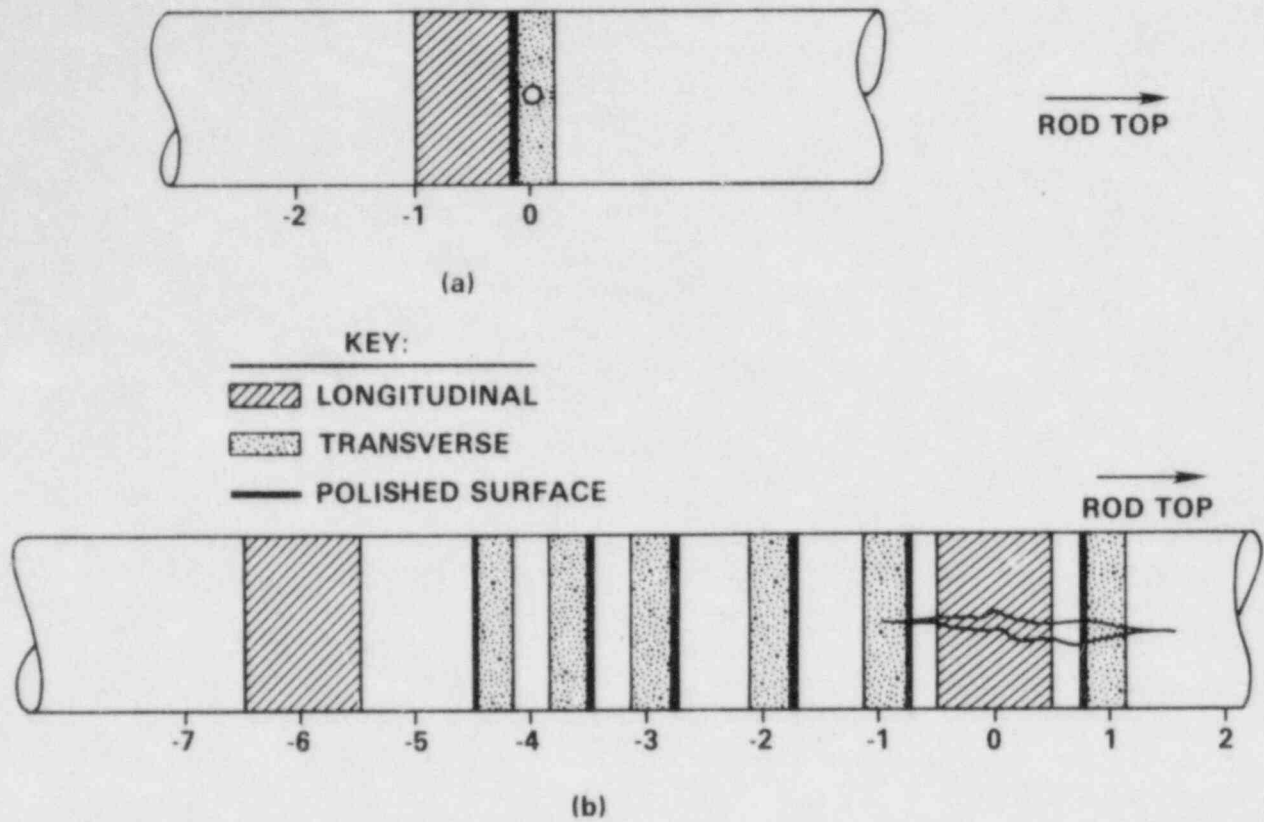
FIGURE 22. Cutting Diagram for Rod PB-PH462-E3. (Original defect location is at 0, and sample locations from the defect are indicated in inches.)
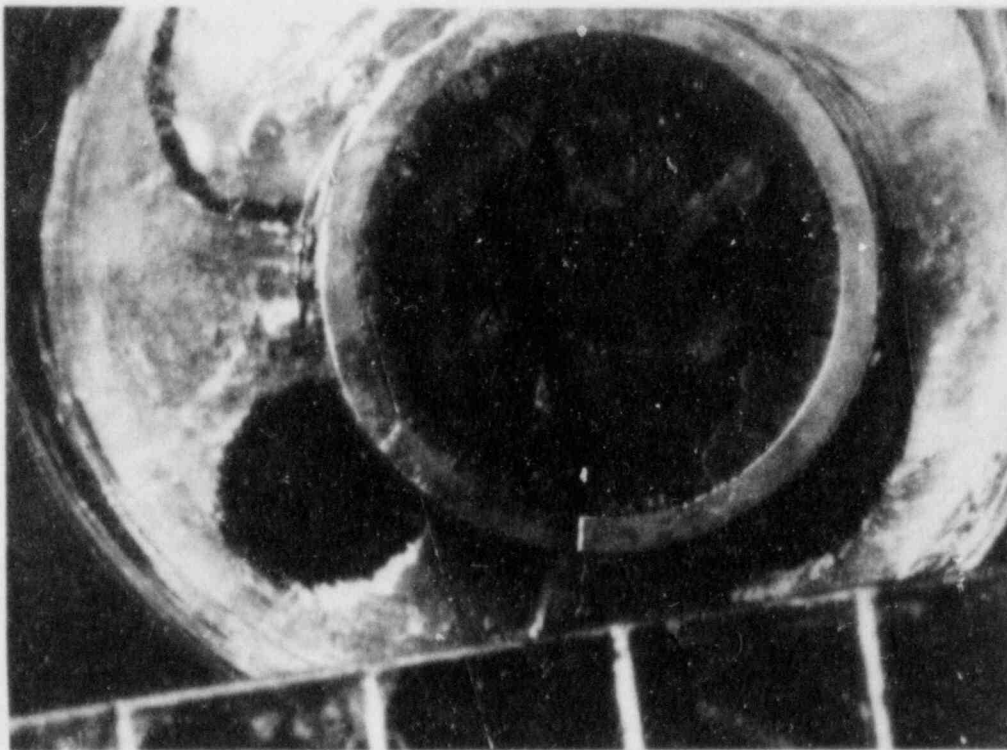
FIGURE 23. As-Polished Transverse Cut Through Center Defect in Rod PB-PH462-E3 After Testing for 5962 Hours at 229°C in Unlimited Air Atmosphere.
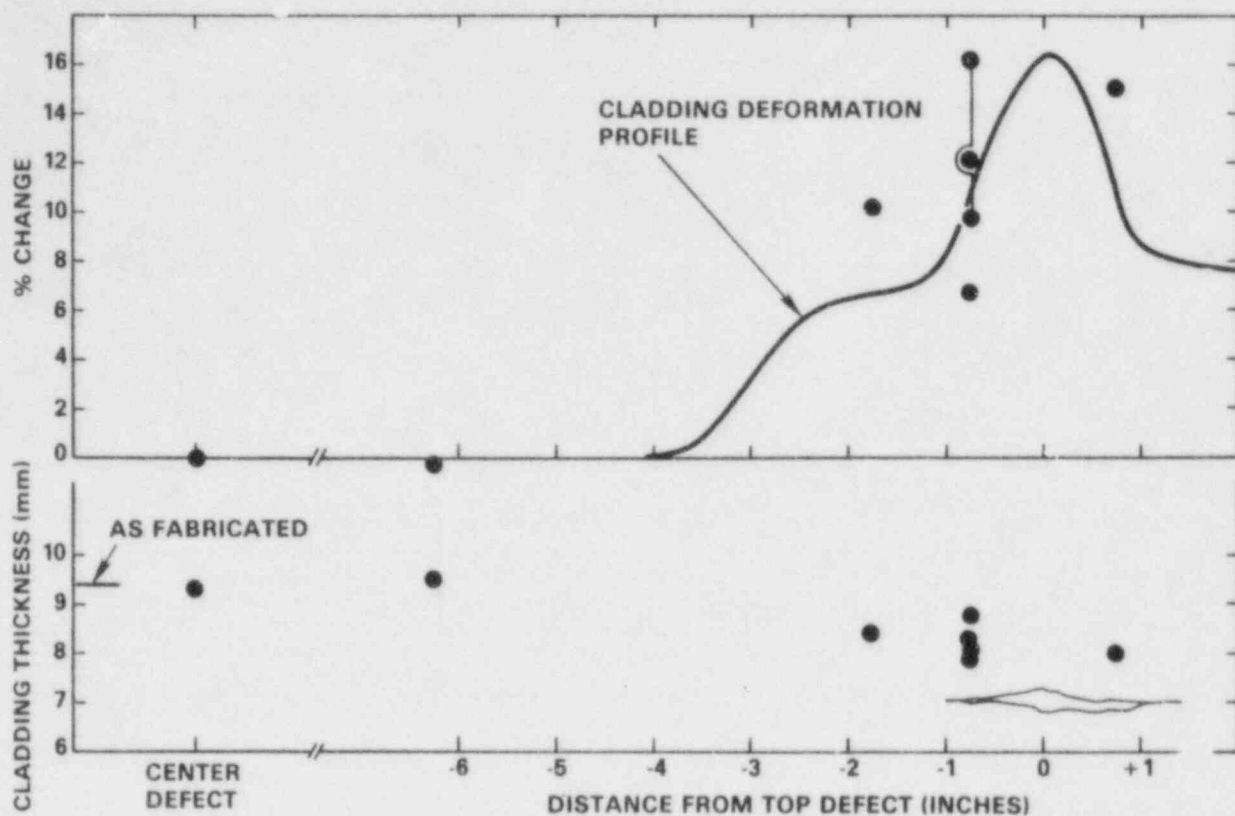
FIGURE 24. Cladding Thickness of Rod PB-PH462-E3 After Testing for 5962
Hours at 229°C in Unlimited Air Atmosphere. (Schematic of split
cladding opening show relative to location 0 of artificial
defect.)

Since the fuel expands to close the cladding gap prior to stressing the
cladding, the closure of the gap is a measure of the extent that degradation
occurred. Measurements of the gap taken near the split defect are given in
Table 23 with typical gap photographs in Figure 25. The as-fabricated clad-
ding gap of 0.15 mm, which allows a volume expansion of the fuel of 5.1%
(~25% conversion of UO_2 to U_3O_8), is essentially completely closed. The
slight gap that does appear is probably due to the difference in the thermal
expansion coefficients of Zircaloy and U_3O_8, which causes the fuel to shrink
relative to the fuel on cooldown.

Insufficient data exists to determine the internal interaction zones or
external oxide layer thickness. As shown in Figure 25b, the internal inter-
action zone is very thin. Illustrations of the external surface oxide are
shown in Figure 26. Six inches below the defect (where there is no cladding
deformation), an oxide layer is present. At 0.075 in. above the defect, the
oxide had spalled due to the substantial cladding deformation. As indicated
by the pretest video examination, there is an axial variation in the surface

67

TABLE 23

FUEL-CLADDING GAP MEASUREMENTS ON ROD PB-PH462-E3
AFTER TESTING FOR 5962 HOURS AT 229°C IN UNLIMITED AIR ATMOSPHERE

Axial Distance* from Upper Defect (in.)	Orientation**	Gap (mm)
-0.75	270	0
-0.75	0	0
-0.75	90	<0.0001
+0.75	90	0.016 - 0.0092
+0.75	270	0.0432
+0.75	180	0.0098
-1.75	0	0.0078
-1.75	90	0 - 0.062

*Positive is towards the top of the rod.
**Zero is the orientation of the original defect.
  Orientations are given in terms of the clockwise
  direction as viewed from the top of the rod.

appearance (Ref. 38). Superimposed on the axial variation is spallation of
the zirconium oxide layer due to cladding deformation. Data are insufficient
to determine if the difference is due to spallation when there is cladding
deformation or to normal oxide layer variations.

The oxidized fuel tended to flow over the cladding surface during the polish-
ing process and to obscure the hydride structure even in the etched state.
The hydrides were clearly present though in the cladding adjacent to the cen-
ter defect (see Figure 27). While remaining rather small, they have aligned
almost completely in the radial direction. This is not the normal circumfer-
ential hydride state usually found in as-irradiated Peach Bottom fuel
(Ref. 38). This reorientation might be indicative of cooldown under stress
caused by swelling fuel.

A number of rather large incipient cracks were found in the cladding adjacent
to the main crack. At 0.75 in. below the defect, a large crack was found at
10°, a small crack at 90° and two small cracks at 165°. When the sample was
repolished, the crack at 165° was no longer evident and a through-the-wall
crack was present at 270°. This is consistent with the external view of the
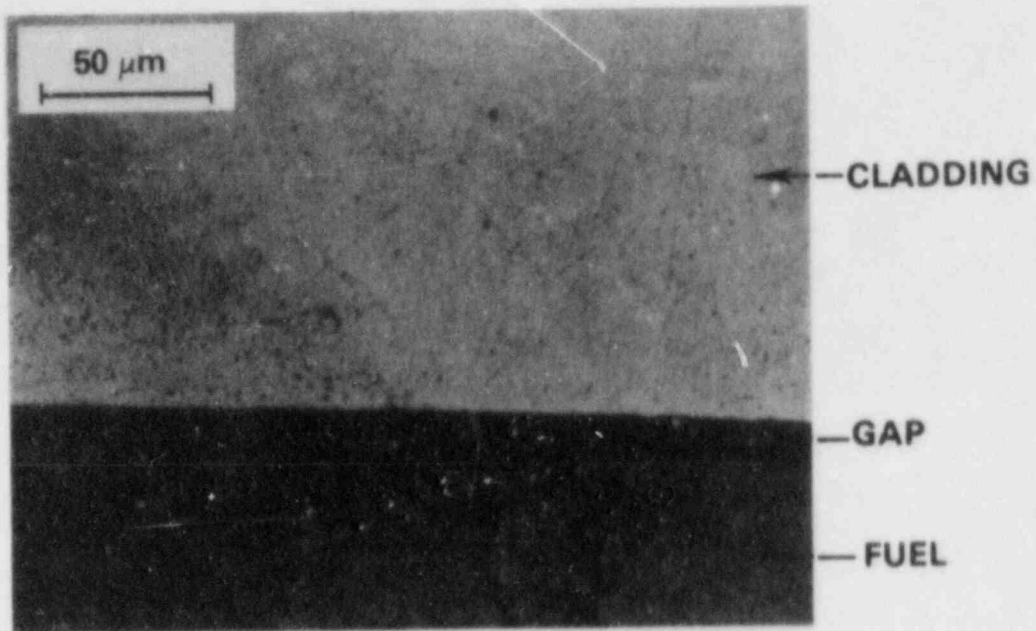
(a)
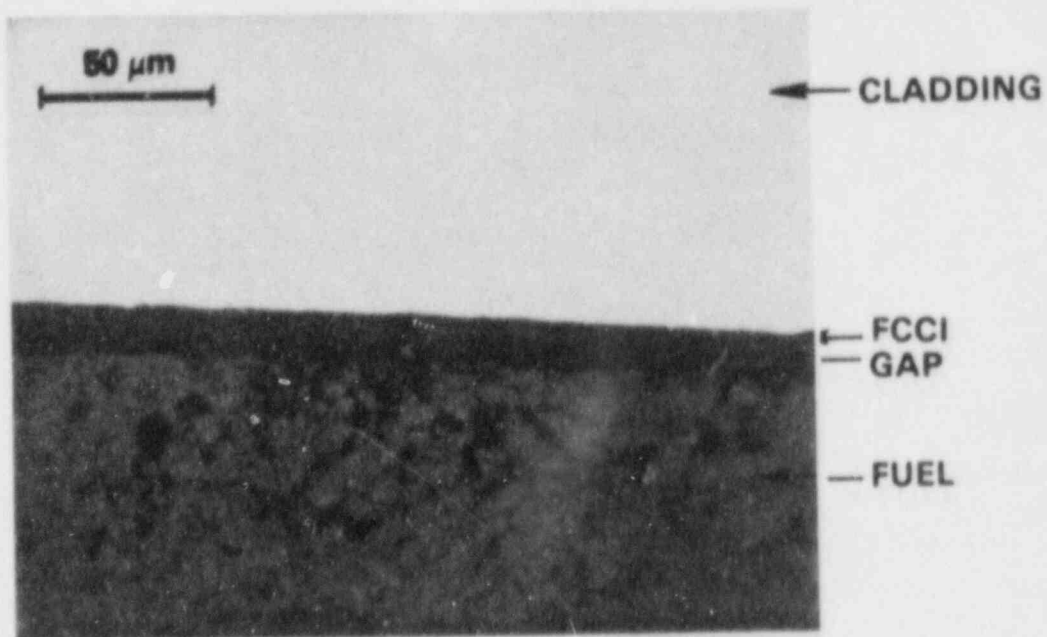
(b)

FIGURE 25. Fuel-Cladding Gap at 0.75 in. Above Split Defect in Rod PB-PH462-E3 After Testing for 5962 Hours at 229°C in Unlimited Air Atmosphere. [As-polished mounts: (a) 90°; (b) 180°.]

CLADDING

EXTERIOR
OXIDE
LAYER

CLADDING

(b)
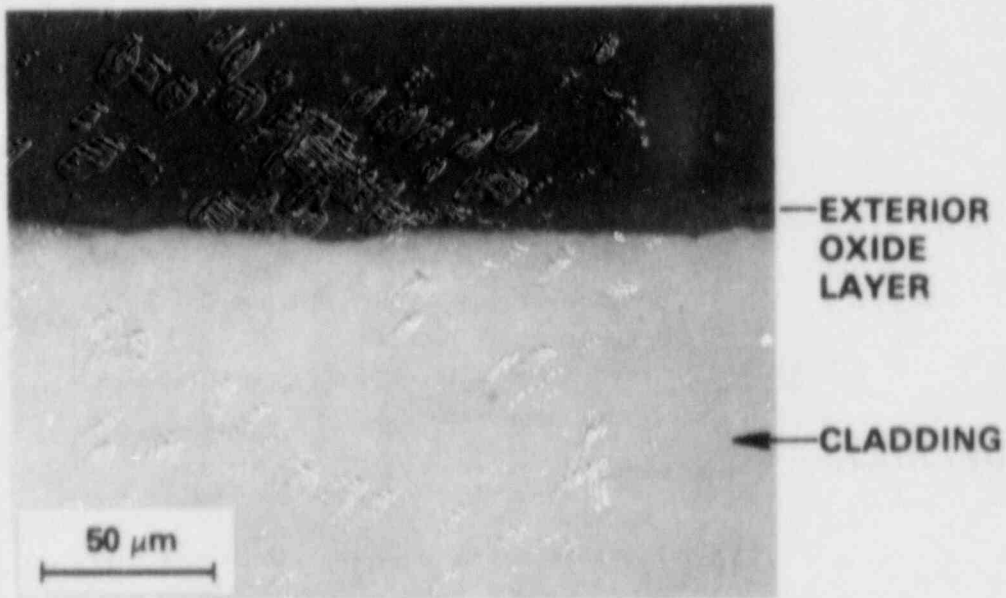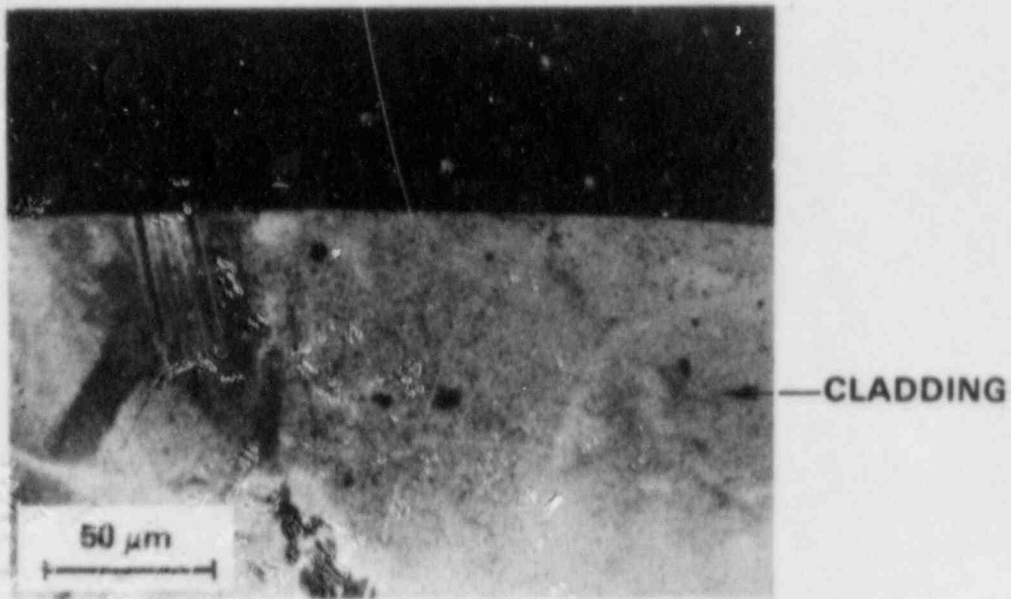
FIGURE 26. External Surface Oxide on Rod PB-PH462-E3 After 5962 Hours at
229°C in Unlimited Air Atmosphere. [Both in as-polished condi-
tion: (a) 90° at +0.75 in. above split defect; (b) 180° at 6 in.
below split defect.]

RADIAL HYDRIDES

247 μm
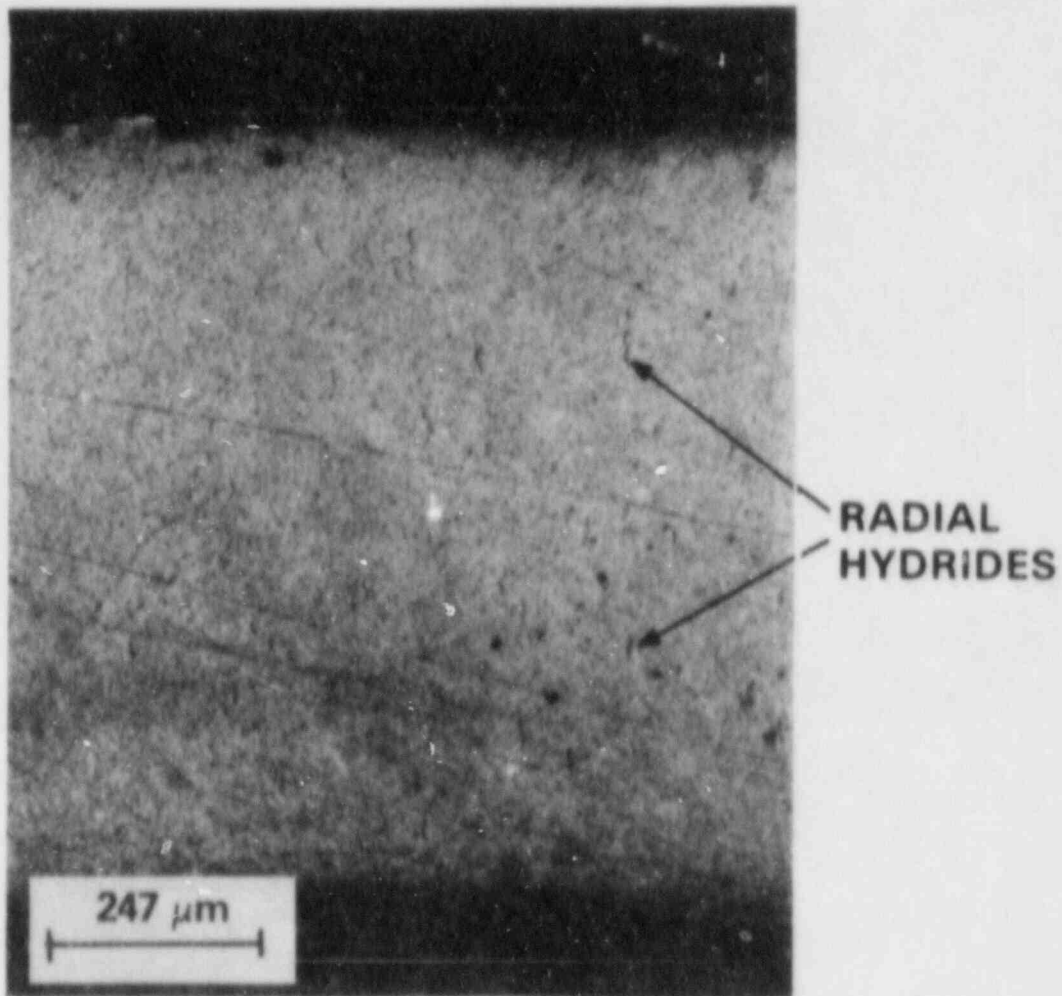
HEDL 8404-173.2

FIGURE 27. Radial Hydride Orientation in Cladding Adjacent to Center Defect in Rod PB-PH462-E3 After Testing for 5962 Hours at 229°C in Unlimited Air Atmosphere. (Etched at 90° orientation.)

71

rod shown in Figure 14. An incipient crack was also found 1.75 in. below the original defect at a 90° orientation. The range of typical defect sizes is shown in Figure 28.

4. Fuel Examination

An ~4.75X as-polished photograph was taken of each metallographic section (see Figures 29 through 31). A number of the samples appear to be etched because of pullout of the friable oxidation products during the polishing procedure. This is more evident the closer the section is to the crack. As an example, Figure 29b shows a section directly under the crack.

By 4-1/2 in. away from the top defect (see Figure 30c) (where there is no cladding deformation), distinct fuel fragments are present, as one would expect in normally irradiated fuel. This is even more evident as you get further away from the defect (Figure 30d). Samples taken in the region of cladding deformation (i.e., closer than 3.5 in. to the upper defect) show no distinct fragment pattern, although one can distinguish where the fragments had been by remnants of the fragment-fragment interface left in the restructured fuel. The pellet-pellet interface is quite clearly defined in Figure 29b by the pellet campher marks at the top and bottom center of the photograph. Since this sample was taken centered on the position of the original defect, it indicates that the original upper defect 138 in. above the bottom of the fuel rod was made at a pellet-pellet interface. In contrast, the defect in the center of the rod was drilled into the side of a pellet, not the pellet-pellet interface. From the gamma scan in Figure 19 it can be seen that the pellets are 0.5 in. long. In Figure 31 the pellet-pellet interface can be seen near the down rod side. This places a second pellet-pellet interface very close to where the fuel fell out of the sample. Since the transverse section through the defect was taken adjacent to the end of the section in Figure 31b, the defect had to be drilled into the side of a pellet.

It is obvious from the appearance of the fuel in Figures 29a through 30b and Figure 31, that there has been fuel restructuring as a result of the test, most likely due to fuel oxidation. The samples were etched with 85% H_2O_2/15% H_2SO_4 and examined at the indicated locations (Figures 29 through 31) prior to removing samples from x-ray diffraction analysis. The fuel structure is illustrated in Figures 32 through 36. Almost all the samples taken from regions where there is cladding dilation exhibited fuel pullout during the polishing process. In some locations, pullout was by individual grain (Figure 32a), and in other areas there was multigrain pullout (Figure 36). This pullout significantly complicated any measurements, such as grain size and axial and radial grain structures. It does indicate a weak intergranular cohesion, possibly due to a surface oxidation process. At the center defect, there was no cladding dilation; but the macrophotographs do indicate that an oxidation process was initiated. In this region, there is fuel that has oxidized to the point of full pullout and that exhibits
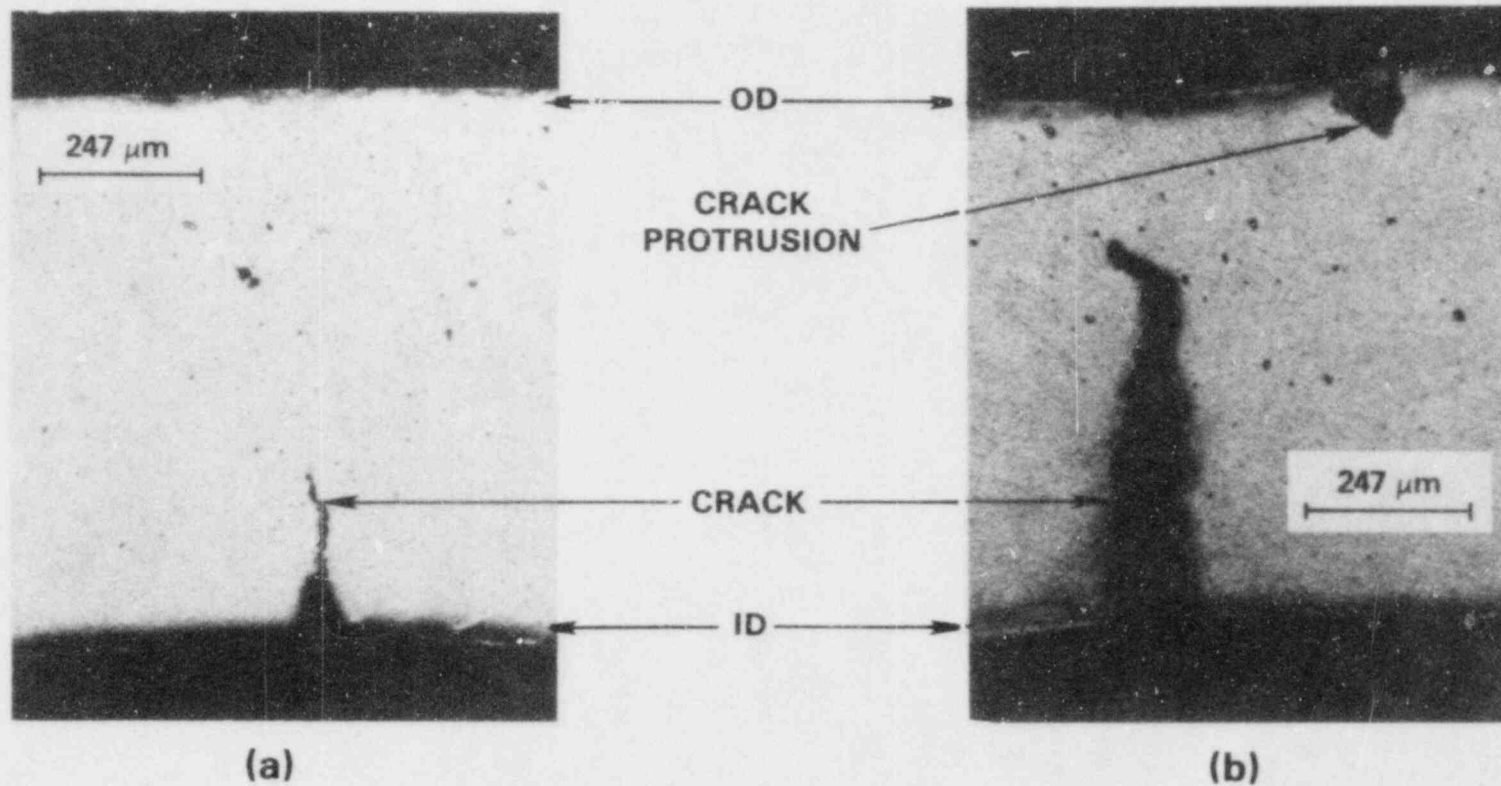
72

FIGURE 28. Typical Range of Incipient Crack Sizes Near Main Crack at Upper Defect on Rod PR-PH462-E3 After Testing for 5962 Hours at 229°C in Unlimited Air Atmosphere. [Etched: (a) 1.75 in. below defect; (b) 0.75 in. below defect.]

HEDL 8404-173.32

TOP OF ROD ────▶

TL

0°

90°

(b) 0 INCHES

(a) +0.75 INCHES

TH

0°

0°

TJ

90°

(d) -1.75 INCHES

(c) -0.75 INCHES
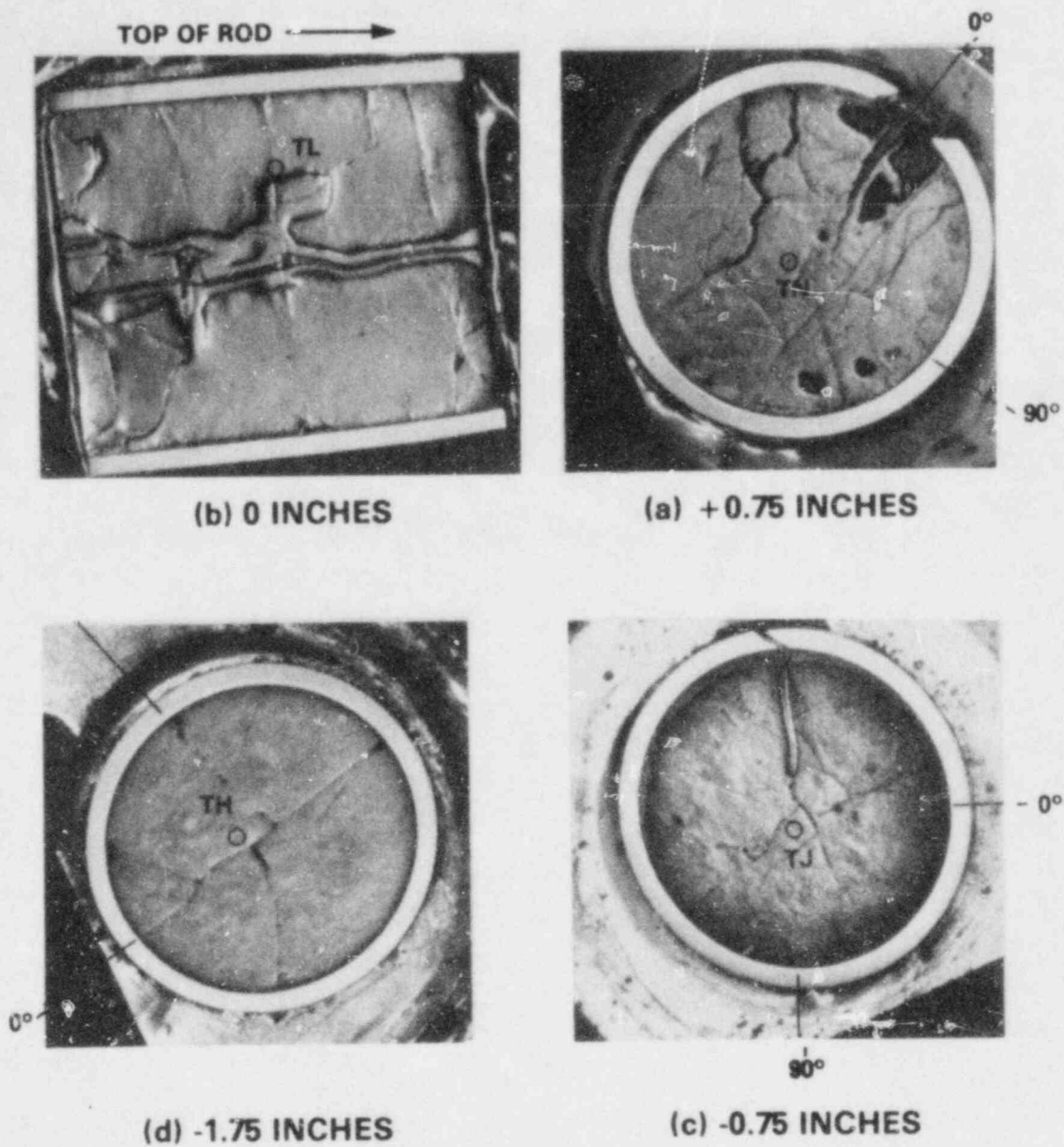
HEDL 8404-173.36

FIGURE 29. As-Polished Ceramographic Sections of Rod PB-PH462-E3 After Testing for 5962 Hours at 229°C in Unlimited Air Atmosphere. (Zero orientation is determined by the position of the original defect. Circled sites are areas where fuel was removed for x-ray analysis.)
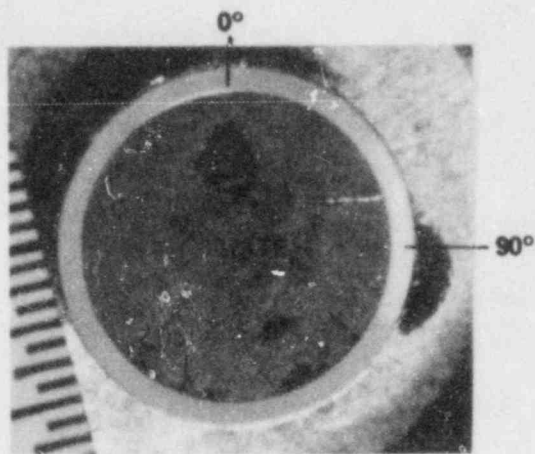
(b) -3 1/2 INCHES
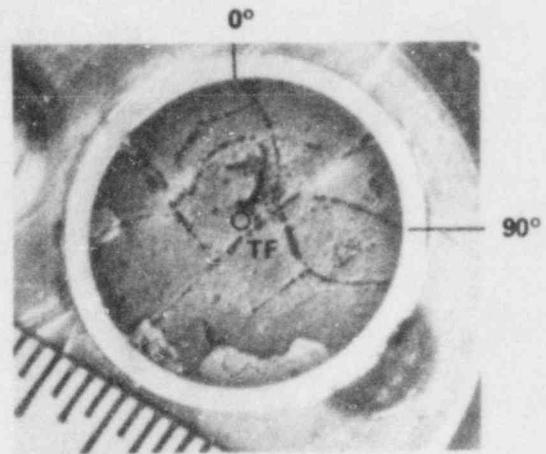
(a) -2 3/4 INCHES
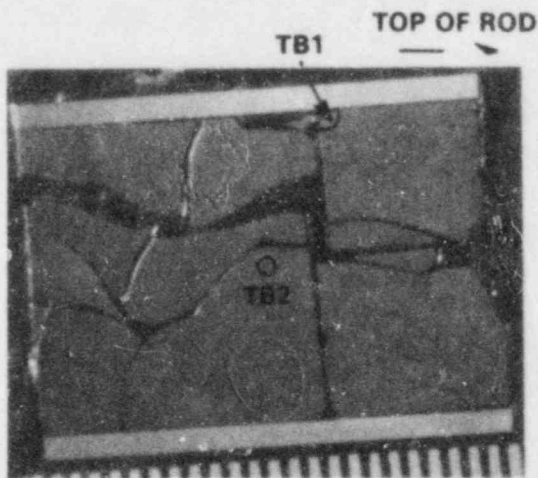
(d) -6 INCHES
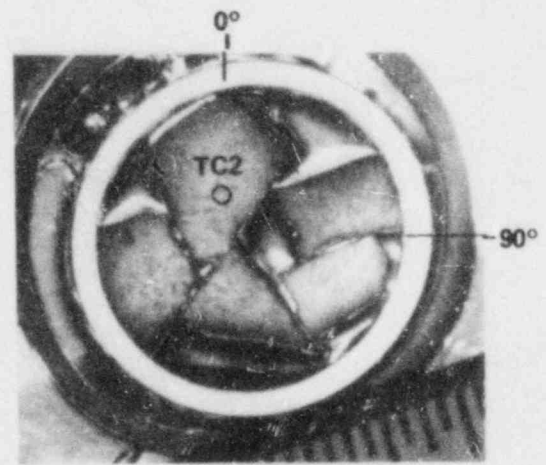
(c) -4 1/2 INCHES

HEDL 8604-173.34

FIGURE 30. As-Polished Ceramographic Sections of Rod PB-PH462-E3 After Testing for 5962 Hours at 229°C in Unlimited Air Atmosphere. (Zero orientation is determined by the position of the original defect. Circled sites are areas where fuel was removed for x-ray analysis.)
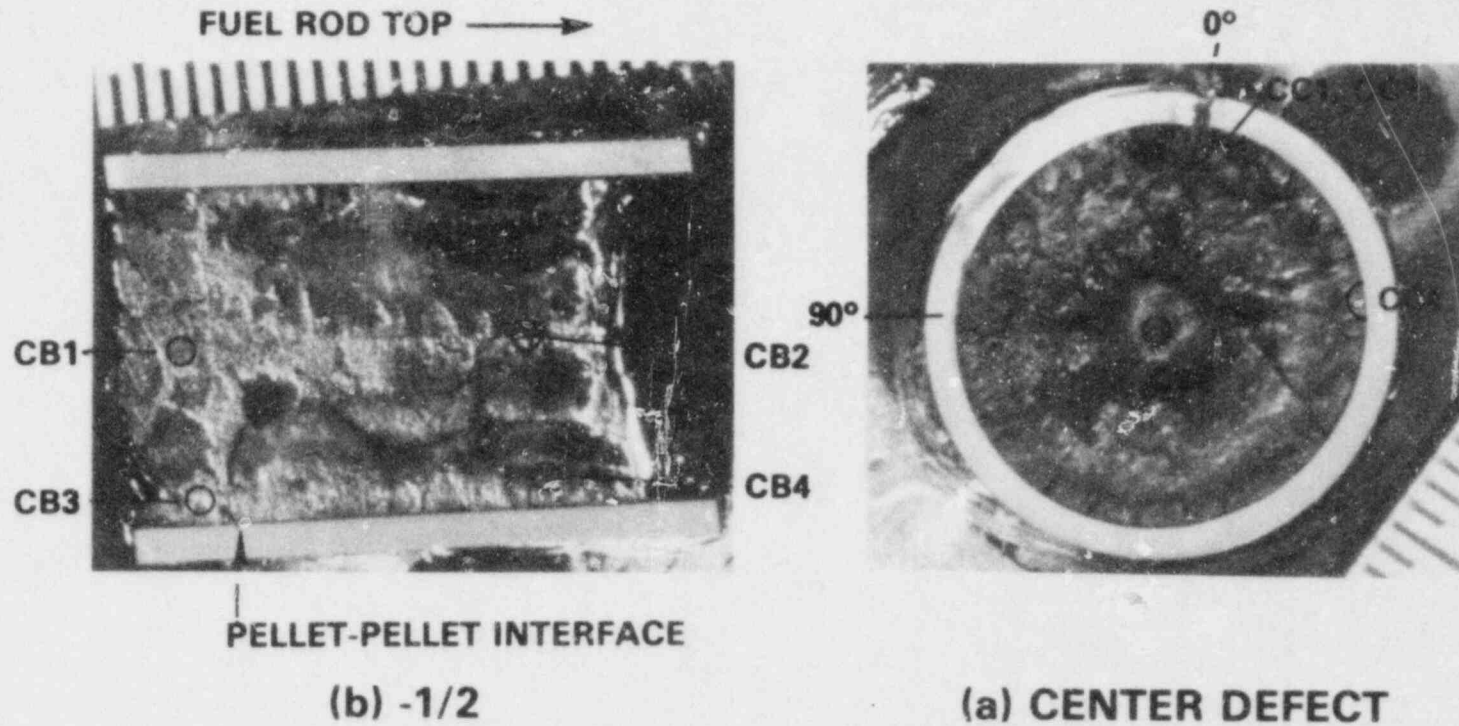
FIGURE 31. As-Polished Ceramographic Sections of Rod PB-PH462-E3 After Testing for 5962 Hours at 229°C in Unlimited Air Atmosphere. (Zero orientation is determined by the position of the original defect. Circled sites are areas where fuel was removed for x-ray analysis.)
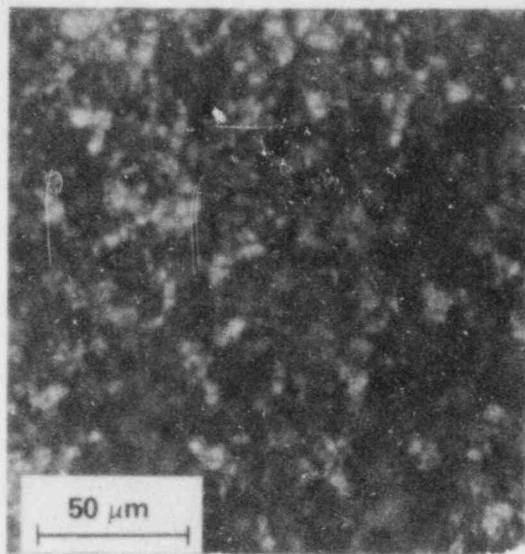
(b) TL, 0 INCHES
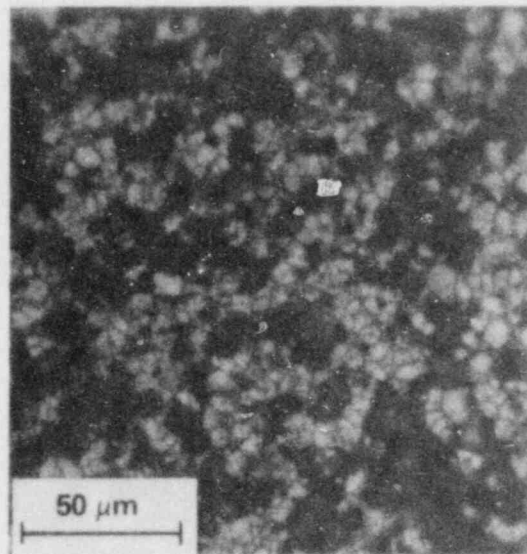
(a) TN, +0.75 INCHES
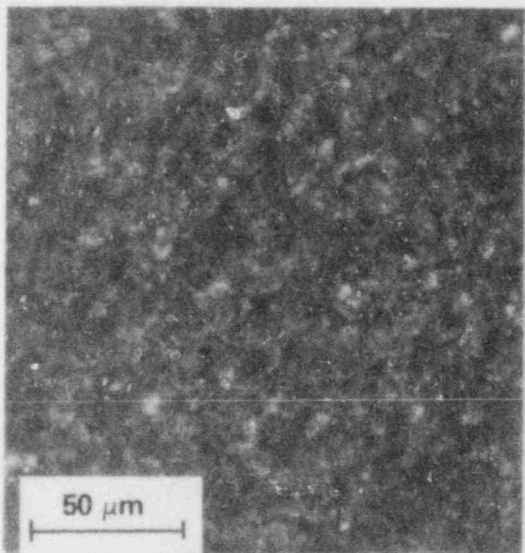
(d) TH, -1.75 INCHES
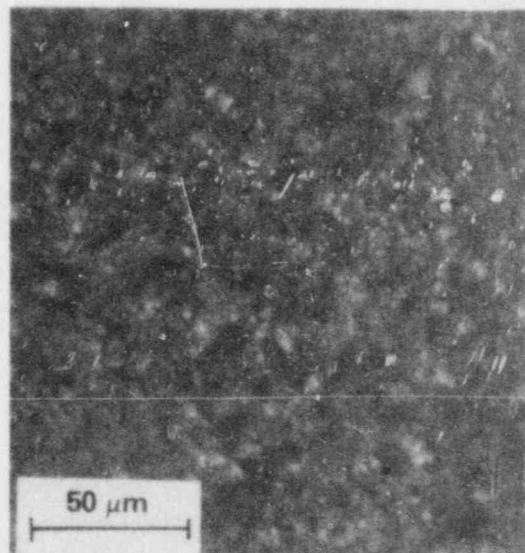
(c) TJ, -0.75 INCHES

HEDL 8404-173.3

FIGURE 32. Micrographs of Etched Fuel Taken from Fuel Centerline Axis of Rod PB-PH462-E3 at Axial Positions Relative to Defect Location After Testing for 5962 Hours at 229°C in Unlimited Air Atmosphere.
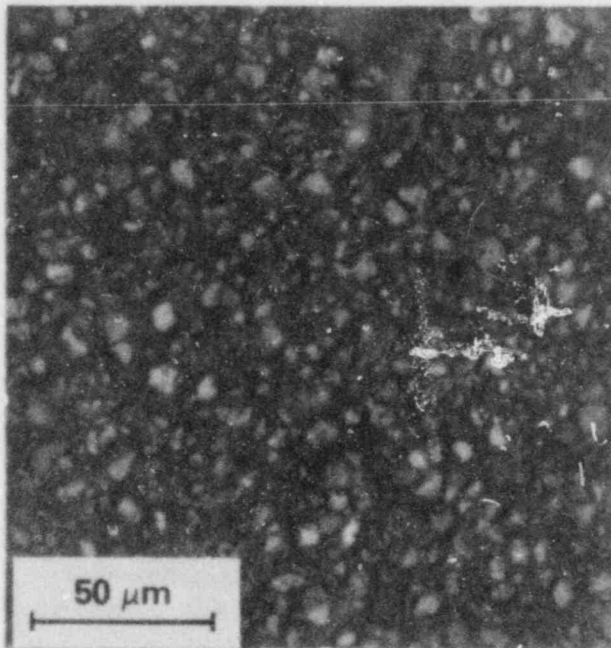
(a) TF, -2 3/4 INCHES
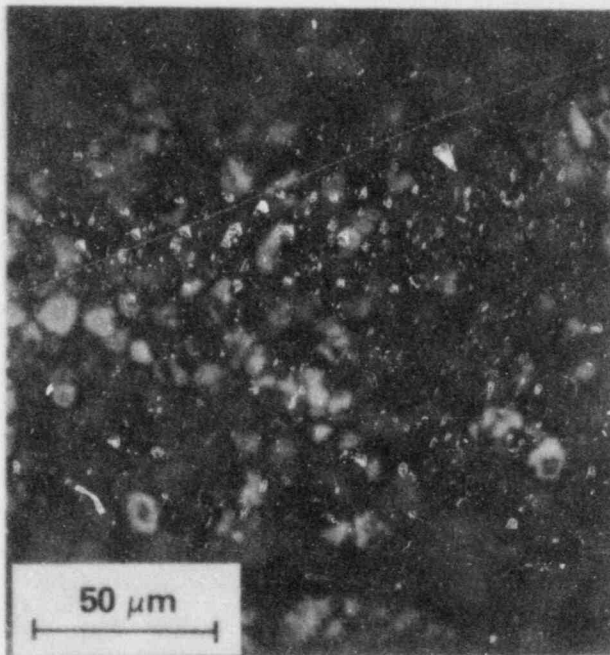
(b) TE, -3 1/2 INCHES

FIGURE 33. Micrographs of Etched Fuel Taken from Fuel Centerline Axis of Rod PH-PH462-E3 at Axial Positions Relative to Defect Locations After Testing for 5962 Hours at 229°C in Unlimited Air Atmosphere.
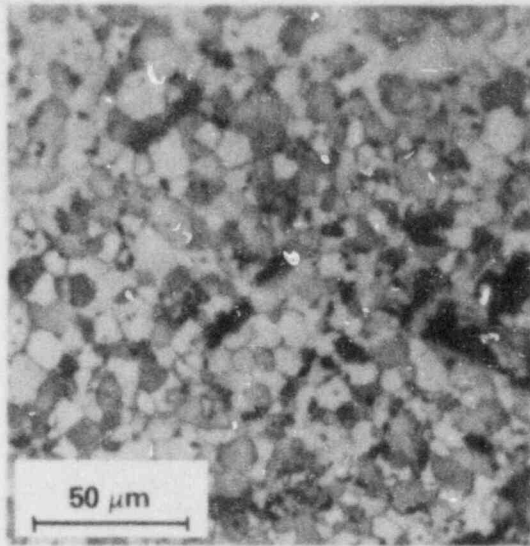
(b) TB1, FUEL EDGE, -6 INCHES
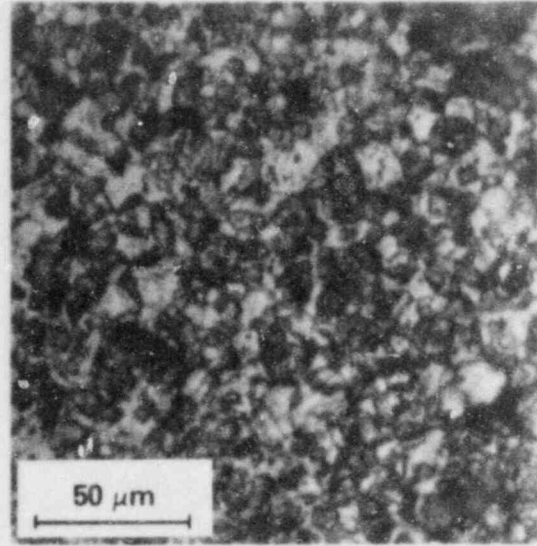
(a) TC2, FUEL CENTERLINE,
-4 1/2 INCHES
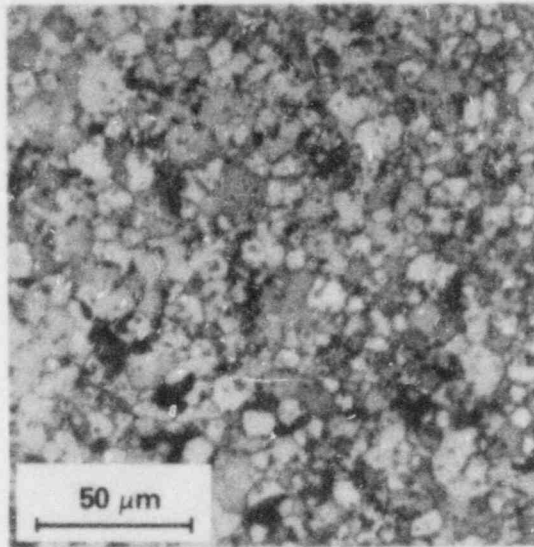
(c) TB2, FUEL CENTERLINE, -6 INCHES

HEDL 8404-173.6

FIGURE 34.   Micrographs of Etched Fuel Taken from Fuel Centerline of Rod
PH-PH462-E3 at Positions Relative to Defect Location After
Testing for 5962 Hours at 229°C in Unlimited Air Atmosphere.
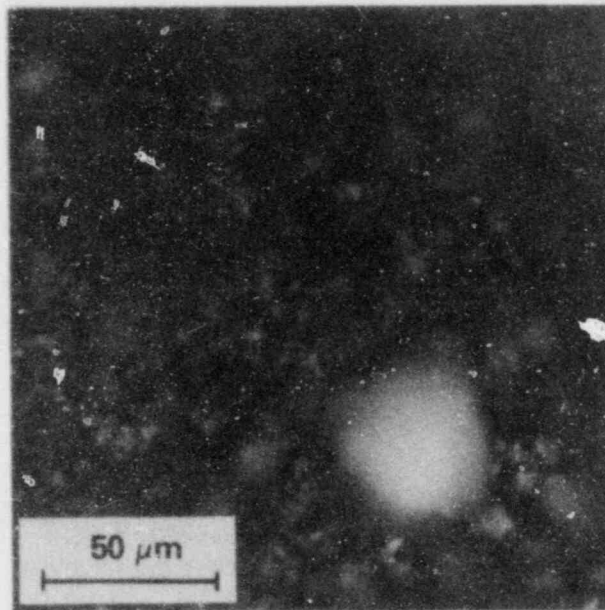
**(a) CC4, NEAR CLADDING,
CENTER DEFECT**
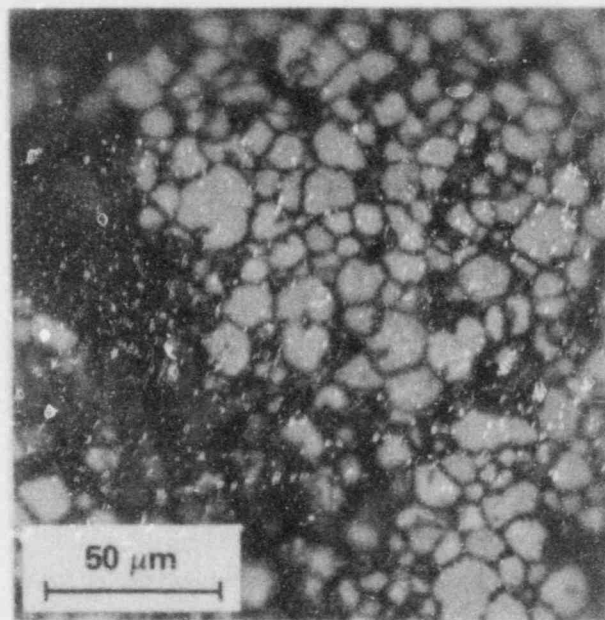
**(b) CC3, FUEL CENTERLINE,
CENTER DEFECT**

HEDL 8404-173.5

FIGURE 35. Micrographs of Etched Fuel Taken from Center Defect of Rod
PB-PH462-E3 After Testing for 5962 Hours at 229°C in Unlimited
Air Atmosphere.

80
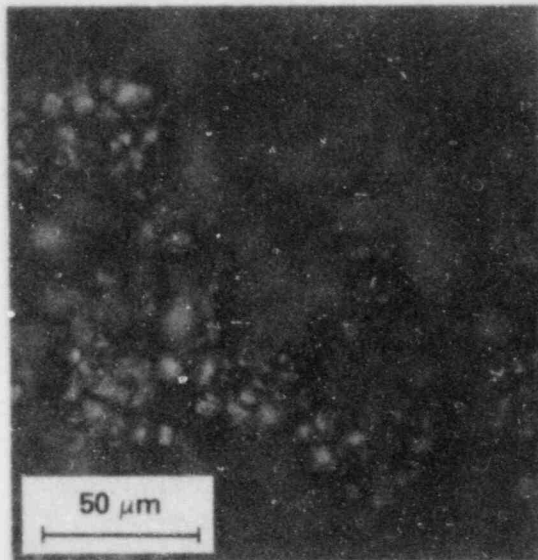
(a) CB1, CENTERLINE, -3/4 INCH   (b) CB2, CENTERLINE, -1/4 INCH
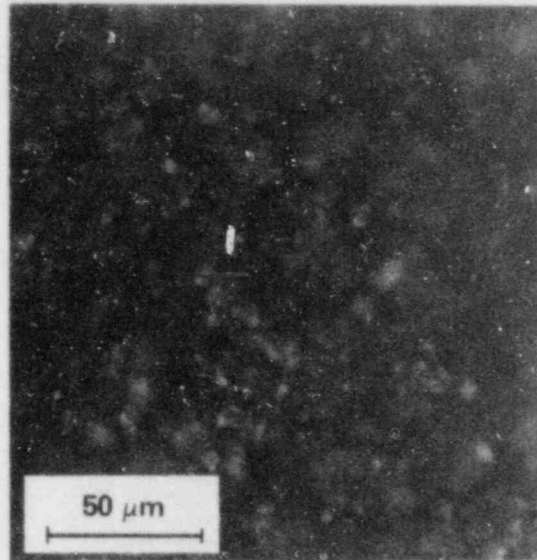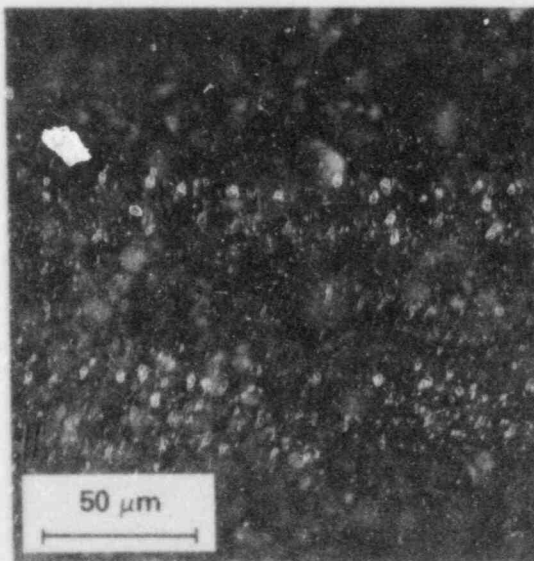
(c) CB3, FUEL EDGE, -3/4 INCH   (d) CB4, FUEL EDGE, -1/4 INCH
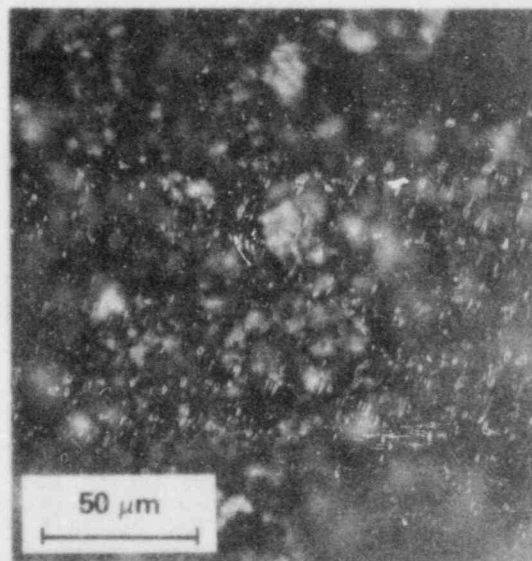
HEDL 8404-173.4

FIGURE 36. Fuel Micrographs of Etched Fuel Taken from Longitudinal Metal-
lographic Section Adjacent to Center Defect in Rod PB-PH462-E3
After Testing for 5962 Hours at 229°C in Unlimited Air
Atmosphere.

81

significant intergranular attack (see Figure 35b). In contrast, samples taken from regions with no cladding dilation (see Figure 34) show a tight grain structure with no surface layers, a typical irradiated UO_2 structure.

At each of the locations indicated on the macrophotographs (Figures 29 through 31), samples were removed for x-ray determination of the fuel structure. The powder diffraction method previously described was used. The results in terms of "d" spacings are given in Tables 24 and 25 along with the x-ray spectrum for the identification standards. As expected, in many instances there was no clear-cut single oxide but rather a mixture of oxides. Only a gross quantitative identification was made (summarized in Table 26).

The oxide structures can be directly correlated with the cladding dilation near the top defect. As seen in Figure 37, the highest dilation at the upper defect occurs when there is only U_3O_8 and steadily decreases until there is no dilation when there is only UO_2 present. At the center defect where there is no dilation, the U_3O_8 occurs in mixtures with U_3O_7 and U_4O_9. At the center defect, where the higher oxides are just starting to form, there is no clear-cut oxidation front (Figure 38).

TABLE 24

X-RAY DIFFRACTION "d" VALUES AND RELATIVE INTENSITIES FROM SAMPLES TAKEN NEAR UPPER SPLIT DEFECT ON ROD PB-PH462-E3 AFTER TESTING FOR 5962 HOURS AT 229°C IN UNLIMITED AIR ATMOSPHERE

"d" Space	Standards* UO2	U4O9	U3O7	α-U3O8	β-U3O8	UO3	Samples TN	TL	TJ	TH	TF	TE2	TC2	TB1	TB2
4.157						58									
4.150					100					85					
4.142				66											
4.137							100								
4.134								100							
4.132									100						
3.530					35										
3.421						100									
3.410										100					
3.406				100											
3.400							70								
3.394								100							
3.389									60						
3.350					25										
3.171													100		
3.166															100
3.161												100			
3.157	100														
3.151													100		
3.144											100				
3.140		100													
3.137								5		50					
3.132							5		10						
3.120			90												
2.745												35			
2.739														35	
2.735	48														70
2.729													35		
2.721		45												15	
2.710			60												
2.690					20										
2.641						72									
2.636													5		
2.631				65											
2.626								25							
2.622							60		80						
2.620										50					
2.610															
2.600					45										
2.135													5		
2.078						7									
2.074									10						
2.071			9		25			10							
2.068							25				35				
2.004					30										
1.990															
1.975					25										
1.967			21												
1.954							20	10							
1.950															

TABLE 24 (Cont'd)

"d" Space	UO_2	U_4O_9	U_3O_7	α-U_3O_8	β-U_3O_8	UO_3	TN	TL	TJ	TH	TF	TE2	TC2	TB1	TB2
				Standards*						Samples					
1.942														50	
1.938													60		65
1.934	49														
1.928													40		
1.926											50				
1.924		50													
1.918			90												
1.907					10										
1.800					18										
1.784					16	25									
1.776				23			32								
1.773									60				5		
1.770				28	25										
1.767							50	20			65				
1.710						10									
1.703				9											
1.680															
1.654														50	60
1.652													50		
1.649	47														
1.643												25			
1.641		50								40					
1.636			100												
1.582							12				10		15	5	15
1.579	13														
1.575				11						5					
1.574												15			
1.571		16													
1.568										5					
1.567			53												
1.438					10										
1.426				10			15	5							
1.382							5	5							
1.368	9												15	5	15
1.360		10													
1.359			30											30	
1.352											10				
1.316										5					
1.280										5					
1.258													30		
1.255	18														20
1.253															
1.251													20		
1.248		30													
1.226														5	15
1.223	15												25		
1.217		25													
1.116	13														
1.111		20													
1.052	15														

*Joint Committee for Powder Diffraction Standards, International Center for Diffraction Data, Swarthmore, PA (1982). Reference File Card Nos.: UO_2 (5-550), U_4O_9 (20-1344), U_3O_7 (9-206), α-U_3O_8 (31-1425), β-U_3O_8 (23-1460), UO_3 (31-1416).

TABLE 25

X-RAY DIFFRACTION "d" VALUES AND RELATIVE INTENSITIES FROM SAMPLES TAKEN NEAR CENTER DEFECT ON ROD PB-PH462-E3 AFTER TESTING FOR 5962 HOURS AT 229°C IN UNLIMITED AIR ATMOSPHERE

"d" Space	Standards*						Samples							
	UO_2	U_4O_9	U_3O_7	$\alpha\text{-}U_3O_8$	$\beta\text{-}U_3O_8$	UO_3	CC1	CC2	CC3	CC4	CB1	CB2	CB3	CB4
4.157						58								
4.150					100									
4.142				66						65	35			
3.530					35									
3.421						100								
3.406				100						25				
3.398										45				
3.350					25									
3.200										100				
3.171												100		
3.157	100													
3.153														100
3.149							100							
3.140		100												
3.135										100	80			
3.132								100					100	
3.120			90											
2.735	48		90											
2.733												50		
2.729														70
2.721		45							30					
2.716								25					50	
2.713								25	20					
2.710			60											
2.690					20									
2.641						72								
2.631				65						25				
2.615											15			
2.610														
2.600					45									
2.078						7								
2.074									5					
2.071			9		25									
2.004					30									
1.990														
1.975					25									
1.967			21											
1.950														
1.934	49													
1.932												40		
1.928														80
1.924		50					45		25				60	
1.922											10			
1.920								70						
1.918			90							45				
1.907					10									
1.800					18									
1.784					16	25								
1.776				23		32								
1.775										30				
1.770				28	25									

TABLE 25 (Cont'd)

"d" Space	Standards*						Samples							
	UO$_2$	U$_4$O$_9$	U$_3$O$_7$	α-U$_3$O$_8$	β-U$_3$O$_8$	UO$_3$	CC1	CC2	CC3	CC4	CB1	CB2	CB3	CB4
1.767										25				
1.710						10								
1.703			9											
1.680														
1.649	47													
1.646												45		40
1.641		50					45	75						
1.639											35		15	
1.636			100						45	30				
1.582						12								
1.579	13													
1.575				11			20		30			20		
1.574														10
1.571		16												
1.569								35						
1.567			53											
1.438					10									
1.426				10						5				
1.368	9													
1.360		10												
1.359			30								15			
1.255	18													
1.253														15
1.251							15					30		
1.248		30							30		50			
1.223	15													10
1.219												10		
1.217		25					15	5			35			
1.116	15													
1.111		20												
1.052	15													

*Joint Committee for Powder Diffraction Standards, International Center for Diffraction Data, Swarthmore, PA (1982). Reference File Card Nos.: UO$_2$ (5-550), U$_4$O$_9$ (20-1344), U$_3$O$_7$ (9-206), α-U$_3$O$_8$ (31-1425), β-U$_3$O$_8$ (23-1460), UO$_3$ (31-1416).

TABLE 26

OXIDE IDENTIFICATION BY X-RAY ANALYSES

Sample ID	Axial* Location (in.)	Radial** Location	Oxide Major	Oxide Minor
TN	+0.75	0	α-U_3O_8	Hint β-U_3O_8
TL	0	R/2	α/β-U_3O_8	U_4O_9
TJ	-0.75	0	α-U_3O_8	Weak U_4O_9
TH	-1.75	0	β-U_3O_8	
TF	-2.75	0	U_4O_9	
TE2	-3.5	0	UO_2	Some U_4O_9, Weak U_3O_8
TC2	-4.5	0	UO_2	
TB1	-6	R	UO_2	
TB2	-6	0	UO_2	
CC1	Center Defect	R-0°	U_4O_9, UO_2	
CC2	Center Defect	R-0°	U_4O_9	U_3O_7
CC3	Center Defect	0	α-U_3O_8	U_4O_9, U_3O_7
CC4	Center Defect	R-270°	U_4O_9	α/β-U_3O_8, U_3O_7
CB1	-3/4	0	U_4O_9	U_3O_7
CB2	-1/4	0	UO_2	U_4O_9
CB3	-3/4	R	U_4O_9	
CB4	-1/4	R	UO_2	U_4O_9

---

*Minus is toward bottom of rod; plus is toward top of rod (measured with respect to the defect).

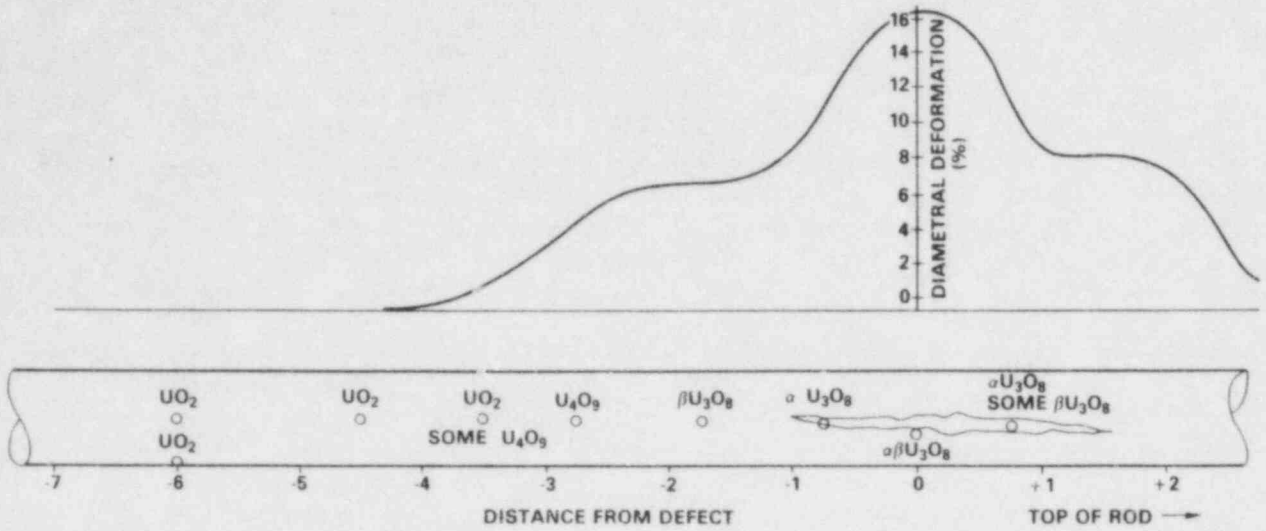**Zero is the center of the fuel; R is the exterior surface of the fuel.

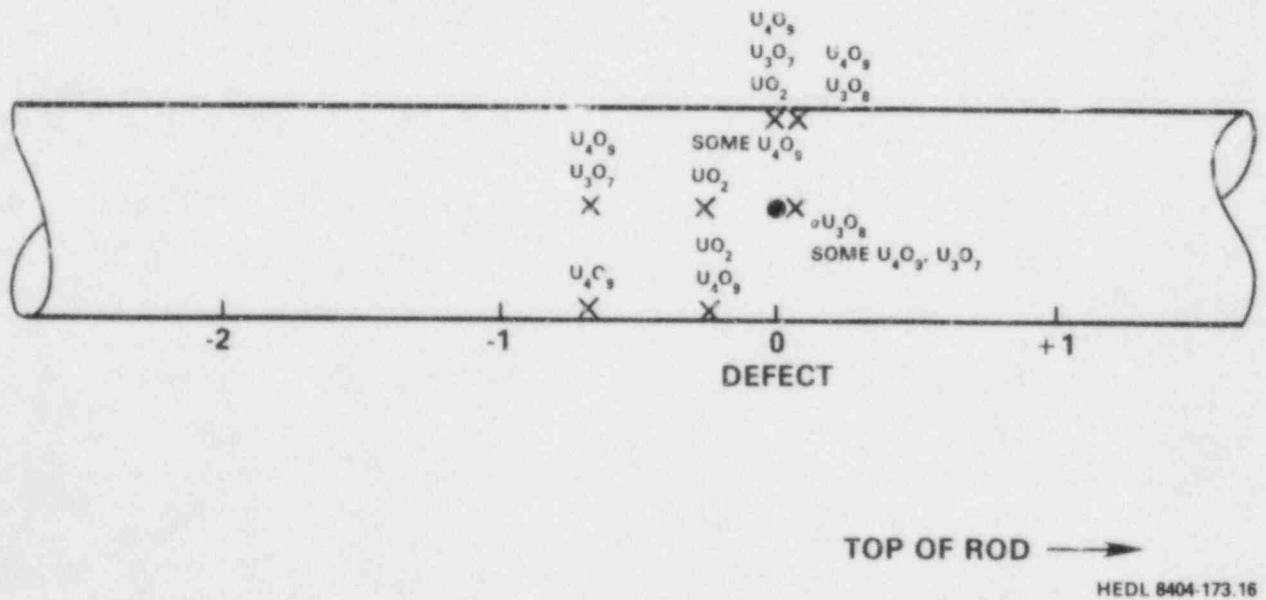FIGURE 37. Fuel Oxidation States as a Function of Distance from Top Defect and Compared With Fuel Rod Dilation.

FIGURE 38. Fuel Oxidation States as a Function of Distance from Center Defect.

VI. DISCUSSION OF RESULTS

A. ROD PERFORMANCE

Of the eight rods tested, four contained two drilled defects each. After
5962 hours of testing at 229°C, the two defected rods that were tested in
an inert argon atmosphere showed no signs of fuel oxidation as would be
expected. Of the two rods tested in unlimited air, the H. B. Robinson PWR
rod showed no signs of deterioration of either of the defects when examined
visually, by gamma scanning, or by diametral measurements. The Peach Bottom
BWR rod developed an ∿0.5-in. long crack at the defect near the upper end
of the fuel column by 2235 hours. The crack growth after 5962 hours was
accompanied by diametral growth as large as 16%, which extended beyond the
crack tip. The defect in the center of the fuel column of the Peach Bottom
rod showed no signs of deterioration when visually examined, gamma scanned
or diametrally measured.

Early studies suggested that below 250°C fuel should not convert to U_3O_8,
hence a defect should not split open. White et al. (Ref. 65) indicated that
spallation of unirradiated UO_2 should start at about 250 hours at a weight
gain of ∿2 mg/cm^2. They also indicated that irradiated spent fuel should
reach this weight gain earlier, hence spall earlier, than unirradiated UO_2.
Simpson and Wood (Ref. 63) found that unirradiated UO_2 started spalling at
230°C in ∿900 hours and at 250°C irradiated fuel spalled faster than
unirradiated fuel. Hastings and Novak (Ref. 64) also found that irradiated
fuel oxidized faster than unirradiated fuel. With predictions of spallation
and U_3O_8 formation starting in less than 250 hours, why did only one of four
defects show any outward appearance of oxidation after 5962 hours?

Filter analysis indicated air was circulating in the capsule containing the
PWR rod, and obviously air was in the capsule containing the BWR rod since
the upper defect continued to grow. Stack monitoring indicated that at least
the center defect in the H. B. Robinson rod was penetrating the cladding.
Penetrations of the upper defect can only be confirmed after destructive
examination of the rod. Metallographic examination (Figure 23) indicated
that the center defect in the Peach Bottom rod was penetrating the cladding.
Nothing found during the metallographic examination indicated a cladding
abnormality that should cause premature splitting near the upper defect in
the Peach Bottom rod. While no evidence of crack propagation exists at the
center defect in Rod PB-PH462-E3, there is evidence that the fuel itself had
passed the incubation stage for weight gain and conversion to U_3O_8. X-ray
analyses of the fuel under the center defect indicated that the oxidation
process began with U_4O_9 and that some U_3O_8 had formed. It was also evident
from the hydride reorientation near the center defect (see Figure 27) and
from gap measurements that the fuel was starting to put stress on the
cladding by 5962 hours.

Examination indicated that the upper defect in the Peach Bottom rod was
placed directly above a pellet-pellet interface, while the center defect was
above the side of a pellet. The positions of the defects in the

H. B. Robinson rod are not exactly known; but if one considers a reasonable pellet-pellet interface of 1.0 mm and a 15.2-mm long pellet, there is only a 14% probability of at least one of the defects in the H. B. Robinson rod being over the pellet-pellet interface. The pellet-pellet interface with its dished pellet ends allows much freer access of air to the fuel than a nominal 0.15-mm fuel-cladding gap (Ref. 70). Likewise, in the H. B. Robinson rod with its creepdown 0.03-mm gap (Ref. 70), the pellet-pellet interfaces present a much easier access of air to the fuel. In all likelihood, the upper defect in the Peach Bottom rod was subjected to incubation and oxidation of the fuel, which had as free access to air as bare fuel. Plotting the split length up and down the rod at 2235 hours and 5962 hours and assuming that the rate of crack propagation is linear with time (which probably is inaccurate), cladding splitting should have started at ~1200 ± 500 hours. Fuel oxidation, which had to incubate earlier than cladding splitting, may well have been in the range of <900 hours, as predicted by studies on bare fuel. On the other hand, when the defect was over the pellet side, the cladding and the juxtaposition of the fuel pellet side retarded the access of oxygen to the fuel; hence incubation occurred at a slower rate than would be expected for bare fuel with free access to air.

Assuming that rods with gross breaches are screened, if a rod is put in storage with an undetected breach, the breach will most likely be a small SCC crack. These cracks usually occur at a pellet-pellet interface where the in-reactor stress is high and where more Cs and iodine are released from the pellet. The behavior of the upper defect in the Peach Bottom rod should not be considered a fluke but rather, quite possibly, the type of behavior of more than 7% of the rods with an undetected breach that are stored in an air atmosphere at 230°C.

B.   DILATION AS A MEASURE OF OXIDATION

Novak et al. (Ref. 66) found that, until there was sufficient oxidation to produce 2% cladding deformation, a crack would not propagate. They estimated that 15% conversion of UO_2 to U_3O_8 (0.6% weight gain) was necessary to produce 2% dilation and thus established 0.6% weight gain as a criterion for incubation of spent CANDU fuel. As indicated in Figure 37, ~6.5% strain is necessary to propagate a crack in the Peach Bottom fuel. A similar strain criterion could be determined from the profile at 2235 hours (Figure 16). The difference between the strains at crack propagation for the CANDU fuel and for the BWR fuel is not surprising. Assuming that the oxidizing fuel puts the same pressure on the cladding of the BWR and CANDU rod, the hoop stress is almost 2.5 times higher in the CANDU rod cladding than in the BWR cladding.

Johnson et al. (Ref. 67) claim that the oxidation front in the BWR rod at 325°C coincides very closely with the cladding deformation and cladding cracking. A similar effect was found by Boase and Vandergraaf (Ref. 22). As seen in Figure 37, in the present test the oxidation front measured by x-ray diffraction travels considerably ahead of the crack tip. The front,

somewhere between -2 and -3 in. from the split defect after 5962 hours, corresponds to ~6.5% cladding deformation. Therefore, ~6.5% cladding strain will be used as a measure of oxidation front position. From Figure 16, the U_3O_8 oxidation front at 2235 hours extended in one direction between 0.5 and 1 in. from the defect. If a constant linear rate with only two points was assumed, a velocity of the oxidation front between 2 and 3×10^{-5} cm/min was found with an incubation period of ~1000 hours. Based on the relationship between the UO_2 fraction converted to U_3O_8 and the cladding strain (developed in Appendix C), 6.5% strain corresponds to essentially 100% conversion of UO_2 to U_3O_8. Figure 39 shows the percentage of UO_2 converted to U_3O_8 as a function of cladding strain. (The conversion is non-zero at zero strain since the fuel-cladding gap can accommodate some fuel oxidation.) Even at 2% strain, there is 50% conversion for the BWR rod. If 50% instead of 100% conversion is used as a criterion, the incubation period shortens but the steady-state rate does not change. As seen in Figure 40 this oxidation rate agrees quite well with the velocity front determined by Boase and Vandergraaf (Ref. 22).

C. CRUD AND FUEL DISPERSAL

Compared to the amount of fuel in the vicinity of the split cladding, very little fuel fell out of the rod. The fact that the particulate stays in the rod may be due to the horizontal orientation of the test. It appears that, as the UO_2 oxidizes to U_3O_8, the crystal structure is disrupted, causing a fuel powder to form. While this expanding fuel is stressing the cladding, the resistance of the cladding is acting as a compacting force on the fuel powder. As indicated by the capsule smear results in Table 14, some of this compact fuel falls out of the crack as a powder but most stays in the rod. Further cladding splitting with longer times would probably increase the fallout. When chunks of the compacted fuel are removed from the rod, they are easily broken.

A partial sample of the swab from the capsule containing the spent Peach Bottom rod contained more than 67 µg of fissile material. Many times more material was released into the capsule since only a fraction of the swab sample was counted and much loose powder was lost in the sampling process. The filters on this capsule (Figure 9) trapped only ~0.2 µg in the respirable range of 2 to 15 µm. This indicates that, while fuel is released from the rod, it does not become easily airborne. Defective rods tended to release ^{137}Cs to the capsule, but only fractions of a percent of the cesium became airborne in the respirable range.

Crud and ZrO_2 spallation were appreciable only with significant cladding deformation. This is substantiated by the post-test smears, which collected only 500 µCi of ^{60}Co after 5962 hours (~2% to 7% of the calculated crud). Like the fuel, this crud did not tend to become airborne. Less than 0.01 µCi in the respirable range was found on the filters.
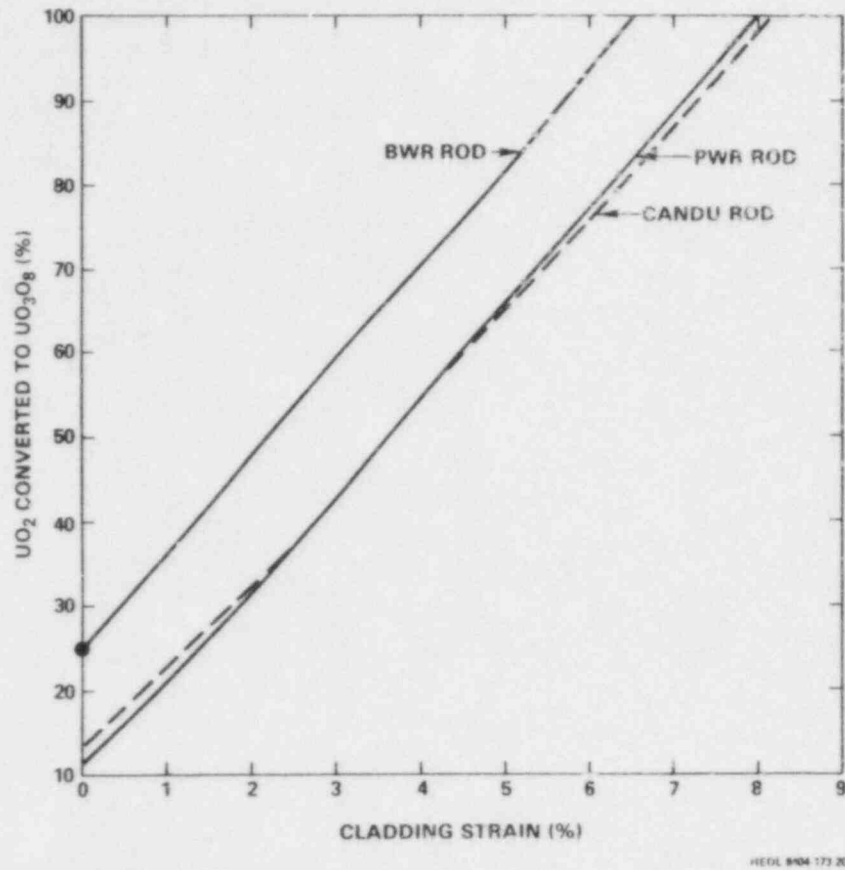
FIGURE 39. Cladding Strain as a Function of the Fraction of UO_2 Converted to U_3O_8
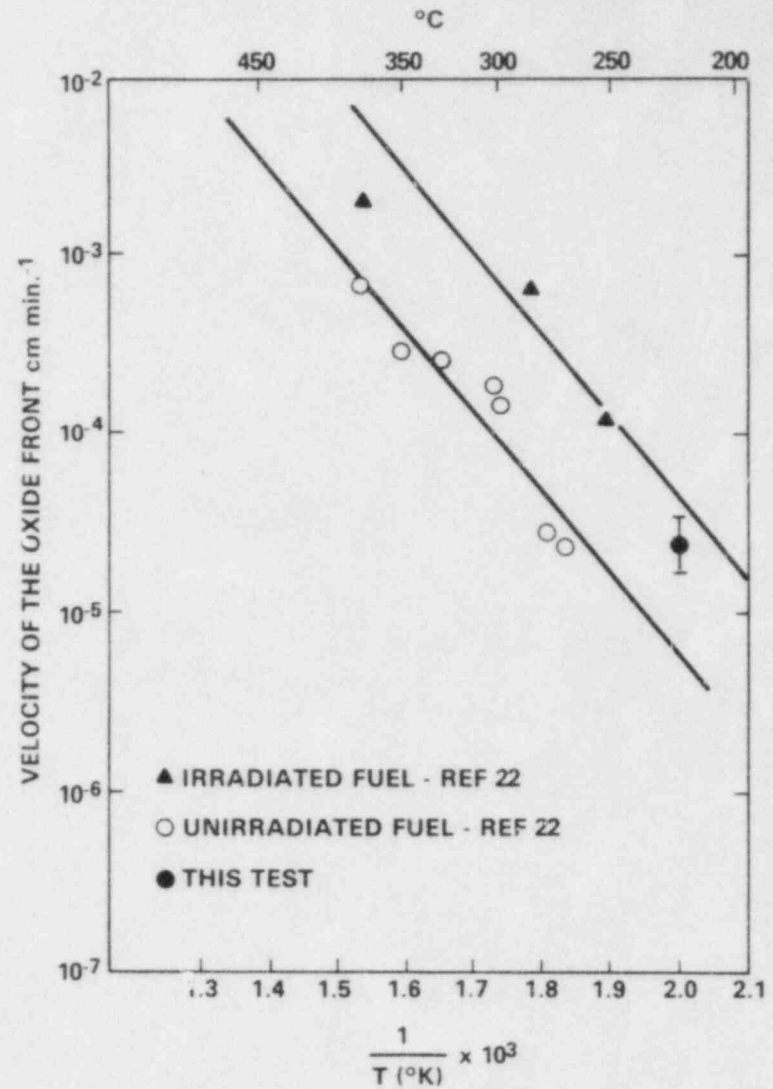
FIGURE 40. Oxidation Front Velocity in Defected Fuel Elements.

VII. CONCLUSIONS

Eight LWR spent fuel rods were individually tested at 229°C for 5962 hours to determine rod performance and crud spallation and dispersal characteristics under selected potential dry storage conditions. These eight included BWR and PWR rods, with and without artificial defects, in air or inert atmosphere. Interim nondestructive testing and capsule smears were conducted on four rods; one rod was destructively examined. The major conclusions from this test are as follows:

1) The oxidation of spent LWR fuel to U_3O_8 at 229°C can incubate in ~1000 hours or less. Once oxidation reaches steady state, the rate is similar to that found for CANDU fuel. A LWR rod with a cladding defect large enough to admit air would split end-to-end in ~17 years at 230°C.

2) The geometry of the defect and of the gap determines the effectiveness of the cladding in inhibiting oxidation. A defect over a pellet-pellet interface, which allows the fuel freer access to air has a shorter incubation period for oxidation than does a defect over a pellet surface where the air access is much more inhibited.

3) Since PCI cracks are the most likely type of small breach to be put in storage without detection and since these cracks most commonly occur at pellet-pellet interfaces, the oxidation behavior of fuel under a defect at the pellet-pellet interface should be considered the limiting case.

4) X-ray analyses indicated that by 5962 hours, oxidation (although no cladding cracking) had started under the BWR rod cladding defect over a pellet face. This defect would probably have split open shortly. In the same vein, the fact that the PWR rod showed no signs of cladding splitting or dilation by 5962 hours should not be taken as an indication that PWR rods perform better than BWR rods. In all likelihood, the variability of the behavior observed in these tests is a result of the probability of defect placement with respect to the pellet-pellet interface.

5) More cladding strain (~6.5%) can be accommodated in a BWR rod than in a CANDU rod (~2%) before cladding splitting starts from large circular defects.

6) When the crystalline structure was disrupted by the oxidation process, the fuel formed a powdery compact. Even with the cladding split more than 2.5 in., very little fuel fell out into the test capsule. This may be due to the horizontal position of the test and not indicative of the behavior in storage orientation. Of the fuel that fell from the rod, very little in the respirable range of 2 to 15 μm became airborne. Longer splits or more extensive handling could reasonably be expected to enhance the fallout.

93

7) If no fuel dispersal <u>inside</u> the confinement system is a storage
    criteria then air should not be used as a storage atmosphere at
    temperatures greater than 230°C when rods with large defects may
    be present.

8) Crud spallation was much more noticeable with cladding dilation.
    Only 10% or less of the crud spalled. Less than 0.1% of the
    spalled crud was airborne in the respirable range of 2 to 15 μm.
    In all likelihood, crud spallation will not be a problem in a
    static storage system.

9) Defected rods stored in a dry inert atmosphere show no gross
    detrimental effects.

The behavior of the fuel used in this test should be representative of a
large portion of the spent fuel population. While spent fuel is a variable,
the pretest characterization indicates that the rods used in this test are
representative of a large portion of the spent fuel population. Therefore,
the behavior of the fuel used in this test should also be representative of
a large portion of the spent fuel population.

VIII. REFERENCES

1. Code of Federal Regulations, "Licensing Requirements for the Storage of Spent Fuel in an Independent Spent Fuel Storage Installation," Title 10, Part 72; and Radwaste News 1, p. 234, December 1980.

2. F. Garzarolli, R. Von Jan and H. Stehle, "The Main Causes of Fuel Element Failure in Water Cooled Power Reactors," Atomic Energy Review 17 (1), p. 31, 1979.

3. J. T. A. Roberts et al., LWR Fuel Performance Program: Progress in 1978," EPRI NP-1024-SR, Electric Power Research Institute, Palo Alto, CA, February 1979.

4. R. J. Bahorich, "Spent Fuel Encapsulation and Dry Storage Demonstration," Trans. Am. Nucl. Soc. 34, p. 834, 1980.

5. L. D. Ramspotts et al., Technical Concept for a Test of Geological Storage of Spent Reactor Fuel in the Climax Granite, Nevada Test Site, UCRL-52796, University of California, Radiation Laboratory, Berkeley, CA, 1979.

6. A. K. Miller, K. D. Challenger and A. Tasooji, SCCIG: A Phenomenological Model for Iodine Stress Corrosion Cracking of Zircaloy, EPRI NP-1798, Vol. 1, Electric Power Research Institute, Palo Alto, CA, April 1981.

7. L. D. Blackburn, D. G. Farwick, S. R. Field, L. A. James and R. A. Moen, Maximum Allowable Temperature for Storage of Spent Nuclear Reactor Fuel, HEDL-TME 78-37, Hanford Engineering Development Laboratory, Richland, WA, May 1978.

8. R. E. Einziger, S. D. Atkin, D. E. Stellrecht and V. Pasupathi, "High Temperature Postirradiation Materials Performance of Spent Pressurized Water Reactor Fuel Rods Under Dry Storage Conditions," Nucl. Technol. 57, p. 65, April 1982.

9. R. B. Davis, Data Report for the Nondestructive Examination of Turkey Point Spent Fuel Assemblies B02, B03, B17, B41 and B43, HEDL-TME 79-68, Hanford Engineering Development Laboratory, Richland, WA, May 1980.

10. S. D. Atkin, Destructive Examination of 3-Cycle LWR Fuel Rods from Turkey Point Unit 3 for the Climax - Spent Fuel Test, HEDL-TME 80-89, Hanford Engineering Development Laboratory, Richland, WA, June 1981.

11. R. B. Davis, Pretest Nondestructive Examination Data Summary Report on Turkey Point Spent Fuel Assemblies D01, D04, D06, for the Climax - Spent Fuel Test, HEDL-TME 80-83, Hanford Engineering Development Laboratory, Richland, WA, June 1981.

12. R. B. Davis and V. Pasupathi, Data Summary for the Destructive Examination of Rods G7, G9, J8, I9 and H6 from Turkey Point Fuel Assembly B17, HEDL-TME 80-85, Hanford Engineering Development Laboratory, Richland, WA, April 1981.

13. F. R. Larson and J. Miller, "A Time-Temperature Relationship for Rupture and Creep Stresses," Trans. Am. Soc. Mech. Eng. 74, p. 765, 1952.

14. R. E. Einziger and R. Kohli, "Low-Temperature Rupture Behavior of Zircaloy Clad Pressurized Water Reactor Fuel Rods Under Dry Storage Conditions," accepted for publication in Nucl. Technol., November 1984.

15. D. Cubicciotti and R. L. Jones, EPRI-NASA Cooperative Project on Stress Corrosion Cracking of Zircaloys, EPRI NP-717, Electric Power Research Institute, Palo Alto, CA, March 1978.

16. D. Cubicciotti and J. A. Davies, "The Release of Iodine from Iodine Salts by Gamma Radiolysis," Nucl. Sci. Eng. 60, p. 314, 1976.

17. D. Cubicciotti, R. L. Jones and B. C. Syrett, Stress Corrosion Cracking of Zircaloys, EPRI NP-1329, Electric Power Research Institute, Palo Alto, CA, March 1980.

18. A. Tasooji, R. E. Einziger and A. K. Miller, "Modelling of Zircaloy Stress Corrosion Cracking: Texture Effects and Dry Storage Spent Fuel Behavior," accepted for publication in Proc. of 6th ASTM Symposium on Zirconium in the Nuclear Industry, Vancouver, B.C., June 28-30, 1982, August 1984.

19. A. K. Miller and A. Tasooji, "Estimating the Limiting Temperature for Dry Storage with Respect to Stress Corrosion Cracking," Proc. of NRC Workshop on Spent Fuel/Cladding Reaction During Dry Storage, NUREG/CP-0049, August 17-18, 1983, Gaithersburg, MD, D. Reisenweaver, ed., March 1984.

20. R. D. Watson, On the Oxidation of Zirconium Alloys in Air and the Dimensional Changes Associated with Oxidation, AECL-3375, Atomic Energy of Canada Ltd., Chalk River, Ontario, Canada, June 1969.

21. E. Hillner, Corrosion and Hydriding Performance Evaluation of Three Zircaloy-2 Clad Fuel Assemblies After Continuous Exposure in PWR Cores 1 and 2 at Shippingport, PA, WAPD-TM-1412, Westinghouse Electric Corporation, Atomic Power Division, Pittsburgh, PA, January 1980.

22. D. G. Boase and T. T. Vandergraaf, "The Canadian Spent Fuel Storage Canister: Some Materials Aspects," Nucl. Technol. 32, p. 60. January 1977.

23. D. O. Pickman, "Internal Cladding Corrosion Effects," Nucl. Eng. Des. 33, p. 141, 1975.

24. R. P. Marshall and M. R. Loutham, "Tensile Properties of Zircaloy with Orientated Hydrides," Trans. Am. Soc. Met. 56, p. 693, 1963.

25. M. R. Loutham and R. P. Marshall, "Control of Hydride Orientation in Zircaloy," J. Nucl. Mater. 9, (2), 1963, pp. 170-184.

26. R. P. Marshall, "Influence of Fabrication History on Stress-Oriented Hydrides in Zircaloy Tubing," J. Nucl. Mater. 24, pp. 34-38, 1967.

27. D. O. Pickman, "Properties of Zircaloy Cladding," Nucl. Eng. Des. 21, pp. 212-236, 1972.

28. D. Hardie and M. W. Shanahan, "Stress Reorientation of Hydrides in Zr-2.5%Nb," J. Nucl. Mater. 55, pp. 1-13, 1975.

29. D. O. Northwood and U. Kosasih, "Hydrides and Delayed Hydrogen Cracking in Zirconium and its Alloy," Int. Met. Reviews 28, (2), p. 92, 1983.

30. A. Garlick, R. Sumerling and G. L. Shires, "Crud-Induced Overheating Defects in Water Reacator Fuel Pins," J. Br. Nucl. Energy Soc. 16, (1), January 1977.

31. G. Vesterlund and T. Olsson, Degradation Mechanisms During Pool Storage and Handling of Spent Power Reactor Fuel, ASEA-ATOM RB 78-29, ASEA-ATOM, Vaesteraas, Sweden, January 1978.

32. L. Lunde, "External Corrosion of Fuel Cladding in BWRs," Nucl. Eng. Des. 33, pp. 178-195, 1975.

33. V. F. Urbanic, R. Gray and D. H. Lister, Review of In-Reactor Zircaloy Corrosion and Crud Deposition Experience at AECL, EPRI NP-1254, Electric Power Research Institute, Palo Alto, CA, December 1979.

34. G. E. Zima, Comments on Fuel Crud as a Safety and Operational Factor of Independent Spent Fuel Storage Installations (ISFSI), NUREG/CR-0163, PNL-2657, Battelle Pacific Northwest Laboratories, Richland, WA, November 1978.

35. J. Blok, S. G. Sawochka and D. T. Snyder, "Corrosion Product Deposits in Fuel at the Nine Mile Point BWR," Trans. Am. Nucl. Soc. 16, p. 116, June 1972.

36. M. Reier, F. Keneshea and J. Younger, Fuel-Clad Failure Detection Final Report - Task 1, DOE-ET-47906-2, US Department of Energy, Washington, DC, November 16, 1979.

37. M. G. Balfour, E. Roberts, E. DeQuindt and P. Blanc, Zorita Research and Development Program: Vol. 1 Final Report, WCAP-10180, Vol. 1, Westinghouse Electric Corporation, Atomic Power Division, Pittsburgh, PA, September 1982.

38. R. E. Einziger and J. A. Cook, Pre-Test Visual Examination and Crud Characterization of LWR Rods Used in the Long-Term Low-Temperature Whole Rod Test, NUREG/CR-3285, HEDL-TME 83-9, Hanford Engineering Development Laboratory, Richland, WA, March 1984.

39. M. J. Bannister, "The Storage Behavior of Uranium Dioxide Powders - Review Article," J. Nucl. Mater. 26, pp. 174-184, 1968.

40. T. Wadsten, "The Oxidation of Polycrystalline Uranium Dioxide in Air at Room Temperature," J. Nucl. Mater. 64, p. 315, 1977.

41. D. A. Dominey, "Oxidation of UO_2 by Oxygen at 66°C and 80°C," J. Inorg. Nucl. Chem. 30, p. 1757, 1968.

42. H. R. Hockstra, A. Santos and S. Siegel, "The Low-Temperature Oxidation of UO_2 and U_4O_9," J. Inorg. Nucl. Chem. 18, p. 166, 1961.

43. M. L. Smith and J. M. Leitnaker, Atmosphere Contamination of Uranium Dioxide Powder, ORNL-4704, Oak Ridge National Laboratory, Oak Ridge, TN, June 1971.

44. G. C. Allen, P. M. Tucker and J. W. Tyler, "Oxidation of Uranium Dioxide a 298K Studied by Using X-Ray Photoelectron Spectroscopy," J. Phys. Chem. 86, p. 224, 1982.

45. P. Taylor, E. A. Burgess and D. S. Owens, "An X-Ray Diffractor Study of the Formation of β-$UO_{2.33}$ on UO_2 Pellet Surfaces in Air at 229 to 275°C," J. Nucl. Mater. 88, p. 153, 1980.

46. R. E. DeMarco, H. A. Heller, R. C. Abbott and W. Burkhardt, "Oxidation of UO_2 to U_3O_8," Bull. Cer. Soc. 38, (7), p. 360, 1959.

47. S. Aronson, R. B. Ronf and J. Belle, "Kinetic Study of the Oxidation of Uranium Dioxide," J. Chem. Phys. 27, (1), p. 137, July 1957.

48. H. Landspersky and M. Voboril, "Oxidation of UO_2 Containing Small Additions of Other Oxides," J. Inorg. Nucl. Chem. 29, p. 250, 1967.

49. D. Kolar, E. D. Lynch and J. H. Handwerk, "Influence of Gas Flow in DTA Curves of UO_2," J. Am. Cer. Soc. 45, (3), p. 141, March 1962.

50. J. Iwasaki, T. Sakurai, N. Ishikawa and Y. Kobayaski, Oxidation Pulverization of UO_2 Pellet, JAERI-1174, Japan Atomic Energy Research Institute, Tokyo, Japan, March 1969.

51. R. Wang, Probable Mechanisms for Oxidation and Dissolution of Single-Crystal UO_2 Surfaces, PNL-3566, Battelle Pacific Northwest Laboratory, Richland, WA, March 1981.

52. M. Iwasaki, T. Sakurai, N. Ishikawa and Y. Kobayashi, "Oxidation of UO_2 Pellets in Air - Effects of Heat-Treatment of Pellet in Particle Size Distribution of Powders Produced," J. Nucl. Sci. & Technol. 5, (12), p. 652, December 1968.

53. P. E. Blackburn, J. Weissbart and E. A. Gulbransen, "Oxidation of Uranium Dioxide," J. Phys. Chem. 62, p. 902, 1958.

54. K. A. Peakall and J. E. Antill, "Oxidation of Uranium Dioxide in Air at 350-1000°C, *J. Nucl. Mater.* 2, pp. 191-195, 1960.

55. K. T. Harrison, C. Padgett and K. T. Scott, "The Kinetics of the Oxidation of Irradiated Uranium Dioxide Spheres in Dry Air," *J. Nucl. Mater.* 23, p. 121, 1967.

56. H. Ohashi, E. Noda and T. Morozume, "Oxidation of Uranium Dioxide," *J. Nucl. Sci. & Technol.* 11, (10), p. 445, October 1974.

57. E. U. Kuzmicheva, L. . Kovba and E. A. Ippolitova, "Oxidation of Uranium Dioxide at Temperatures Below 270°C," *Soc. Radiochem.* 13, p. 877, 1971.

58. Q. E. Y. Walker, "The Oxidation of Uranium Dioxides," *J. Appl. Chem.* 15, p. 128, March 1965.

59. K. T. Scott and K. T. Harrison, "Some Studies of the Oxidation of Uranium Dioxides," *J. Nucl. Mater.* 8, (3), p. 307, 1963.

60. M. Iwasaki and N. Ishkiawa, "Air-Oxidation of UO_2 Pellets at 800 and 900°C, *J. Nucl Mater.* 36, p. 116, 1970.

61. T. Smith, *Kinetics and Mechanism of the Oxidation of Uranium Dioxide and Uranium Dioxide Plus Fissia Sintered Pellets*, NAA-SR-4677, North American Aviation, Inc., Downey, CA, November 1960.

62. J. Schmets, *Pretreatment of Irradiated Fuels, Quarterly Report 14, July 1 - September 30, 1963*, EURAEC-884, US-EURATOM Joint Research and Development Program, 1963.

63. K. A. Simpson and P. Wood, "Uranium Dioxide Fuel Oxidation in Air Below 350°C," *Proc. of NRC Workshop on Spent Fuel/Cladding Reaction During Dry Storage*, NUREG/CP-0049, August 17-18, 1983, Gaithersburg, MD, D. Reisenweaver, ed., March 1984.

64. I. J. Hastings and J. Novak, "Behavior in Air at 175-250°C of UO_2 Fuel Fragments Extracted from Irradiated Elements," *Proc. of NRC Workshop on Spent Fuel/Cladding Reaction During Dry Storage*, NUREG/CP-0049, August 17-18, 1983, Gaithersburg, MD, D. Reisenweaver, ed., March 1984.

65. G. D. White, C. A. Knox, E. R. Gilbert and A. B. Johnson, Jr., "Oxidation of UO_2 at 150 to 350°C," *Proc. of NRC Workshop on Spent Fuel/Cladding Reaction During Dry Storage*, NUREG/CP-0049, August 17-18, 1982, Gaithersburg, MD, D. Reisenweaver, ed., March 1984.

66. J. Novak and I. J. Hastings, "Post-Irradiation Behavior of Defected UO Fuel Elements in Air at 220-250°C," *Proc. of NRC Workshop on Spent Fuel/Cladding Reaction During Dry Storage*, NUREG/CP-0049, August 17-18, 1982, Gaithersburg, MD, D. Reisenweaver, ed., March 1984.

67. A. B. Johnson, E. R. Gilbert, D. Stahl, V. Pasupathi and R. Kohli, "Exposure of Breached BWR Fuel Rods at 325°C to Air and Argon," Proc. of NRC Workshop on Spent Fuel/Cladding Reaction During Dry Storage, NUREG/CP-0049, August 17-18, 1982, Gaithersburg, MD, D. Reisenweaver, ed., March 1984.

68. R. A. Lorenz et al., Fission Product Release from Highly Irradiated LWR Fuel, ORNL/NUREG/TM-287, Oak Ridge National Laboratory, Oak Ridge, TN, February 1980.

69. R. E. Einziger, R. L. Fish and R. L. Knecht, A Technical Description of the NRC Long-Term Whole Rod and Crud Performance Test, NUREG/CR-2889, HEDL-TME 82-32, Hanford Engineering Development Laboratory, Richland, WA, September 1982.

70. R. E. Einziger and R. L. Fish, Characterization of LWR Spent Fuel Rods Used in the NRC Low-Temperature Whole Rod and Crud Performance Test, NUREG/CR-2871, HEDL-TME 82-27, Hanford Engineering Development Laboratory, Richland, WA, September 1982.

71. P. H. Larson, Core Design and Operating Data for Cycles 1 & 2 of Peach Bottom-II, EPRI NP-563, Electric Power Research Institute, Palo Alto, CA, June 1978.

72. D. E. Owen, Interim Report on the Postirradiation Examination of Peach Bottom-II BWR Fuel Rods, TFBP-TR-264, EG&G, Idaho Falls, ID, March 1978.

73. Nuclear Power Plant Operating Experience 1976, NUREG-0366, Nuclear Regulatory Commission, Washington, DC, 1976.

74. J. T. A. Roberts, F. E. Gelhaus, H. Ocken, N. Hoppe, S. T. Oldberg, G. R. Thomas and D. Franklin, LWR Fuel Performance Program Progress in 1978, EPRI NP-1024-SR, Electric Power Research Institute, Palo Alto, CA, February 1979.

75. "The World List of Nuclear Power Plants," Nuclear News, p. 71, February 1984.

76. S. J. Dagbjartsson, B. A. Murdock, D. E. Owens and P. E. MacDonald, Axial Gas Flow in Irradiated PWR Fuel Rods, TREE-NUREG-1158, Nuclear Regulatory Commission, Washington, DC, September 1977.

77. A. A. Bauer, L. M. Lowry and J. S. Perrin, Progress on Evaluating Strength and Ductility of Irradiated Zircaloy During April through June 1975, BMI-1935, Battelle Memorial Institute, Columbus, OH, June 1975.

78. L. M. Lowry, A. J. Markworth, J. S. Perrin and M. P. Landow, Evaluating Strength and Ductility of Irradiated Zircaloy Task 5, Experimental Data Final Report, NUREG/CR-1729, BMI-2066, Vol. 1, Battelle Memorial Institute, Columbus, OH, May 1981.

79. A. A. Bauer, L. M. Lowry and J. S. Perrin, Evaluating Strength and Ductility of Irradiated Zircaloy, BMI-NUREG-1976, Battelle Memorial Institute, Columbus, OH, July 1977.

80. Progress on Evaluating Strength and Ductility of Irradiated Zircaloy During July through September 1975, BMI-1938, Battelle Memorial Institute, Columbus, OH, p. 3, 1975.

81. A. A. Bauer, L. M. Lowry and J. S. Perrin, Evaluating Strength and Ductility of Irradiated Zircaloy, BMI-1942, Battelle Memorial Institute, Columbus, OH, December 1975.

82. S. M. Gehl and L. R. Kelman, "Fuel Characterization," Light Water Reactor Safety Research Program: Quarterly Report for July - September 1975, ANL-75-72, Argonne National Laboratory, Argonne, IL, p. 42, 1975.

83. Light Water Reactor Safety Research Program: Quarterly Progress Report for January - March 1976, ANL-76-49, Argonne National Laboratory, Argonne, IL, 1976.

84. A. E. Norris, Fission Product Release, April 1 - June 30, 1979, LA-7969-PR, Los Alamos National Laboratory, Los Alamos, NM, 1979.

85. R. A. Lorenz, J. L. Collins and S. R. Manning, Quarterly Progress Report on Fission Product Release from LWR Fuel for the Period October - December 1975, ORNL/TM-290, Oak Ridge National Laboratory, Oak Ridge, TN, p. 30, March 1976.

86. A. A. Bauer, L. M. Lowry and J. S. Perrin, Evaluating Strength and Ductility of Irradiated Zircaloy, BMI-NUREG-1967, Battelle Memorial Institute, Columbus, OH, January 1977.

87. S. M. Gehl and M. G. Seitz, "Burnup Analysis," Light Water Reactor Safety Research Program: Quarterly Report for October - December 1975, ANL-76-15, Argonne National Laboratory, Argonne, IL, p. 50, 1975.

88. Y. B. Katayamo, D. J. Bradley and C. O. Harvey, Status Report on LWR Spent Fuel LAEA Leach Tests, PNL-3173, Battelle Pacific Northwest Laboratory, Richland, WA, March 1980.

89. Y. B. Katayama, Spent LWR Fuel Leach Tests, PNL-2982, Battelle Pacific Northwest Laboratory, Richland, WA, April 1979.

90. A. E. Norris, (Ed.), Fission Product Release, January 1 - March 31, 1980, LA-8389-PR, Los Alamos National Laboratory, Los Alamos, NM, p. 3, June 1980.

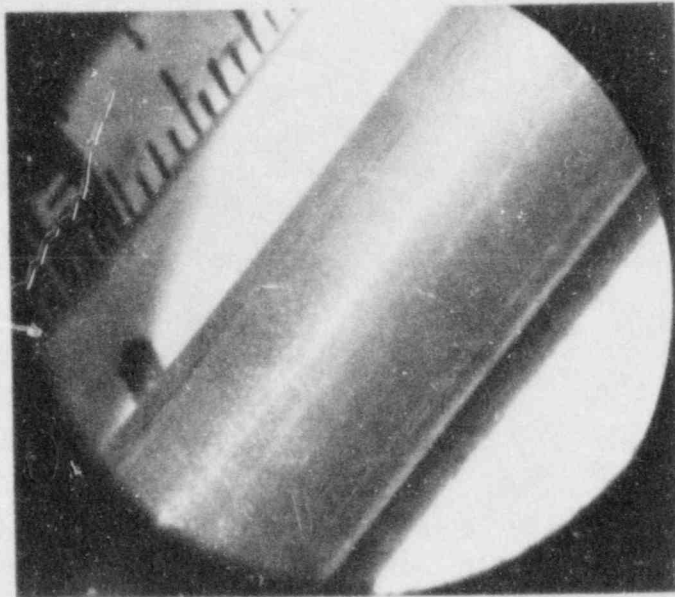APPENDIX A

VISUAL EXAMINATION OF FUEL RODS

FIGURE A1. Visual Examination 12 in. from Top of Rod PB-PH462-D6 After Testing for 5962 Hours at 229°C in Argon Atmosphere.
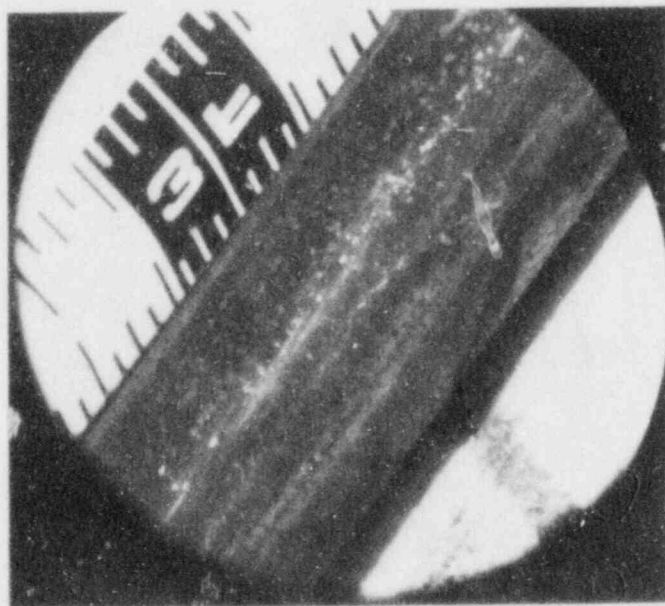

FIGURE A2. Visual Examination 36 in. from Top of Rod PB-PH462-D6 After Testing for 5962 Hours at 229°C in Argon Atmosphere.
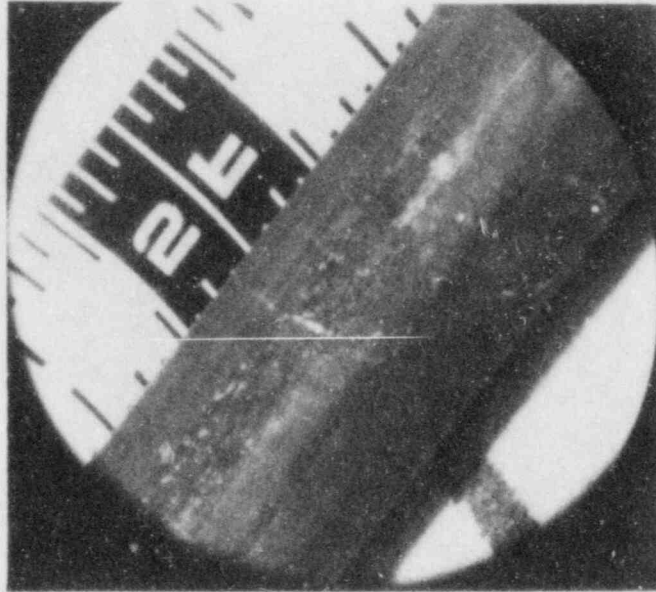
FIGURE A3. Visual Examination 60 in. from Top of Rod PB-PH462-D6 After
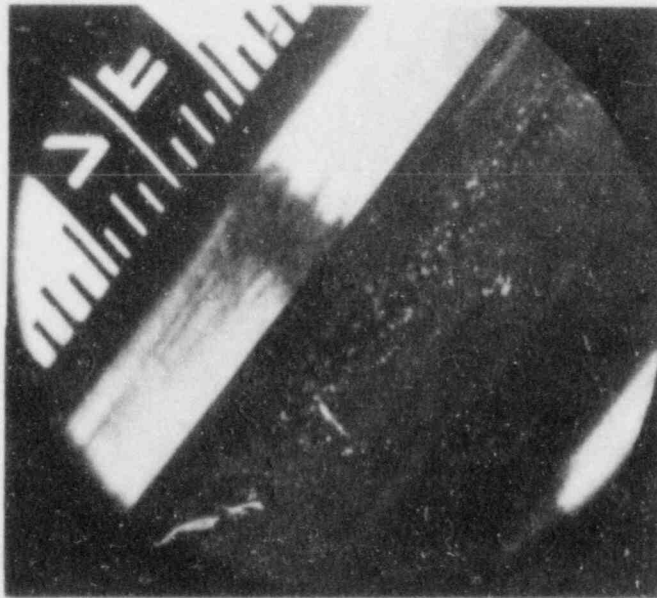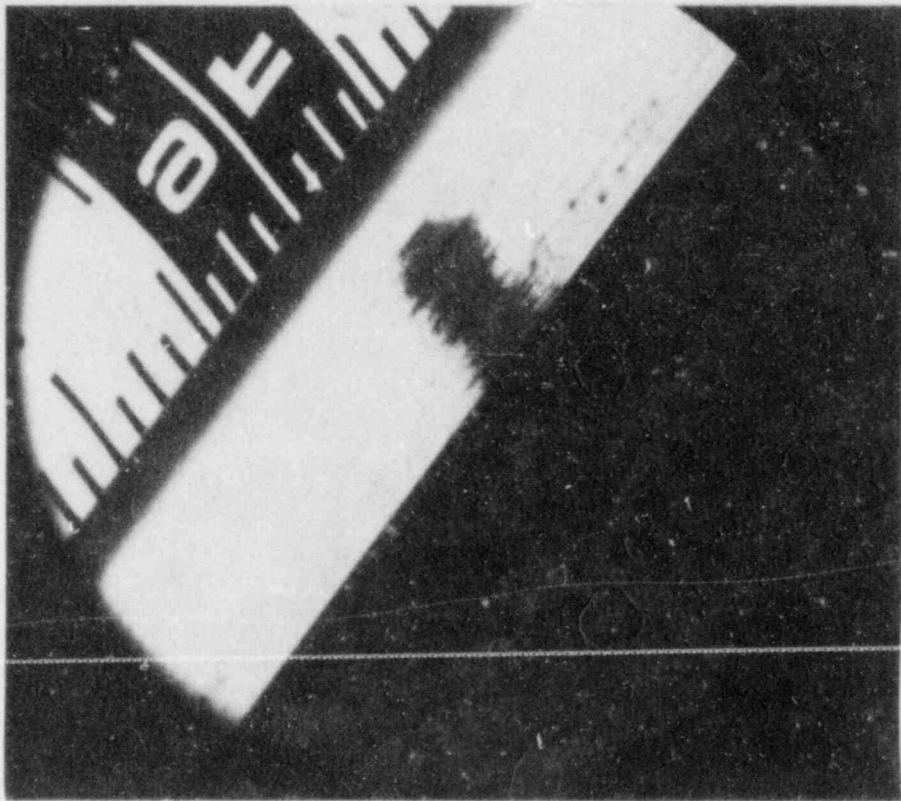Testing for 5962 Hours at 229°C in Argon Atmosphere.

FIGURE A4. Visual Examination 84 in. from Top of Rod PB-PH462-D6 After
Testing for 5962 Hours at 229°C in Argon Atmosphere.

HEDL 8404-173.22

FIGURE A5. Visual Examination 108 in. from Top of Rod PB-PH462-D6 After
Testing for 5962 Hours at 229°C in Argon Atmosphere.

(a)   **(b)**   **(c)**

FIGURE A6.   Artificial Defect at 70.5 in. from Top of Rod HBR-B05-E7:   (a) Pretest, (b) After Testing for 2235 Hours and (c) After Testing for 5962 Hours at 229°C in Argon Atmosphere.

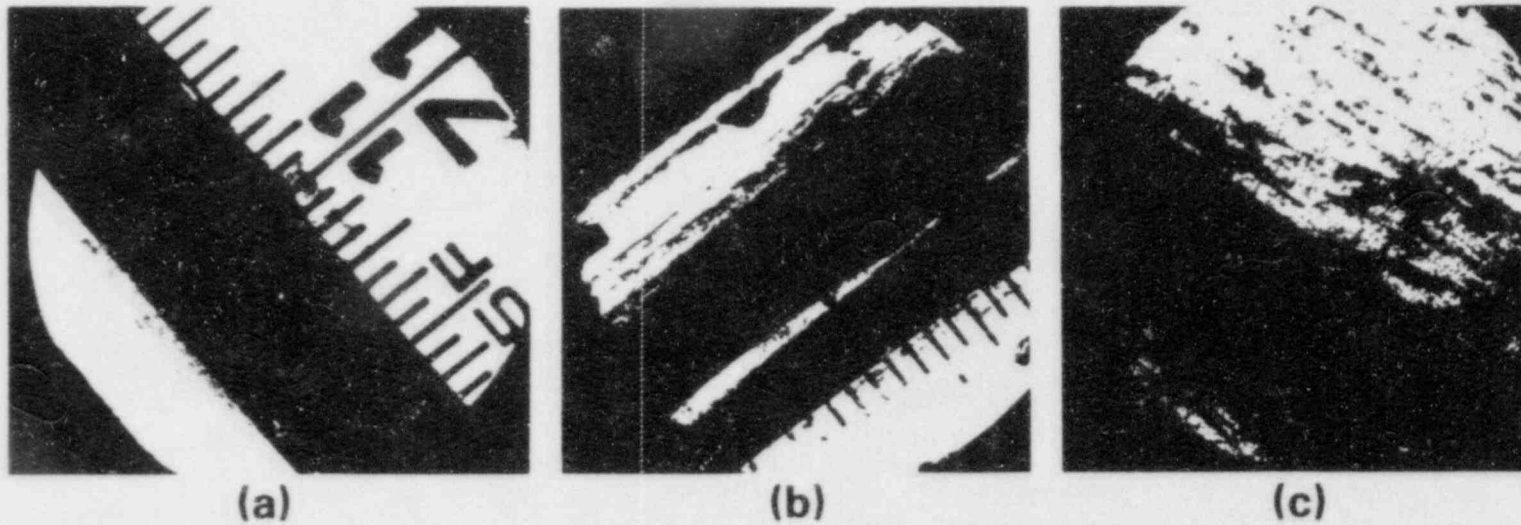**NO PHOTO TAKEN**

(a)   **(b)**   **(c)**

FIGURE A7.   Artificial Defect at 14 in. from Top of Rod HBR-B05-E7:   (a) Pretest, (b) After Testing for 2235 Hours and (c) After Testing for 5962 Hours at 229°C in Argon Atmosphere.

FIGURE A8. Artificial Defect at 81 in. from Top of Rod HBR-B05-D7: (a) Pre-
test and (b) After Testing for 2235 Hours at 229°C in Argon
Atmosphere.

(a)

(b)

HEDL 8404-173.37

FIGURE A9. Artificial Defect at 11 in. from Top of Rod HBR-B05-D7: (a) Pre-test and (b) After Testing for 2235 Hours at 229°C in Argon Atmosphere.
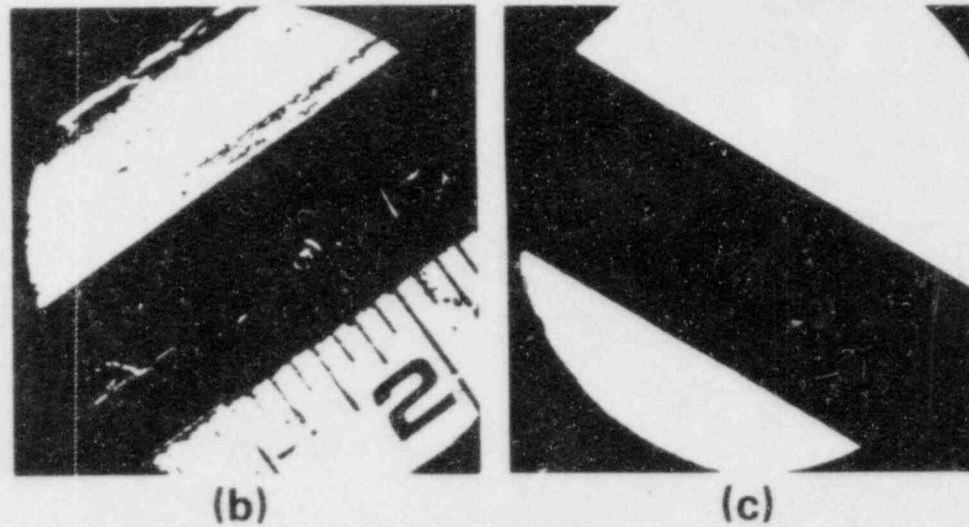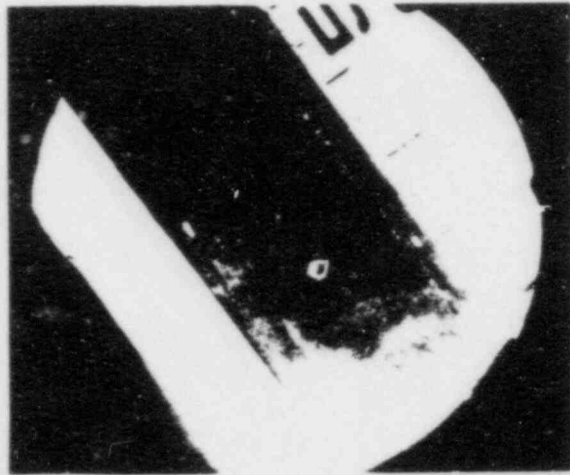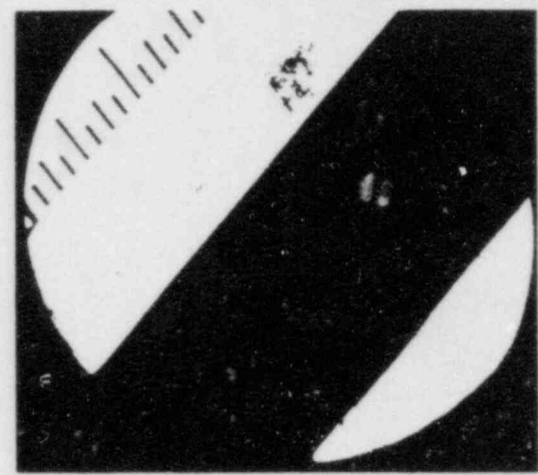
(a)   (b)   (c)

FIGURE A10.   Artificial Defect at 88.5 in. from Top of Rod PB-PH462-D6:   (a) Pretest, (b) After Testing for 2235 Hours and (c) After Testing for 5962 Hours at 229°C in Argon Atmosphere.
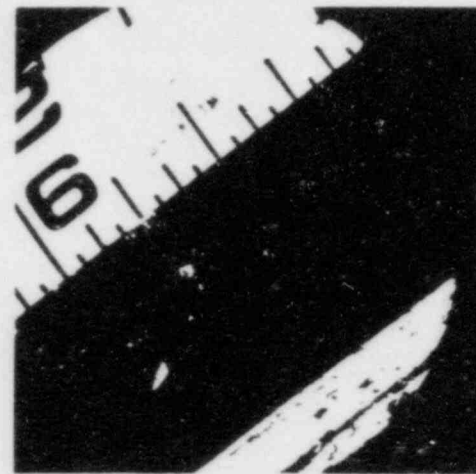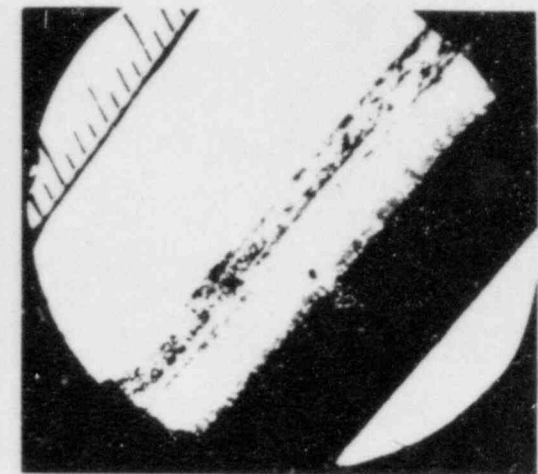
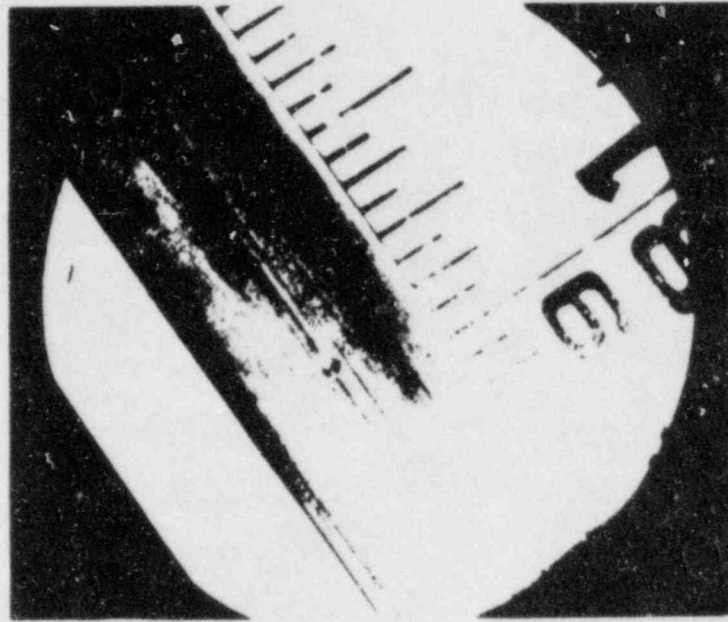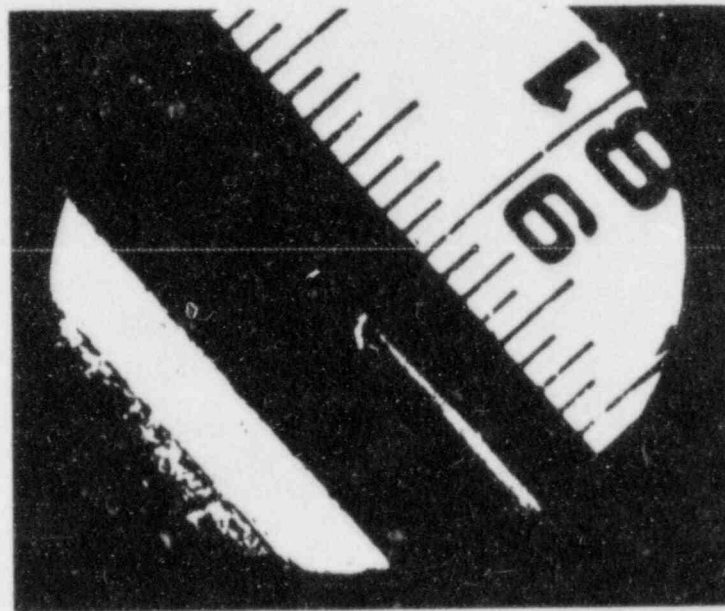(a)   (b)   (c)

FIGURE A11.   Artificial Defect at 205 in. from Top of Rod PB-PH462-D6:   (a) Pretest, (b) After Testing for 2235 Hours and (c) After Testing for 5962 Hours at 229°C in Argon Atmosphere.
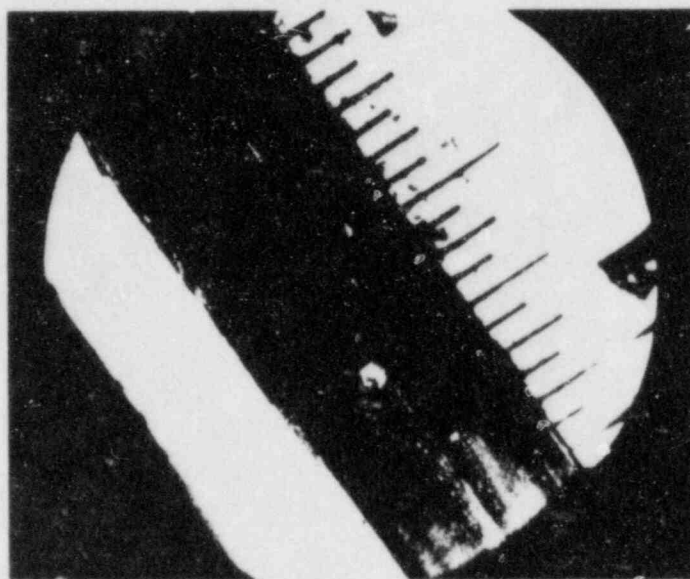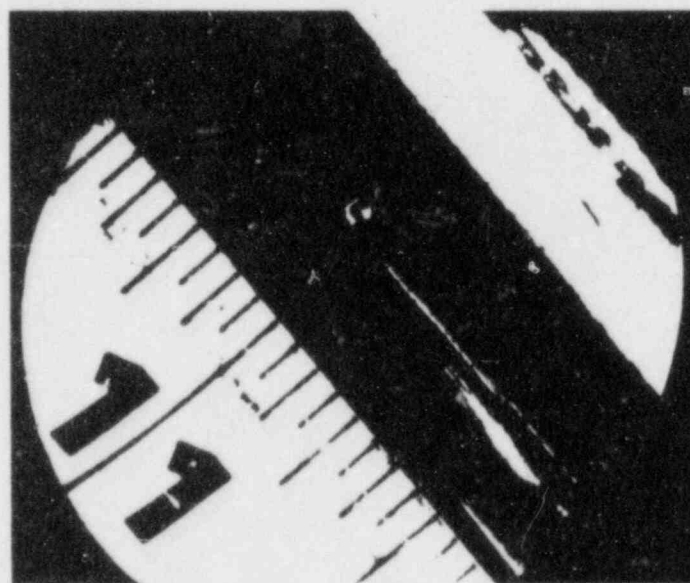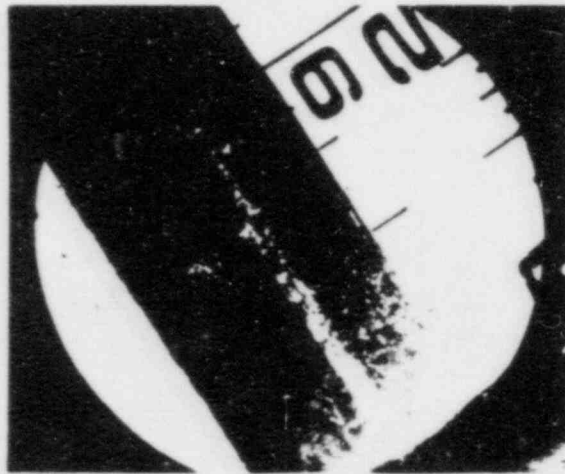
APPENDIX B

ISOTOPIC GAMMA SCANS AFTER 5962 HOURS AT 229°C

TABLE B1

ISOTOPIC GAMMA SCAN OF ROD HBR-B05-E7
AFTER TESTING FOR 5962 HOURS AT 229°C IN UNLIMITED AIR ATMOSPHERE

Distance from Bottom of Fuel Rod (in.)	Activity (ct/s)			
	^{134}Cs	^{137}Cs	^{254}Eu	^{60}Co
0.4	--	146.15	0.50	0.26
6.4	16.72	274.51	1.84	0.33
12.4	27.55	354.81	2.80	0.25
18.4	30.29	361.76	3.05	0.27
24.4	32.97	378.28	3.34	0.28
30.4	36.28	415.15	3.63	--
36.4	37.80	427.85	3.93	0.33
42.4	37.86	423.63	3.95	0.25
48.4	36.80	419.64	3.85	0.32
54.4	33.70	396.44	3.64	0.29
60.4	37.15	422.52	3.87	0.31
66.4	--	419.67	3.80	0.28
72.4	34.58	392.63	3.55	0.31
78.4	34.18	396.32	3.68	0.26
84.4	36.53	412.36	3.69	0.30
90.4	36.90	419.73	3.85	0.32
96.4	36.89	418.24	3.95	--
102.4	36.81	413.89	3.95	0.32
108.4	35.53	406.25	3.77	0.28
114.4	36.55	408.87	3.55	0.31
120.4	34.17	389.32	3.46	0.29
126.4	30.66	370.77	3.22	0.28
132.4	4.37	60.98	0.49	0.29
138.4	14.49	243.80	1.47	0.33
144.4	5.46	163.23	0.53	0.29
150.4	ND*	0.18	ND	1.36
156.4	ND	0.15	ND	0.25

---

*ND (Not Detected) means <0.1 ct/s.

B-3

TABLE B?

ISOTOPIC GAMMA SCAN OF ROD PB-PH462-D6
AFTER TESTING FOR 5962 HOURS AT 229°C IN ARGON ATMOSPHERE

Distance from Bottom of Fuel Rod (in.)	Activity (ct/s)		
	^{134}Cs	^{137}Cs	^{60}Co
--	ND*	0.18	0.24
4	3.32	118.02	0.31
10	9.50	202.80	0.28
16	15.62	254.99	0.37
22	--	--	0.41
28	25.68	333.75	0.46
34	30.08	361.31	0.44
40	28.54	338.42	0.39
46	29.99	353.05	0.44
52	29.48	342.91	0.41
58	26.29	316.98	0.38
64	25.73	308.21	0.36
70	24.09	287.93	0.39
76	26.11	311.47	0.37
82	23.65	284.72	0.37
88	24.95	292.64	0.36
94	25.95	299.74	0.36
100	--	--	0.37
106	24.65	287.34	0.39
112	23.51	279.72	0.41
118	22.47	277.09	0.38
124	18.73	250.50	0.39
130	14.54	222.19	0.33
136	8.83	172.91	0.30
142	3.80	119.18	0.28
148	ND	0.17	19.71
154	ND	0.20	7.78
160	ND	0.18	8.34

---

*ND (Not Detected) means <0.1 ct/s.

^{54}Mn, ^{152}Eu and ^{154}Eu were also not detected.

B-4

TABLE B3

ISOTOPIC GAMMA SCAN OF ROD PB-PH462-E5
AFTER TESTING FOR 5962 HOURS AT 229°C IN ARGON ATMOSPHERE

Distance from Bottom of Fuel Rod (in.)	Activity (ct/s)			
	^{154}Eu	^{60}Co	^{134}Cs	^{137}Cs
--	ND*	0.29	ND	0.20
--	ND	0.31	ND	0.16
5.4	0.24	0.31	3.89	131.86
11.4	0.63	0.33	8.86	191.34
17.4	1.07	0.38	15.17	257.67
23.4	1.41	0.41	20.73	301.10
29.4	1.78	0.48	24.32	323.94
35.4	1.94	0.44	26.84	337.37
41.4	1.96	0.41	26.77	335.25
47.4	1.98	0.40	26.86	329.33
53.4	1.84	0.39	23.94	302.19
59.4	1.54	0.35	21.52	282.63
65.4	1.68	0.39	21.50	275.87
71.4	1.62	0.33	21.96	278.10
77.4	1.67	0.34	20.76	269.22
83.4	1.61	0.35	20.49	265.28
89.4	1.80	0.35	23.19	283.89
95.4	1.74	0.38	22.84	281.77
101.4	1.69	0.33	20.60	262.81
107.4	1.79	0.37	21.32	268.19
113.4	1.72	0.33	21.08	266.55
119.4	1.56	0.37	18.72	250.01
125.4	1.35	0.36	16.39	236.67
131.4	0.97	0.32	11.95	201.70
137.4	0.48	0.31	6.32	146.37
143.4	0.27	0.30	4.54	137.07
149.4	ND	14.49	ND	0.10
155.4	ND	10.57	ND	0.17
161.4	ND	0.26	ND	0.17

*ND (Not Detected) means <0.1 ct/s.

^{54}Mn, ^{152}Eu and ^{154}Eu were also not detected.

TABLE B4

ISOTOPIC GAMMA SCAN OF ROD PB-PH462-E3
AFTER TESTING FOR 5962 HOURS AT 229°C IN UNLIMITED AIR ATMOSPHERE

Distance from Bottom of Fuel Rod (in.)	Activity (ct/s)					
	^{60}Co	^{106}Ru-^{106}Rh	^{125}Sb	^{134}Cs	^{137}Cs	^{154}Eu
0.0	ND*	ND	ND	ND	ND	ND
0.1	11.3 ± 0.4	ND	ND	0.13 ± 0.03	0.26 ± 0.06	ND
0.1	7.46 ± 0.22	ND	ND	ND	0.15 ± 0.08	ND
0.2	9.59 ± 0.29	ND	ND	0.32 ± 0.04	15.6 ± 0.2	ND
0.6	ND	0.12 ± 0.04	0.29 ± 0.05	0.73 ± 0.05	44.9 ± 0.9	ND
2.4	ND	0.14 ± 0.02	0.24 ± 0.04	0.94 ± 0.04	46.2 ± 0.9	ND
8.4	ND	0.28 ± 0.03	0.50 ± 0.05	3.78 ± 0.09	95.9 ± 1.3	0.22 ± 0.02
14.4	ND	0.45 ± 0.03	0.70 ± 0.08	7.01 ± 0.21	133 ± 2	0.42 ± 0.03
20.4	ND	0.51 ± 0.04	0.96 ± 0.07	9.87 ± 0.13	157 ± 2	0.60 ± 0.02
26.4	ND	0.58 ± 0.04	1.01 ± 0.16	12.7 ± 0.1	182 ± 3	0.76 ± 0.02
32.4	ND	0.66 ± 0.04	1.00 ± 0.13	14.6 ± 0.3	195 ± 3	0.93 ± 0.02
38.4	ND	0.59 ± 0.05	1.13 ± 0.08	14.7 ± 0.2	190 ± 2	0.96 ± 0.02
44.4	ND	0.73 ± 0.05	1.17 ± 0.08	16.7 ± 0.2	205 ± 2	1.05 ± 0.03
50.4	ND	0.75 ± 0.08	1.20 ± 0.09	15.9 ± 0.2	198 ± 3	1.05 ± 0.03
59.3	ND	0.73 ± 0.04	1.03 ± 0.08	14.0 ± 0.2	173 ± 2	0.96 ± 0.02
62.3	ND	0.71 ± 0.06	1.13 ± 0.08	14.4 ± 0.4	175 ± 2	0.96 ± 0.03
68.3	ND	0.73 ± 0.04	0.99 ± 0.07	16.0 ± 0.2	190 ± 2	0.97 ± 0.04
74.3	ND	0.71 ± 0.05	0.95 ± 0.08	15.1 ± 0.2	185 ± 2	0.96 ± 0.02
80.3	ND	0.68 ± 0.04	0.97 ± 0.07	12.6 ± 0.2	162 ± 2	0.81 ± 0.02
86.3	ND	0.64 ± 0.06	1.11 ± 0.13	15.0 ± 0.3	188 ± 3	0.91 ± 0.02
92.3	ND	0.71 ± 0.04	0.98 ± 0.08	15.2 ± 0.3	188 ± 3	0.87 ± 0.02
98.3	ND	0.75 ± 0.05	1.00 ± 0.07	15.2 ± 0.3	190 ± 3	0.89 ± 0.02
104.3	ND	0.67 ± 0.06	1.10 ± 0.08	14.9 ± 0.3	184 ± 3	0.97 ± 0.04
110.3	ND	0.64 ± 0.05	1.13 ± 0.03	13.8 ± 0.2	169 ± 3	0.95 ± 0.03
116.3	ND	0.63 ± 0.04	1.06 ± 0.08	13.5 ± 0.3	166 ± 2	0.98 ± 0.04
122.3	ND	0.60 ± 0.05	0.87 ± 0.07	11.9 ± 0.1	158 ± 2	0.83 ± 0.03
128.0	ND	0.39 ± 0.05	0.90 ± 0.07	10.6 ± 0.3	150 ± 2	0.70 ± 0.03
128.2	ND	0.39 ± 0.03	0.63 ± 0.06	7.52 ± 0.15	111 ± 1	0.57 ± 0.02
128.4	ND	0.40 ± 0.03	0.87 ± 0.11	9.77 ± 0.21	140 ± 1	0.66 ± 0.22
134.3	NC	0.37 ± 0.03	0.63 ± 0.6	7.04 ± 0.26	119 ± 2	0.51 ± 0.02
140.3	ND	0.19 ± 0.04	0.51 ± 0.05	3.01 ± 0.05	75.9 ± 1	0.21 ± 0.01
146.3	10.9 ± 0.2	ND	ND	ND	ND	ND
152.3	4.79 ± 0.10	ND	ND	ND	ND	ND
158.3	2.72 ± 0.10	ND	ND	ND	ND	ND
160.4	2.58 ± 0.08	ND	ND	ND	ND	ND
160.7	12.4 ± 0.2	NC	ND	ND	ND	ND
161.0	0.69 ± 0.04	ND	ND	ND	ND	ND
161.1	1.18 ± 0.09	ND	ND	ND	ND	ND

*ND (Not Detected) means <0.1 ct/s.

APPENDIX C

FUEL OXIDATION AND CLADDING STRAIN

APPENDIX C

FUEL OXIDATION AND CLADDING STRAIN

A. ISOTROPIC OXIDATION

Consider a pellet of UO_2 with radius R_0 that oxidizes from the outside surface inward. It is actually a two-step process when the UO_2 converts directly to U_3O_8. Since the UO_2 has a higher density than the U_3O_8, as the oxidation proceeds, the radius of the pellet will increase to R_2 but the core of UO_2 will shrink to a radius R_1 (see Figure C1a). The volume of UO_2 at time t is $4/3 \pi R_1^3$ and the volume of U_3O_8 is $4/3 \pi (R_2^3 - R_1^3)$. The weight of UO_2 that is oxidized is $4 \pi/3 (R_0^3 - R_1^3)\rho_0$, when ρ_0 is the density of the UO_2. Since 3 moles of UO_2 react with 1 mole of O_2 to form 1 mole of U_3O_8, the weight gain is given by:
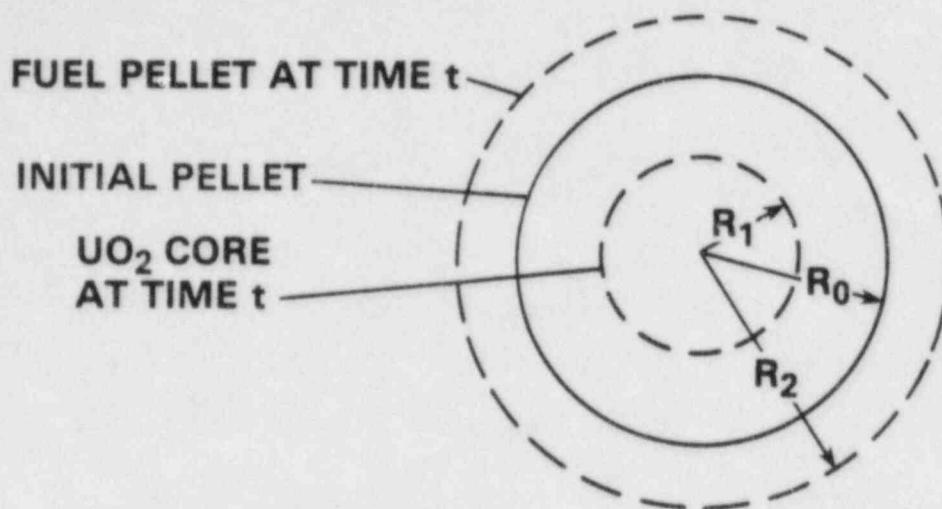
$$\text{Weight gain} = \frac{32}{270} \times \frac{1}{3} \times \frac{4\pi}{3} (R_0^3 - R_1^3)\rho_0 \qquad (C1)$$

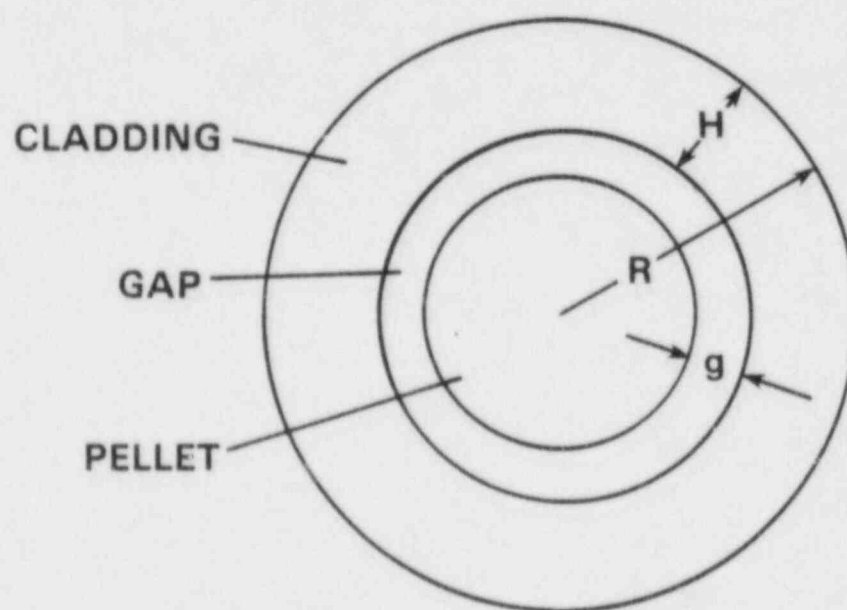and the fractional weight gain (f) is given by:

$$f = 3.95 \times 10^{-2} \left[1 - \left(\frac{R_1}{R_0} \right)^3 \right] \qquad (C2)$$

The fractional weight gain can also be expressed as

$$f = \frac{V_{UO_2}^t \rho_0 + V_{U_3O_8}^t \rho_1}{V_{UO_2}^i \rho_0} - 1 \qquad (C3)$$

(a) TIME-DEPENDENT PELLET RELATIONSHIP

(b) PELLET-CLADDING RELATIONSHIP

HEDL 8404-173.19

FIGURE C1. Pellet Oxidation.

C-4

where $V_{UO_2}^t$ is the volume of UO_2 at time t, $V_{U_3O_8}^f$ is the fuel volume of U_3O_8 at time t, $V_{UO_2}^i$ is the initial volume of UO_2, and ρ_1 is the density of U_3O_8. Eq. (C3)^2 can be expressed as:

$$f = \left(\frac{R_1}{R_0}\right)^3 + \left[\left(\frac{R_2}{R_0}\right)^3 - \left(\frac{R_1}{R_0}\right)^3\right] \frac{\rho_1}{\rho_0} - 1 \tag{C4}$$

Letting $\beta = (R_1/R_0)^3$ and equating Eqs. (C2) and (C4), we can obtain the expression:

$$\beta = \frac{1.0395 - \left(\frac{R_2}{R_0}\right)^3 \left(\frac{\rho_1}{\rho_0}\right)}{1.0395 - \rho_1/\rho_0} \tag{C5}$$

Now consider the relationship of the pellet and the cladding shown in Figure (Cb), where R is the midwall cladding radius, H is the wall thickness, and g is the gap width. After the system comes to thermal equilibrium, the fuel radius (R_0) and inner cladding radius (R_{Co}) can be expressed:

$$R_0 = (R - H/2 - g)(1 + \alpha_f \Delta T)$$

$$\tag{C6}$$

$$R_{Co} = (R - H/2)(1 + \alpha_{zr} \Delta T)$$

where α_f and α_{zr} are the radial coefficients of thermal expansion of the fuel and of Zircaloy, respectively. Notice that R_0 in Eqs. (C6) is the same as R_0 in Eq. (C5). After oxidation of the fuel has started and the fuel expands to contact the cladding, $R_{Co} = R_2$. At this point the cladding is placed under a stress from the oxidizing fuel and starts to strain an amount s. For 1% strain, s = 0.01, so R_2 can be expressed as

$$R_2 = (R - H/2)(1 + \alpha_{zr} \Delta T)(1 + s) \tag{C7}$$

Substituting β into Eq. (C2), and Eqs. (C7) and (C6) into β, one obtains the set of equations for determining the fractional weight gain:

$$f = 3.95 \times 10^{-2} (1 - \beta)$$

where:

$$\beta = \frac{1.0395 - \left(\frac{R_2}{R_0}\right)^3 \left(\frac{\rho_1}{\rho_0}\right)}{1.0395 - \rho_1/\rho_0} \tag{C8}$$

and

$$\frac{R_2}{R_0} = \frac{(R - H/2) (1 + \alpha_{zr} \Delta T) (1 + s)}{(R - H/2 - g) (1 + \alpha_f \Delta T)}$$

$$\alpha_{zr} = 2.07 \times 10^{-6}/°C$$

$$\alpha_f = 2.77 \times 10^{-6}/°C$$

$$\rho_1 = 8.35 \text{ g/cc}$$

Other parameters depend on the fuel rod and are listed in Table C1.

TABLE C1

FUEL ROD CHARACTERISTICS FOR DETERMINING FRACTIONAL WEIGHT GAIN
AS A FUNCTION OF CLADDING STRAIN (Ref. C1)

Parameter	Symbol	PWR	BWR	CANDU
Midwall Radius (mm)	R	5.04	6.68	7.43*
Wall Thickness (mm)	H	0.62	0.94	0.38
Gap (mm)	G	0.05**	0.15	0.1*
UO$_2$ Density (g/cc)	ρ_0	10.42	10.42	10.6

*Ref. C3.
**Ref. C2.

C-6

B. RADIAL FUEL GROWTH

If one assumes that the remainder of the fuel column restricts the fuel growth in the axial direction so that all the growth must be accommodated in the radial direction, then the only modification to Eq. (C8) is that $(R_2/R_0)^3$ must be replaced with $(R_2/R_0)^2$.

REFERENCES

C1. R. E. Einziger, R. L. Fish and R. L. Knecht, A Technical Description of the NRC Long-Term Whole Rod and Crud Performance Test, NUREG/CR-2889, HEDL-TME 82-32, Hanford Engineering Development Laboratory, Richland, WA, September 1982.

C2. R. E. Einziger and R. L. Fish, Characterization of LWR Spent Fuel Rods Used in the NRC Low-Temperature Whole Rod and Crud Performance Test, NUREG/CR-2871, HEDL-TME 82-27, Hanford Engineering Development Laboratory, Richland, WA, September 1982.

C3. J. Novak and J. J. Hastings, "Post-Irradiation Behavior of Defected UO Fuel Elements in Air at 220-250°C," Proc. of NRC Workshop on Spent Fuel/ Cladding Reaction During Dry Storage, NUREG/CP-0049, August 17-18, 1983, Gaithersburg, MD, D. W. Reisenweaver, ed., March 1984.

DISTRIBUTION

RJ

DOE-RL/Office of
Assistant Manager for Energy
P.O. Box 550
Richland, WA 99352

    KR Absher, Chief, Technology
       Development Branch

DOE/Nevada Operations Office
P.O. Box 14100
Las Vegas, NV 89114

    D. Vieth

Argonne National Laboratory (2)
Materials Science Division
9700 South Cass Avenue
Argonne, IL 66439

    LA Neimark
    RV Strain

HEDL (39)
c/o Supervisor, Document Processing
P.O. Box 1970, W/C-123
Richland, WA 99352

EG&G Idaho, Inc. (4)
P.O. Box 1625
Idaho Falls, ID 83415

    JA Cook (2)
    RR Hobbins
    CS Olson

Lawrence Livermore National Laboratory (2)
P.O. Box 808
Livermore, CA 94550

    V. Oversby
    L. Ballou

Westinghouse
Advanced Energy Systems Division
P.O. Box 158
Madison, PA 15663

    CR Bolmgren

JM Dahlke	W/C-115	
RE Einziger (2)	W/D-40	
RL Knecht	W/A-40	
WF Sheely	W/C-44	
HD Smith	W/A-40	
HH Yoshikawa	W/C-44	

Spent Fuel Files (27)	
c/o RE Einziger	W/C-40
Central Files (2)	W/C-110
Document Services (2)	W/C-123
Microfilm Services	W/C-123

3 TITLE AND SUBTITLE	4 RECIPIENT'S ACCESSION NUMBER
LWR SPENT FUEL DRY STORAGE BEHAVIOR AT 229°C	5 DATE REPORT COMPLETED
	MONTH: May — YEAR: 1984

6 AUTHOR(S)	7 DATE REPORT ISSUED
Robert E. Einziger (WHC)	MONTH: August — YEAR: 1984
James A. Cook (EG&G Idaho, Inc.)	9 PROJECT/TASK/WORK UNIT NUMBER

8 PERFORMING ORGANIZATION NAME AND MAILING ADDRESS (Include Zip Code)	
Westinghouse Hanford Company	10 FIN NUMBER
P.O. Box 1970	
Richland, WA 99352	B2435

14 ABSTRACT (200 words or less)

A whole rod test was conducted at 229°C to investigate the long-term stability of spent fuel rods under a variety of possible dry storage conditions. All combinations of BWR or PWR rods, inert or air atmospheres, and intact or defected rods were tested. After 2235 hours, visual observations, diametral measurements and radiographic smears were used to assess the degree of cladding deformation and particulate release. The same examinations plus metallography and x-ray analysis were conducted after 5962 hours.

None of the intact rods, the rods tested in inert atmosphere, or the defected PWR rod tested in unlimited air showed any measurable change from the pretest condition. The upper defect on the BWR rod tested in unlimited air had split open ∿0.5 in. after 2235 hours and had ∿10% cladding deformation. The crack grew to ∿2.5 in. after 7962 hours. X-ray analysis indicated that the UO_2 had oxidized to U_3O_8. The difference in behavior of the upper and lower defects is attributed to the air's accessibility to the fuel because of the deflect's position with respect to the pellet-pellet interface.

The oxidized fuel appeared to form a powdery compact that remained for the most part in the split cladding. Only a fraction of the fuel that fell out of the cladding became airborne. Some crud spalled from the rods but appeared to have no airborne particulate in the 2- to 15-μm respirable range. This report discusses the details and meaning of the data from this test.

15a KEY WORDS AND DOCUMENT ANALYSIS	15b DESCRIPTORS	
DRY STORAGE	FUEL OXIDATION	BWR
AIR STORAGE	WHOLE ROD TESTING	LWR
SPENT FUEL	H. B. ROBINSON	PWR
DEFECTIVE FUEL	PEACH BOTTOM	

16 AVAILABILITY STATEMENT	17 SECURITY CLASSIFICATION (This report)	18 NUMBER OF PAGES
Unlimited	Unclassified	
	19 SECURITY CLASSIFICATION (This page)	20 PRICE
		$